Studies on Electrochemical Reactions at Interface between Graphite and Solution(Dissertation_全文)

AUTHOR(S):

Yamada, Yuki

Studies on Electrochemical Reactions at Interface between Graphite and Solution

Yuki Yamada

2010

Studies on Electrochemical Reactions at Interface between Graphite and Solution

Yuki Yamada

Department of Energy and Hydrocarbon Chemistry
Graduate School of Engineering
Kyoto University
Kyoto, Japan

2010

Preface

The present thesis is a compilation of "Studies on Electrochemical Reactions at Interface between Graphite and Solution," which were carried out at Department of Energy and Hydrocarbon Chemistry, Graduate School of Engineering, Kyoto University during 2005–2010.

The present work has been conducted under the supervision of *Professor Zempachi Ogumi* and *Professor Takeshi Abe*, Department of Energy and Hydrocarbon Chemistry, Graduate School of Engineering, Kyoto University. The author would like to express his deepest gratitude to them for providing him a prime opportunity to study as a Ph.D student. Their sincere instruction, constructive discussion, and invaluable advice were of immense significance not only for this work but also for the author's life.

The author is also deeply grateful to *Professor Takashi Kakiuchi* and *Professor Masashi Inoue*, Graduate School of Engineering, Kyoto University, whose fruitful discussion and comments were of great value for this work.

The author's heartfelt appreciation goes to *Professor Yasutoshi Iriyama* (Shizuoka University), *Professor Tomokazu Fukutsuka* (Kyoto University), and *Dr. Kohei Miyazaki* (Kyoto University) for their dedicated guidance and discussion.

The author would like to appreciate *Professor Soon-Ki Jeong* (Soonchunhyang University) and *Dr. Fumihiro Sagane* (Kyoto University) for their helpful suggestions and discussion.

The author is indebted to all the members of Professor Ogumi's laboratory and Professor Abe's laboratory for their hearty support and encouragement. In particular, the author wishes to thank *Mr. Yasuhiro Koyama* and *Mr. Yasuyuki Takazawa* for their excellent contribution to this work.

Finally, the author wishes to express his special thanks to his parents and brothers for their warm encouragement and deep understanding toward accomplishing this work.

Yuki Yamada

Kyoto, Japan

2010

Contents

Part 2

Activation Energy of Electrochemical Lithium Intercalation into Graphite

Chapter 3

Kinetics of Lithium-Ion Transfer at the Interface between $Li_{0.35}La_{0.55}TiO_3$ and Binary Electrolytes

Chapter 4

Kinetics of Lithium Ion Transfer at the Interface between Graphite and Liquid Electrolytes: Effects of Solvent and Surface Film

Chapter 5

Kinetics of Electrochemical Insertion and Extraction of Lithium Ion at SiO

Part 3

Frequency Factor of Electrochemical Lithium Intercalation into Graphite

Chapter 6

Variation in Density of Electronic States at the Surface of Graphite and Its Influence on the Kinetics of Heterogeneous Electron Transfer

Chapter 7

Role of Edge Orientation in Kinetics of Electrochemical Intercalation of Lithium-Ion at Graphite

General Introduction

Background of the work

1. Graphite as Electrode Material [1]

Graphite has long been in an important position as an electrode material in a wide variety of fields. The application of a graphite electrode ranges from fundamental chemistry (e.g., analytical, physical, inorganic, and organic chemistry) to industries (e.g., iron and aluminum manufacturing). Such extensive applicability of a graphite electrode stems from its various advantages: chemical and thermal stability, high electric conductivity, low cost, and innocuity, etc. In addition to the conventional use, of recent interest are the applications to electrochemical energy storage/conversion devices such as lithium-ion batteries and hybrid capacitors. Due to the growing public concern about environmental and energy issues, graphite plays an increasingly crucial and indispensable role as an electrode of electrochemical devices, driving many researchers to study the electrochemistry of graphite.

Another reason for the great interest in a graphite electrode is its characteristic electrochemical behavior. For example, an electric double layer and a heterogeneous electron transfer reaction at a graphite electrode are quite different from those at metal electrodes. Furthermore, graphite can accommodate various ions by electrochemical driving force, which is an essential reaction of the negative electrode in lithium-ion batteries. All of these electrochemical behaviors of graphite are explained in relation to its unique structure and physical property.

2. Structure and Physical Property of Graphite

2.1. Structure of Graphite

Graphite is an allotrope of carbon with a layered structure (Fig. 1). In each layer, sp^2-hybridized carbon atoms compose an infinite plane with a honeycomb structure, which is usually referred to as a graphene sheet. Graphite consists of many graphene sheets stacked with van der

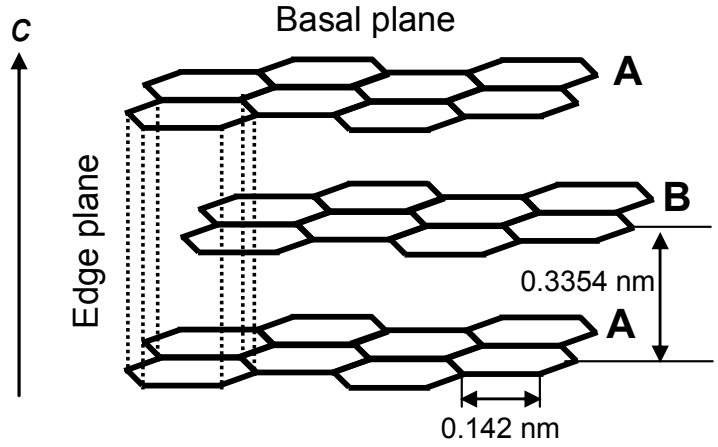

Fig. 1 Schematic illustration of structure of graphite.

Waals interplanar interaction. Graphite has two kinds of stacking as ABAB... (hexagonal) and ABCABC... (rhombohedral), and the more stable one is A-B stacking. In ideal graphite with A-B stacking, the C–C bond length is 0.142 nm and the interplanar spacing is 0.3354 nm. Due to such a layered structure, there are two planes exposed on the surface of graphite. A plane parallel to the graphene sheets is referred to as a basal plane, and one perpendicular to the graphene sheets is an edge plane. Such an anisotropic structure of graphite leads to characteristic electrochemical behaviors.

One of the common model electrodes for graphite is highly oriented pyrolytic graphite (HOPG), which is a polycrystalline block of graphite. On the basal surface of HOPG, the edge plane exists only at defects or grain boundaries and thus, the amount of edge planes is extremely small. According to Bard *et al*. [2], McCreery *et al.* [3], and Compton *et al*. [4], the fraction of edge planes on the basal surface of HOPG is reported to be 0.1–10 %. Therefore, the basal surface of HOPG is flat at an atomic level and it is widely used as a model electrode of graphite. In contrast to HOPG, polished glassy carbon is used as a model graphite electrode with many edge planes [1]. In glassy carbon, small graphitic planes are randomly interwined and there are many edge planes exposed on the surface.

2.2. Electronic Structure of Graphite

Many researchers have studied the electronic structure of graphite by using some models [5–8]. A band structure of graphite is depicted in Fig. 2. The σ and π orbitals of sp^2-hybridized carbon atoms form filled valence bands, whereas the antibonding orbitals form conduction bands.

The valence and conduction bands slightly overlap with each other at Fermi level (E_F), leading to free movement of π electrons occupying the π^+ band. Such π electrons serve as electric charge carriers, which provide graphite with electric conductivity. The density of states (DOS) at Fermi level is 0.002 states $atom^{-1}$ eV^{-1} at graphite [9]. In contrast, the DOS's of metals at Fermi level are higher; for example, gold shows 0.28 states $atom^{-1}$ eV^{-1} [10]. As a result, although graphite is not a semiconductor, the DOS at Fermi level is much lower than those of metals. Due to such properties, graphite is sometimes referred to as a semimetal.

2.3. Surface Structure of Graphite

There are many functional groups at the edge plane of graphite, which usually derive from reactions of dangling edge planes with oxygen and water in air [1]. The surface functional groups were identified by X-ray photoelectron spectroscopy and mass spectroscopy, etc. Figure 3 shows some functional groups commonly observed at the edge plane of graphite. Although a hydrogen atom is the simplest terminal group, the amount of the group is small. Instead, terminal groups including oxygen atoms (e.g., hydroxyl, carbonyl, lactone, and carboxyl) make up the largest number. These surface functional groups influence the double-layer capacitance and the heterogeneous electron transfer at a graphite electrode, as shown later.

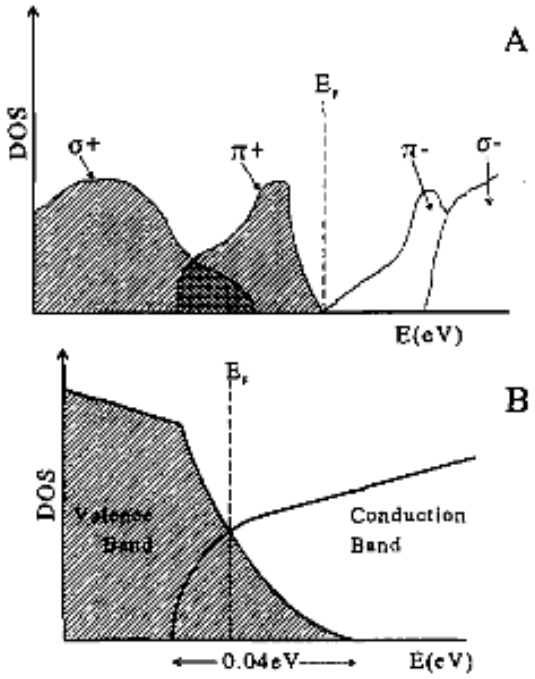

Fig. 2 A) Band structure for a graphite crystal. B) Enlarged figure of the band-overlapped region.

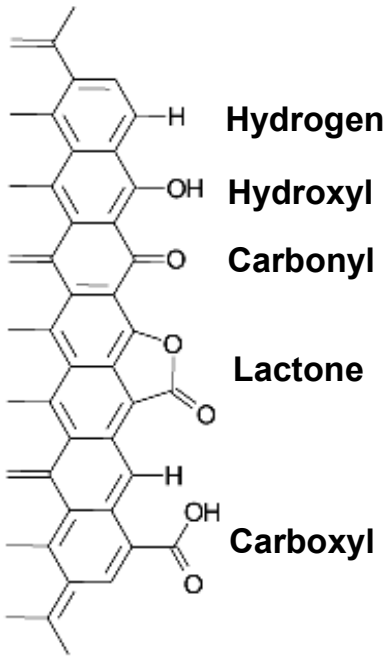

Fig. 3 Examples of terminal groups at the edge plane of graphite.

3. Electric Double Layer at Interface between Graphite and Solution

Graphite has a characteristic double-layer structure. A generally-accepted model for electric double layer at an electrode/solution interface is Stern model (Fig. 4) [11,12], in which two double layers, Helmholtz and diffusion double layers, exist in the solution near the electrode. In contrast, the behavior of a graphite electrode is different from that of Stern model. Randin and Yeager reported that the basal plane of HOPG showed an exceptionally small double-layer capacitance with some characteristic behaviors [13–15], which could not be interpreted by Stern model.

3.1. Presence of Space-Charge Layer inside Graphite

On the basis of the characteristic behaviors of an HOPG basal plane, Randin and Yeager concluded that a space-charge layer existed at the near-surface of an HOPG basal plane in addition to Helmholtz and diffusion double layers in a solution (Fig. 5) [13,14]. Their argument translates to the existence of three capacitors in series at the HOPG/solution interface: space-charge-layer capacitance (C_{SC}), Helmholtz-double-layer capacitance (C_H), and diffusion-double-layer capacitance (C_{diff}). Therefore, the measured capacitance (C_{exp}) is given in the following equation:

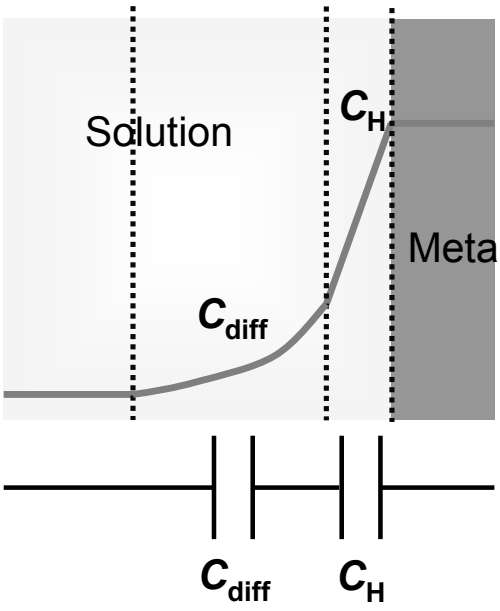

Fig. 4 Structure of electric double layer at metal/solution interface (Stern model) and its equivalent circuit.

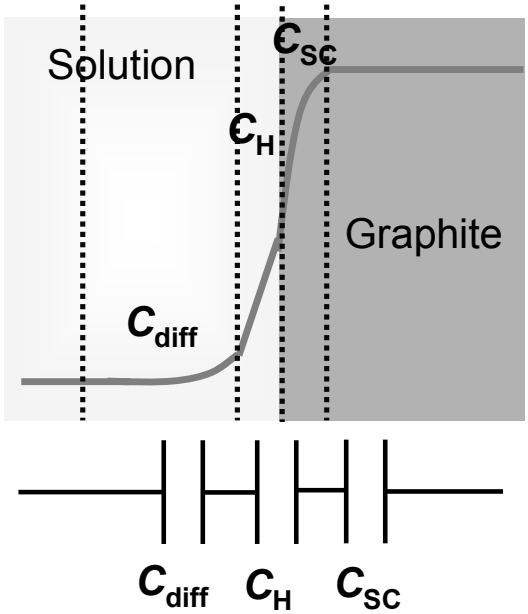

Fig. 5 Structure of electric double layer at graphite/solution interface and its equivalent circuit.

$$\frac{1}{C_{\mathrm{exp}}} = \frac{1}{C_{\mathrm{diff}}} + \frac{1}{C_{\mathrm{H}}} + \frac{1}{C_{\mathrm{SC}}} \qquad (1).$$

Consequently, the measured capacitance is dominated by the smallest capacitance of the three, C_{diff}, C_{H}, and C_{SC}. On the basis of a theory for semiconductor electrodes, the C_{SC} value was roughly estimated to be 4.5 μF cm^{-2} [13,14], assuming that the carrier density was 6×10^{18} carriers cm^{-3} [16] and the relative permittivity was 3.28 [17] at graphite . The C_{SC} value is the smallest of the three capacitances and thus, the measured capacitance is strongly influenced by the C_{SC} value.

The appearance of the space-charge layer at an HOPG basal plane stems from the small carrier density (i.e., small DOS). Gerischer *et al*. reported the following relation between DOS and C_{SC} as a function of the potential drop at a space-charge layer, ϕ_{SC}, in a unit of eV [18],

$$D(\phi_{\mathrm{SC}}) = \frac{1}{e\varepsilon\varepsilon_0}\left[\int_0^{\phi_{\mathrm{SC}}} C_{\mathrm{SC}}(\phi_{\mathrm{SC}})d\phi_{\mathrm{SC}}\,\frac{dC_{\mathrm{SC}}(\phi_{\mathrm{SC}})}{d\phi_{\mathrm{SC}}} + \{C_{\mathrm{SC}}(\phi_{\mathrm{SC}})\}^2\right] \qquad (2),$$

where $D(\phi_{\mathrm{SC}})$ is DOS at the energy level of ϕ_{SC}, e is the charge of electron, ε_0 is the permittivity of free space, and ε is the relative permittivity of graphite. Therefore, the value of C_{SC} is determined by DOS on a graphite electrode.

3.2. Role of Edge Plane in Double-Layer Capacitance

A double-layer capacitance tends to be large at the basal surface of HOPG with many edge planes [14,19]. Likewise, a polished glassy carbon electrode shows a large capacitance [15]. These results indicate that the presence of edge planes on the surface of a graphite electrode increases its measured capacitance. Such an effect of edge planes is generally explained by two factors: 1) functional groups and 2) DOS.

1) Effect of Functional Groups at Edge Plane

Various functional groups exist at the edge plane of graphite. Randin and Yeager reported that a measured capacitance strongly depended on pH of the solution and the direction of potential sweep [14,15]. Such behaviors cannot be explained by a space-charge layer and thus, functional groups at the edge plane should be taken into consideration as one of the factors influencing the measured capacitance. However, the detailed mechanism has not been clear yet.

2) Effect of DOS at Edge Plane

The local density of states (LDOS) is different at the basal and edge planes of graphite. Kobayashi carried out a first-principle calculation on the electronic structure of graphite and clarified that the LDOS is particularly high at the edge plane of graphite [20]. Because the value of C_{SC} is related to DOS, as shown in eq. 2, such an increase in LDOS at edge planes may influence the measured capacitance.

4. Heterogeneous Electron Transfer at Graphite Electrode

4.1. Characteristics of Electron Transfer at Graphite

Generally, the mechanism of heterogeneous electron transfer at an electrode is similar to that of homogeneous electron exchange in a solution. According to Marcus theory [21,22], the standard rate constant (k^o) for heterogeneous electron transfer of a given redox species is related to the rate constant (k_{ex}) for homogeneous electron exchange of the redox species,

$$\left(\frac{k_{ex}}{Z_{ex}}\right)^{1/2} = \frac{k^o}{Z_{el}} \qquad (3)$$

where Z_{ex} and Z_{el} denote the frequency factors for homogeneous and heterogeneous electron transfer, respectively. The values of Z_{ex} and Z_{el} are usually considered to be 10^{11} dm^3 mol^{-1} s^{-1} and 10^4 cm s^{-1}, respectively, and eq. 3 is effective for electron transfer at metal electrodes [23].

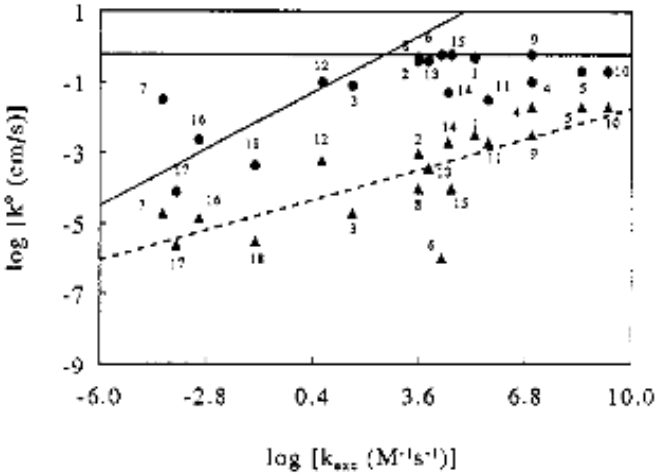

Fig. 6 Correlation of k^0 and k_{ex} for redox systems 1–15 on validated HOPG (triangles) and laser-activated glassy carbon (circles). For systems16–18, triangles are validated HOPG and circles are fractured, unoxidized glassy carbon. Horizontal line is instrumental limit.

Table 1: Kinetic Data for Redox Couples on HOPG

	System	k^0 (cm s^{-1})	k_{ex} (M^{-1} s^{-1})
1	$IrCl_6^{2-/3-}$	0.003	2X10^5
2	$Ru(NH_3)_6^{3+/2+}$	9X10^{-4}	4000
3	$Co(phen)_3^{3+/2+}$	2X10^{-5}	40
4	$MV^{2+/+}$	0.017	10^7
5	$Fe(phen)_3^{3+/2+}$	>0.07	3X10^8
6	$Fe(CN)_6^{3-/4-}$	10^{-6}	2X10^4
7	$Co(en)_3^{3+/2+}$	2X10^{-5}	8X10^{-5}
8	$Ru(en)_3^{3+/2+}$	1X10^{-4}	4000
9	$Fc(COOH)_2$	0.003	10^7
10	$Ru(bpy)_3^{3+/2+}$	>0.02	2X10^9
11	$Ru(NH_3)_5py^{3+/2+}$	0.002	5X10^5
12	$Co(sep)^{3+/2+}$	7X10^{-4}	5
13	$Ru(CN)_6^{3-/4-}$	4X10^{-4}	8000
14	$Mo(CN)_6^{3-/4-}$	0.002	3X10^4
15	$W(CN)_8^{3-/4-}$	4X10^{-4}	>4X10^4
16	$Fe_{aq}^{3+/2+}$	1.4X10^{-5}	1X10^{-3}
17	$Eu_{aq}^{3+/2+}$	2.5X10^{-6}	2X10^{-4}
18	$V_{aq}^{3+/2+}$	<3X10^{-6}	0.05

However, a graphite electrode exhibits an exceptional behavior, as shown by Wightman *et al.* [24] and McCreery *et al.* [25−33]. Figure 6 shows a correlation between k^o and k_{ex} for various redox systems listed in Table 1 at an HOPG basal plane (triangles) [32]. The k^o values at an HOPG basal plane did depend on the k_{ex} values, but were two or three orders of magnitude less than those expected by Marcus theory (a diagonal solid line). These results indicate that the heterogeneous electron transfer at an HOPG basal plane is slow compared to that at metal electrodes.

4.2. Role of Edge Plane in Heterogeneous Electron Transfer at Graphite

In contrast to the behaviors at an HOPG basal plane, the kinetics of heterogeneous electron transfer at glassy carbon or an HOPG edge plane is as fast as that at metal electrodes [24]. There are many edge planes exposed on the surface of these electrodes. Hence, it is reasonable to consider that the edge planes should play an important role in facilitating the heterogeneous electron transfer. In other words, the edge plane serves as a reaction site for heterogeneous electron transfer. As discussed in the previous section, the edge plane has two characteristics: 1) the presence of functional groups and 2) the increase in LDOS.

1) Effect of Functional Groups at Edge Plane

A relation between the presence of functional groups and the kinetics of heterogeneous electron transfer has been extensively studied at a glassy carbon electrode. Meyer *et al.* [34] and Bard *et al.* [35] reported that an oxidation treatment of glassy carbon significantly increased the electron-transfer rate of various redox species. McCreery *et al.* found that the electron-transfer kinetics of particular species clearly depended on the amount of carbonyl groups on the surface of glassy carbon [36,37]. On the basis of these results, they argued that an inner-sphere reaction path existed for the electron transfer of particular species: $Fe_{aq}^{3+/2+}$, $Eu_{aq}^{3+/2+}$, and $V_{aq}^{3+/2+}$, etc. In the case of such inner-sphere reactions, the reaction site is limited to the functional groups on edge planes. Therefore, the frequency factor is small at an HOPG basal plane compared to that at metal electrodes, leading to the smaller rate constants than those expected from Marcus theory.

2) Effect of LDOS at Edge Plane

As mentioned in the previous section, LDOS is quite high at edge plane on graphite [20]. Such high LDOS should facilitate heterogeneous electron transfer. There are some theoretical

considerations on a relation between DOS and the kinetics of heterogeneous electron transfer [38–41]. Lewis and his co-workers used Fermi's golden rule to formulate the rate of electron transfer at a semiconductor electrode [39,40] and a semimetal electrode [41]. According to their theory, the standard rate constant (k^{o}) of electron transfer at a semimetal electrode (e.g., graphite) is expressed in the following equation [41],

$$k^{o} \propto D(\phi_{E})\left(\frac{T}{\lambda}\right)^{1/2} A\exp\left(-\frac{\lambda}{4k_{B}T}\right) \quad (4),$$

where $D(\phi_E)$ is DOS at the energy level corresponding to a formal potential of redox couple, A is a term regarding electronic coupling in Fermi golden rule, λ is reorganization energy, T is absolute temperature, and k_B is Boltzmann constant. This equation indicates that the k^{o} value depends on the DOS of a graphite electrode. However, there are no experimental results about this correlation.

5. Electrochemical Ion Intercalation at Graphite Electrode

Graphite can accommodate various atoms and molecules in its interlayer space [42]. The resultant products are referred to as a graphite intercalation compound (GIC). At an early phase of research on GIC's, a popular synthesis method of GIC's was a chemical synthesis: a gas-phase method and a solution method, etc. In 1990's, the commercialization of lithium-ion batteries brought an important turning point to the research on GIC's. Lithium-ion batteries employ an electrochemical synthesis of Li-GIC (i.e., electrochemical lithium intercalation) as a negative-electrode reaction. Hence, many researchers were driven to study the electrochemical lithium intercalation into graphite. This reaction is unique in the following points.

1) The decomposition of electrolyte solutions is inevitable. This is because Li-GIC shows an extremely low potential (~0 V vs. Li/Li^{+}) [43], which decomposes even organic solvents with high tolerance toward reduction.

2) Ion and electron transfer simultaneously occurs during the reaction. Therefore, the reaction kinetics cannot be explained by a conventional theory of electrochemistry.

Covering such unique behaviors, this section describes recent research on the mechanism and kinetics of the electrochemical lithium intercalation into graphite in organic solutions.

5.1. Compatibility of Graphite Electrode and Electrolyte Solution

The decomposition of electrolyte solutions is inevitable at graphite during electrochemical lithium intercalation. Therefore, the behavior of electrochemical lithium intercalation strongly depends on electrolyte solutions. Ethylene carbonate (EC)-based electrolytes allow for reversible intercalation and deintercalation of lithium-ion at a graphite electrode [44], whereas propylene carbonate (PC) causes the exfoliation of graphite layers accompanied by continuous decomposition of PC [45–47]. Furthermore, in dimethyl sulfoxide (DMSO) or 1,2-dimethoxy ethane (DME), for example, solvated lithium-ion intercalates into graphite, which is referred to as cointercalation of solvents [48–51]. Generally, such a behavior of a graphite electrode is interpreted in relation to a solid electrolyte interphase (SEI) [52], which is formed on the surface of graphite by the reductive decomposition of an electrolyte. The nature of an SEI greatly depends on electrolyte solvents used.

The formation mechanism of an SEI was vigorously studied in the late 1990's. Besenhard *et al.* first proposed a model of the SEI formation (Fig. 7) [53], in which solvated lithium-ion intercalates into graphite, followed by rapid decomposition of the solvated lithium-ion in the interlayer of graphite. The decomposition product serves as an SEI layer to prevent further decomposition of the electrolyte solution. Ogumi and his co-workers used scanning tunneling

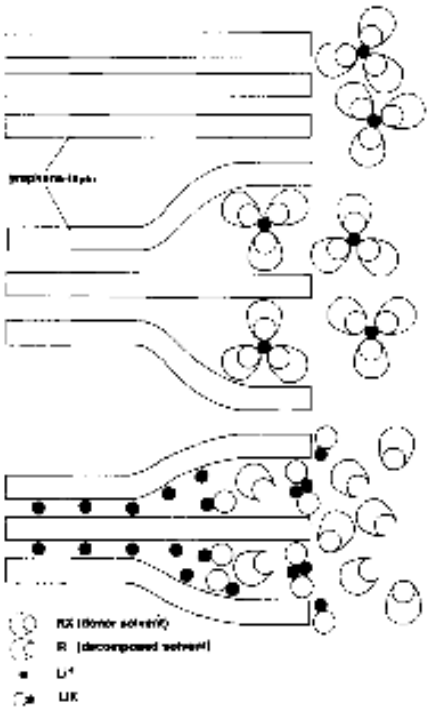

Fig. 7 Besenhard's model of the SEI formation via decomposition of $Li(solv)_yC_n$.

microscopy and atomic force microscopy to carry out *in situ* observation of the basal plane of HOPG during the SEI formation in an EC-based solution, and confirmed the appearance of bumps and blisters near a step edge at the potential of higher than 1 V vs. Li/Li^+ [54,55]. With the height of the bumps considered, the bumps and blisters indicate the intercalation of solvated lithium-ion and its decomposition in the interlayer of graphite, respectively. On the other hand, rapid exfoliation of graphite layers was observed at an HOPG basal plane in a PC-based solution [45–47], suggesting that the cointercalation of PC causes the deterioration of graphite. Chung *et al.* reported that the electrochemical behavior of graphite was completely different in *cis*- and *trans*-isomers of 2,3-butylene carbonate (*c*-BC and *t*-BC) [56]. Because the decomposition product of *c*-BC and *t*-BC is the same, the formation process of an SEI (i.e., intercalation of solvated lithium-ion) should influence the electrochemical behavior of graphite. In summary, the formation process of an SEI is an important factor for determining whether or not the intercalation of lithium-ion occurs.

In contrast to the Besenhard's model, Aurbach *et al.* argued that a decomposition product of electrolyte solvents is a determining factor for the behavior of lithium-ion intercalation into graphite (Fig. 8) [57,58]. According to Aurbach *et al.* [57–59] and Wang *et al.* [60], the SEI

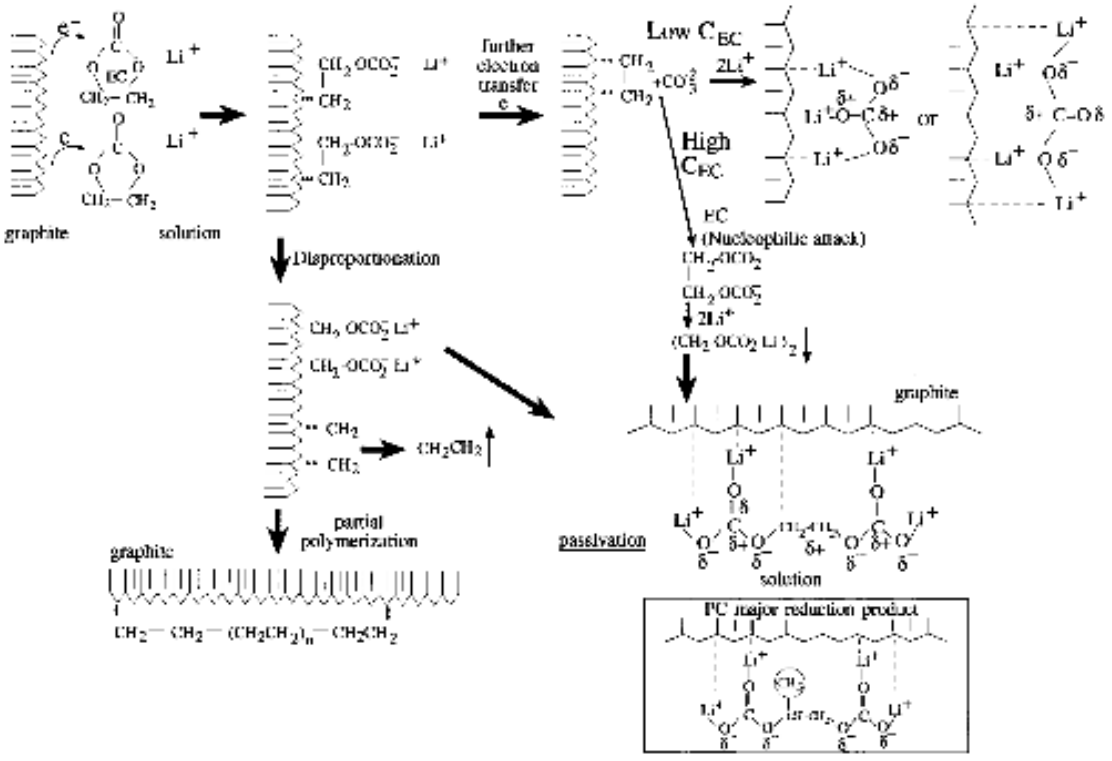

Fig. 8 Aurbach's model of the SEI formation in EC-based solution. The chemical structure of the expected major PC reduction product is also shown for comparison.

formed in an EC-based solution cnsists of both organic and inorganic components: lithium alkyl carbonates (e.g., $(CH_2OCO_2Li)_2$), Li_2CO_3, and Li_2O etc. On the contrary, the SEI formed in a PC-based solution has a different lithium alkyl carbonate, $CH_3CH(OCO_2Li)CH_2OCO_2Li$, which is less adhesive to the surface of graphite [57,61]. In addition, the reduction of PC forms propylene gas bubbles at the surface of graphite, which deteriorate the graphite layers [57]. This is why the intercalation of lithium-ion is impossible in a PC-based solution. However, Aurbach's argument cannot explain the results by Chung *et al.* as mentioned before [56].

In either model, the formation of a stable interface between graphite and solution is important for reversible intercalation and deintercalation of lithium-ion. However, the compatibility of a graphite electrode and electrolyte solutions remains controversial even now, requiring more fundamental researches.

5.2. Kinetics of Electrochemical Lithium Intercalation into Graphite

5.2.1. Contribution of Ion and Electron Transfer

The electrochemical ion intercalation is characterized by the concurrence of ion and electron transfer. The contribution of ion and electron transfer to the whole kinetics was first discussed in electrochemical amalgamation reactions. Fawcett *et al.* argued that the ion-transfer process was the rate-determining step of electrochemical amalgamation [62–64]. On the contrary, Schmickler and Koper argued that a unified treatment of ion and electron transfer was needed to accurately describe an amalgam forming reaction [65,66]. To date, scientists have not reached consensus on the contribution of ion and electron transfer to an amalgam forming reaction.

As for ion-insertion reactions, researchers agree that an ion-transfer process should be the rate-determining step of the reaction. Raistrick reported that the activation enthalpy of lithium-ion insertion at $Li_yNa_xWO_3$ was constant at several electrode potentials [67]. The independence of the activation enthalpy from the electron concentration suggests that the ion-transfer process is the rate-determining step. Bruce and Saidi investigated the kinetics of lithium-ion insertion at layered TiS_2 and reached the same conclusion [68,69].

Levi and Aurbach conducted theoretical consideration on electrochemical lithium intercalation into graphite [70,71]. However, the contribution of ion and electron transfer was not clarified in their reports.

5.2.2. Activation Energy for Electrochemical Lithium Intercalation into Graphite

Ogumi and his co-workers discussed the kinetics of interfacial lithium-ion transfer from a viewpoint of activation energy. They reported that the activation energy was generally over 50 kJ mol^{-1} at various solid/liquid interfaces [50, 72–75]. Such values of the activation energy are larger than those for lithium-ion transport in solid [76–79] or liquid [80–82] phase, indicating that the interfacial lithium-ion transfer is a slow process among several transport processes of lithium-ion. Even at an ideal solid/liquid interface (e.g., solid electrolyte/solution interface) where electron transfer does not occur, the activation energy for lithium-ion transfer was almost the same as those at electrode/solution interfaces [72]. These results suggest that the rate-determining step of electrochemical lithium intercalation is an ion-transfer process, and that the influence of an electron-transfer process is small.

Abe *et al.* studied the kinetics of electrochemical lithium intercalation into graphite [50]. Their discussion provides new insight into the interfacial lithium-ion transfer. In an EC-based solution, the activation energy for the electrochemical lithium intercalation into graphite was over 50 kJ mol^{-1}. In a DMSO solution, however, the activation energy was around 25 kJ mol^{-1}. It should be noted that the intercalation of DMSO-solvated lithium-ion occurs in a DMSO-based solution and thus, a desolvation process of lithium-ion does not exist in this case. All these results considered, the desolvation process of lithium-ion is the rate-determining step of the electrochemical lithium intercalation into graphite (Fig. 9).

Despite the vigorous study, there are several questions about the kinetics of electrochemical lithium intercalation at graphite. One of the questions is the influence of the solvation structure on the activation energy of interfacial lithium-ion transfer. If the desolvation of lithium-ion is the

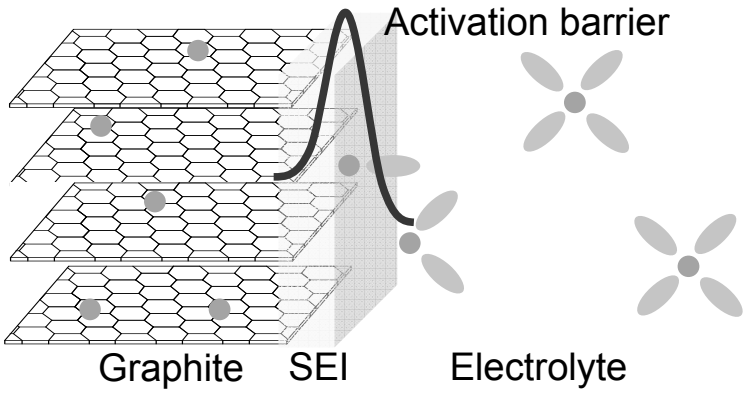

Fig. 9 Schematic diagram of intercalation of lithium-ion into a graphite electrode. Desolvation of lithium-ion occurs at the interface.

rate-determining step, the activation energy should depend on the solvation structure of lithium-ion in the solution. Another question is the influence of the SEI film on the activation energy. One important feature of the graphite/solution interface is the presence of an SEI on the surface of graphite. Therefore, the SEI film may have an impact on the kinetics of electrochemical lithium intercalation into graphite.

5.2.3. Frequency Factor for Electrochemical Lithium Intercalation into Graphite

The kinetics of lithium-ion intercalation is determined by frequency factor as well as activation energy. However, there are few reports on the frequency factor of electrochemical lithium intercalation into graphite.

There are several factors that may influence the frequency factor: 1) density of active sites, 2) activity of lithium-ion in an electrolyte, and 3) activity of lithium-ion in graphite (Li-GIC) etc. Among these factors, insight into 1) the density of active sites is important for designing a graphite electrode for lithium-ion batteries. It is generally accepted that the active site for the intercalation of lithium-ion is the edge plane on graphite. Hence, the frequency factor is expected to depend on the density of edge planes. Funabiki *et al.* reported that the electrochemical lithium-ion intercalation was quite slow at the basal plane of HOPG compared to that at the whole surface (i.e., basal and edge planes) of HOPG [83]. These results imply that the edge plane is the active site for electrochemical lithium intercalation at graphite. However, it is not clear how the kinetics of lithium intercalation is correlated with the density of edge planes at the surface of graphite.

Outline of the work

As discussed in the previous sections, much effort has been devoted to the clarification of the behaviors of electric double layer and heterogeneous electron transfer at graphite electrode. In contrast, fundamental researches on electrochemical lithium intercalation at graphite are inadequate, despite its growing importance in lithium-ion batteries. Furthermore, the complicated behavior of electrochemical lithium intercalation into graphite cannot be explained by present theories of electrochemistry. Therefore, researchers have not reached a complete

understanding of the reaction mechanism of lithium-ion intercalation into graphite, requiring much more fundamental studies. The present work focused its attention to the mechanism and kinetics of the electrochemical lithium intercalation into graphite.

In part 1, the compatibility of a graphite electrode and electrolyte solutions was studied. There are many reports on solvent decompositions on the surface of graphite, but the determining factor for the suppression of them is not clear. The present work investigated electrochemical reactions at a graphite/solution interface from a viewpoint of solvation structure of lithium-ion and discussed the compatibility of graphite and electrolyte solutions.

In chapter 1, the electrochemical reactions at natural graphite were studied in PC-based solutions. The solvation structure of lithium-ion was deliberately varied by the addition of a co-solvent, dimethyl carbonate (DMC), to a PC solution. The electrochemical behaviors of natural graphite clearly depended on the solvation number of PC molecules toward lithium-ion in PC:DMC binary solutions, indicating that the solvation structure of lithium-ion plays an important role in determining the behavior of electrochemical lithium intercalation.

In chapter 2, the electrochemical reaction at natural graphite was studied in DMSO-based solutions. The solvation structure of lithium-ion was varied with two methods: 1) addition of DMC and 2) addition of excess amount of lithium salt to the solution. A clear correlation was observed between the electrochemical behaviors of graphite and the solvation number of DMSO toward lithium-ion, leading to the conclusion that one of the determining factors in electrochemical reactions at the graphite/solution interface is the solvation structure of lithium-ion in the solution.

In part 2, the kinetics of lithium-ion transfer at graphite/solution interface was studied from a viewpoint of activation energies. So far, the kinetics of interfacial lithium-ion transfer has been widely investigated at several electrode materials. In summary, the activation energy for lithium-ion transfer at the interfaces between solid and liquid phases is large compared to those in solid or liquid phase, because the desolvation process of lithium-ion at the interface is the rate-determining step of the reaction. The present study focused its attention on the influences of the

solvation structure of lithium-ion and the composition of an SEI on the activation energy of interfacial lithium-ion transfer.

In chapter 3, the kinetics of lithium-ion transfer at a $Li_{0.35}La_{0.55}TiO_3$/solution interface was studied by ac impedance spectroscopy. Such an interface is ideal for investigating the kinetics of interfacial lithium-ion transfer, because there is no redox reaction (electron transfer), structural change, or SEI. Using a four-probe cell, the activation energy for the interfacial lithium-ion transfer in EC:DMC binary solutions was investigated. As a result, the presence of only a small amount of EC drastically increased the activation energy. With the solvation structure of lithium-ion taken into consideration, it was concluded that the desolvation of lithium-ion from the last solvent molecule is the rate-determining step, and that earlier desolvation process have almost no effect on the kinetics of interfacial lithium-ion transfer.

In chapter 4, the kinetics of lithium-ion intercalation into graphite was studied by ac impedance spectroscopy. Using highly oriented pyrolytic graphite (HOPG) as a model electrode, the activation energies of the interfacial lithium ion transfer were investigated. The results in this study showed that the activation energy of lithium-ion intercalation into graphite depended on two factors: 1) solvation strength of the solvent used and 2) composition of the SEI on graphite.

In chapter 5, the kinetics of lithium-ion insertion at silicon monoxide (SiO) was studied by ac impedance spectroscopy. SiO is one of the promising candidates for a next-generation negative electrode of lithium-ion batteries due to its high energy density [84–92]. Therefore, a comparison of the kinetics at SiO and graphite electrodes is needed. As a result, the activation energy was much lower at SiO than that at a graphite electrode. Furthermore, the activation energy remained unchanged in various electrolytes, suggesting that the kinetics of lithium-ion insertion at SiO is not influenced by the desolvation of lithium-ion.

In part 3, the kinetics of lithium-ion transfer at graphite/solution interface was studied from a viewpoint of frequency factor. One of the determining factors in frequency factor is the amount of reactive sites, as shown in section 5.2.3. It is generally accepted that the intercalation of lithium-ion occurs at the edge plane of graphite, but it is not clear how the amount of edge planes influences the kinetics (i.e., frequency factor) of the reaction. The present study shed light on a relationship between the amount of edge planes and the kinetics of electrochemical lithium intercalation at graphite.

In chapter 6, the kinetics of heterogeneous electron transfer of $Ru(NH_3)_6^{3+/2+}$ on the basal plane of HOPG was studied by cyclic voltammetry. This reaction is useful to quantify the edge planes exposed on the surface of graphite, as shown in chapter 7. Hence, the present study focused its attention on the determining factor in the kinetics of heterogeneous electron transfer of $Ru(NH_3)_6^{3+/2+}$ on an HOPG electrode. In addition, DOS at the near-surface of HOPG was investigated by a capacitance measurement. The results showed that the standard rate constant of $Ru(NH_3)_6^{3+/2+}$ had a proportional correlation with DOS on an HOPG basal plane.

In chapter 7, a relation between the amount of edge planes and the kinetics of electrochemical lithium intercalation into the basal plane of HOPG was studied. First, the amount of edge planes exposed on the surface of an HOPG basal plane was evaluated from the standard rate constant of $Ru(NH_3)_6^{3+/2+}$. Next, the charge-transfer resistance of lithium-ion intercalation into the same HOPG basal plane was measured by ac impedance spectroscopy. A relation between the amount of edge planes and the charge-transfer resistance was approximately inverse proportional, suggesting that the amount of edge planes determined the frequency factor of lithium intercalation.

References

[1] McCreery, R. L. *Chem. Rev.* **2008**, *108***,** 2646.

[2] Chang, H.; Bard, A. J. *Langmuir* **1991**, *7*, 1143.

[3] McDermott, M.T.; McCreery, R. L. *Langmuir* **1994**, *10***,** 4307.

[4] Davies, T. J.; Moore, R. R.; Banks, C. E.; Compton, R. G. *J. Electroanal. Chem.* **2004**, *574***,** 123.

[5] Tatar, R. C.; Rabii, S. *Phys. Rev. B* **1982**, *25***,** 4126.

[6] McClure, J. W. *Phys. Rev.* **1957**, *108***,** 612.

[7] Slonczewski, C.; Weiss, P. R. *Phys. Rev.* **1958**, *109***,** 272.

[8] Johnson, L. G.; Dresselhaus, G. *Phys. Rev. B* **1973**, *7***,** 2275.

[9] Gerischer, H.; McIntyre, R.; Scherson, D.; Storck, W. *J. Phys. Chem.* **1987**, *91***,** 1930.

[10] Kokko, K.; Ojala, E.; Mansikka, K. *J. Phys.: Condens. Matter*, **1990**, *2***,** 4587.

[11] Grahame, D. C. *J. Am. Chem. Soc.* **1954**, *76*, 4819.

[12] Grahame, D. C. *J. Am. Chem. Soc.* **1954**, *79*, 2093.

[13] Randin, J. P.; Yeager, E. *J. Electrochem. Soc.* **1971**, *118*, 711.

[14] Randin, J. P.; Yeager, E. *J. Electroanal. Chem.* **1972**, *36*, 257.

[15] Randin, J. P.; Yeager, E. *J. Electroanal. Chem.* **1975**, *58*, 313.

[16] Klein, C. A. *J. Appl. Phys.* **1962**, *33*, 3338.

[17] Ergun, S.; Yasinsky, J. B.; Townsend, J. R. *Carbon* **1967**, *5*, 403.

[18] Gerischer, H. *J. Phys. Chem.* **1985**, *89*, 4249.

[19] Bauer, H. H.; Spritzer, M. S.; Elving, P. J. *J. Electroanal. Chem*. **1968**, *17*, 299.

[20] Kobayashi, K. *Phys. Rev. B*, **1993**, *48*, 1757.

[21] Marcus, R. A. *J. Phys. Chem.* **1963**, *67*, 853.

[22] Marcus, R. A. *Ann. Rev. Phys. Chem.* **1964**, *15*, 155.

[23] Saji, T.; Yamada, T.; Aoyagui, S. *Electroanal. Chem. Interfacial Electrochem.* **1975**, *61*, 147.

[24] Wightman, R. M.; Deakin, M. R.; Kovach, P. M.; Kuhr, W. G.; Stutts, K. J. *J. Electrochem. Soc.* **1984**, *131*, 1578.

[25] Rice, R. J.; McCreery, R. L. *Anal. Chem.* **1989**, *61*, 1637.

[26] Bowling, R. J.; Packard, R. T.; McCreery, R. L. *J. Am. Chem. Soc.* **1989**, *111*, 1217.

[27] Rice, R. J.; Pontikos, N. M.; McCreery, R. L. *J. Am. Chem. Soc.* **1990**, *112*, 4617.

[28] Robinson, R. S.; Sternitzke, K.; McDermott, M. T.; McCreery, R. L. *J. Electrochem. Soc*. **1991**, *138*, 2412.

[29] McDermott, M. T.; Kneten, K.; McCreery, R. L. *J. Phys. Chem.* **1992**, *96*, 3124.

[30] McDermott, M. T.; McDermott, C. A.; McCreery, R. L. *Anal. Chem.* **1993**, *65*, 937.

[31] Kneten, K. R.; McCreery, R. L. *Anal. Chem.* **1992**, *64*, 2518.

[32] Cline, K. K.; McDermott, M. T.; McCreery, R. L. *J. Phys. Chem.* **1994**, *98*, 5314.

[33] McCreery, R. L.; Cline, K. K.; McDermott, C. A.; McDermott, M. T. *Colloids Surf. A*, **1994**, *93*, 211.

[34] Cabaniss, G. E.; Diamantis, A. A.; Murphy,W. R. Jr.; Linton, R. W.; Meyer, T. J. *J. Am. Chem. Soc.* **1985**, *107*, 1845.

[35] Kepley, L. J.; Bard, A. J. *Anal. Chem.* **1988**, *60*, 1459.

[36] Chen, P.; Fryling, M. A.; McCreery, R. L. *Anal. Chem.* **1995**, *67*, 3115.

[37] McDermott, C. A.; Kneten, K. R.; McCreery, R. L. *J. Electrochem. Soc.* **1993**, *140*, 2593.

[38] Gerischer, H. *J. Phys. Chem.* **1991**, *95*, 1356.

[39] Royea, W. J.; Fajardo, A. M.; Lewis, N. S. *J. Phys. Chem. B* **1997**, *101*, 11152.

[40] Lewis, N. S. *J. Phys. Chem. B* **1998**, *102*, 4843.

[41] Royea, W. J.; Hamann, T. W.; Brunschwig, B. S.; Lewis, N. S. *J. Phys. Chem. B* **2006**, *110*, 19433.

[42] Dresselhaus, M. S.; Dresselhaus, G. *Advances in Physics* **2002**, *51***,** 1.

[43] Dahn, J. R. *Phys. Rev. B* **1991**, *44*, 9170.

[44] Ogumi, Z.; Inaba, M. *Bull. Chem. Soc. Jpn.* **1998**, *71*, 521.

[45] Inaba, M.; Siroma, Z.; Kawatate, Y.; Funabiki, A.; Ogumi, Z. *J. Power Sources* **1997**, *68*, 221.

[46] Jeong, S. K.; Inaba, M.; Iriyama, Y.; Abe, T.; Ogumi, Z. *J. Power Sources* **2003**, *119–121*, 555.

[47] Jeong, S. K.; Inaba, M.; Iriyama, Y.; Abe, T.; Ogumi, Z. *J. Power Sources* **2008**, *175*, 540.

[48] Besenhard, J. O. *Carbon* **1976**, *14*, 111.

[49] Abe, T.; Kawabata, N.; Mizutani, Y.; Inaba, M.; Ogumi, Z. *J. Electrochem. Soc.* **2003**, *150*, A257.

[50] Abe, T.; Fukuda, H.; Iriyama, Y.; Ogumi, Z. *J. Electrochem. Soc.* **2004**, *151*, A1120.

[51] Schoderböck, P.; Boehm, H. P. *Synth. Met.* **1991**, *44*, 239.

[52] Peled, E. *J. Electrochem. Soc.* **1979**, *126*, 2047.

[53] Besenhard, J. O.; Winter, M.; Yang, J.; Biberacher, W. *J. Power Sources* **1995**, *54*, 228.

[54] Inaba, M.; Siroma, Z.; Funabiki, A.; Ogumi, Z.; Abe, T.; Mizutani, Y.; Asano, M. *Langmuir* **1996**, *12*, 1535.

[55] Jeong, S. K.; Inaba, M.; Abe, T.; Ogumi, Z. *J. Electrochem. Soc.* **2001**, *148*, A989.

[56] Chung, G. C.; Kim, H. J.; Yu, S. I.; Jun, S. H.; Choi, J. W.; Kim, M. H. *J. Electrochem. Soc.* **2000**, *147*, 4391.

[57] Aurbach, D.; Markovsky, B.; Weissman, I.; Levi, E.; Ein-Eli, Y. *Electrochim. Acta* **1999**, *45*, 67.

[58] Aurbach, D.; Levi, M. D.; Levi, E.; Schechter, A. *J. Phys. Chem. B* **1997**, *101*, 2195.

[59] Aurbach, D.; Zaban, A.; Ein-Eli, Y.; Weissman, I.; Chusid, O.; Markovsky, B.; Levi, M.; Levi, E.; Schechter, A.; Granot, E. *J. Power Sources* **1997**, *68*, 91.

[60] Wang, Y.; Nakamura, S.; Ue, M.; Balbuena, P. B. *J. Am. Chem. Soc.* **2001**, *123*, 11708.

[61] Wang, Y.; Balbuena, P. B. *J. Phys. Chem. B* **2002**, *106*, 4486.

[62] Baranski, A. S.; Fawcett, W. R. *J. Chem. Soc. Faraday Trans. 1* **1980**, *76*, 1962.

[63] Baranski, A. S.; Fawcett, W. R. *J. Chem. Soc. Faraday Trans. 1* **1980**, *78*, 1279.

[64] Fawcett, W. R. *Langmuir* **1989**, *5*, 661.

[65] Schmickler, W. *Electrochim. Acta* **1996**, *41*, 2329.

[66] Koper, M. T. M.; Schmickler, W. *J. Electroanal Chem.* **1998**, *450*, 83.

[67] Raistrick, I. D. *Solid State Ionics* **1983**, *9/10*, 425.

[68] Bruce, P. G.; Saidi, M. Y. *Solid State Ionics* **1992**, *51*, 187.

[69] Bruce, P. G.; Saidi, M. Y. *J. Electroanal. Chem.* **1992**, *322*, 93.

[70] Levi, M. D.; Aurbach, D. *J. Phys. Chem. B* **1997**, *101*, 4630.

[71] Levi, M. D.; Aurbach, D. *Electrochim. Acta* **1997**, *45*, 167.

[72] Abe, T.; Sagane, F.; Ohtsuka, M.; Iriyama, Y.; Ogumi, Z. *J. Electrochem. Soc.* **2005**, *152*, A2151.

[73] Yamada, I.; Iriyama, Y.; Abe, T.; Ogumi, Z. *J. Power Sources* **2007**, *172*, 933.

[74] Doi, T.; Iriyama, Y.; Abe, T.; Ogumi, Z. *Anal. Chem*. **2005**, *77*, 1696.

[75] Doi, T.; Miyatake, K.; Iriyama, Y.; Abe, T.; Ogumi, Z.; Nishizawa, T. *Carbon* **2004**, *42*, 3183.

[76] Inaguma, Y.; Chen, L. Q.; Itoh, M.; Nakamura, T *Solid State Ionics* **1994**, *70/71*, 196.

[77] Inaguma, Y.; Chen, L. Q.; Itoh, M.; Nakamura, T.; Uchida, T.; Ikuta, H.; Wakihara, M. *Solid State Commun.* **1993**, *86*, 689.

[78] Bohnke, O.; Bohnke, C.; Fourquet, J. L. *Solid State Ionics* **1996**, *91*, 21.

[79] Fu, J. *Solid State Ionics* **1997**, *96*, 195.

[80] Ding, M. S.; Jow, T. R. *J. Electrochem. Soc.* **2003**, *150*, A620.

[81] Ding, M. S.; Xu, K.; Jow, T. R. *J. Electrochem. Soc.* **2005**, *152*, A132.

[82] Ding, M. S. *J. Electrochem. Soc.* **2004**, *151*, A40.

[83] Funabiki, A.; Inaba, M.; Ogumi, Z. *J. Power Sources* **1997**, *68*, 227.

[84] Yang, J.; Takeda, Y.; Imanishi, N.; Capiglia, C.; Xie, J. Y.; Yamamoto, O. *Solid State Ionics* **2002**, *152–153*, 125.

[85] Netz, A.; Huggins, R. A.; Weppner, W. *J. Power Sources* **2003**, *119–121*, 95.

[86] Netz, A.; Huggins, R. A. *Solid State Ionics* **2004**, *175*, 215.

[87] Nagao, Y.; Sakaguchi, H.; Honda, H.; Fukunaga, T.; Esaka, T. *J. Electrochem. Soc.* **2004**, *151*, A1572.

[88] Tabuchi, T.; Yasuda, H.; Yamachi, M. *J. Power Sources* **2005**, *146*, 507.

[89] Miyachi, M.; Yamamoto, H.; Kawai, H.; Ohta, T.; Shirakata, M. *J. Electrochem. Soc.* **2005**, *152*, A2089.

[90] Miyachi, M.; Yamamoto, H.; Kawai, H. *J. Electrochem. Soc.* **2007**, *154*, A376.

[91] Kim, T.; Park, S.; Oh, S. M. *J. Electrochem. Soc.* **2007**, *154*, A1112.

[92] Yang, X.; Wen, Z.; Xu, X.; Lin, B.; Huang, S. *J. Power Sources* **2007**, *164*, 880.

Part 1

Compatibility of Graphite Electrode and Electrolyte Solution

Chapter 1

Correlation between Charge-Discharge Behavior of Graphite and Solvation Structure of the Lithium Ion in Propylene Carbonate-Containing Electrolytes

1.1. Introduction

Natural graphite plays an important role as a negative electrode in lithium-ion batteries due to its relatively high energy density (372 mAh g^{-1}) and excellent cycling ability. During charging, a lithium - graphite intercalation compound (Li-GIC) is formed by the electrochemical intercalation of lithium-ion into graphite and the resultant GIC shows a low potential, which is almost equal to that of lithium metal [1]. The low potential of Li-GIC leads to extremely high energy densities as compared with other rechargeable batteries and lithium-ion batteries now play an important role in portable electronic devices. However, the low potential of the negative electrode raises a problem. At such potentials (~0 V vs. Li/Li^+), organic electrolytes are thermodynamically unstable and are reduced to form decomposition products on a graphite electrode. These decomposition products are generally referred to as a solid electrolyte interphase (SEI) [2] and act as a passivation film to suppress the further decomposition of electrolytes.

The properties of SEI strongly depend on the electrolyte composition. Therefore, the choice of electrolyte components is important for the reversible intercalation/de-intercalation of lithium-ion at a graphite electrode [3–6]. Since lithium-ion batteries were commercialized in 1991, ethylene carbonate (EC)-based solutions have been widely used as electrolytes. This is because EC-derived SEI is stable and allows for the highly reversible intercalation and de-intercalation of lithium-ion at a graphite electrode. On the other hand, electrochemical lithium-ion intercalation into a graphite electrode cannot take place in a propylene carbonate (PC)-based electrolyte [7,8]. It is generally accepted that PC has poor SEI-forming ability and that the continuous decomposition of PC accompanied by the exfoliation of graphite occurs instead of the reversible intercalation and de-intercalation of lithium-ion at a graphite electrode. The incompatibility of graphite with PC has restricted the use of PC-based electrolytes in lithium-ion batteries. Many

researchers have attempted to use PC-based electrolytes, since PC-based electrolyte shows much better lithium-ion conductivity than EC-based electrolyte at lower temperatures [9], which is quite important for the application of these batteries in automobiles. Therefore, although there are many papers [3,10-19] on the electrochemical properties of graphite in PC-based electrolytes, there is still some controversy regarding the mechanism of exfoliation of a graphite electrode.

It is widely accepted that the first step in SEI formation (at around 1 V vs. Li/Li^+) is the intercalation of solvated lithium-ion into graphite in EC-based electrolyte. In the case of pure PC solution, PC-solvated lithium-ion intercalates into graphite and causes the exfoliation of graphite and continuous decomposition of the solvent. In fact, the intercalation of solvated lithium-ion and the exfoliation of graphite have been observed in various solutions by *in situ* electrochemical scanning tunneling microscopy (STM) [1,10] and atomic force microscopy (AFM) [15,19] of the basal plane of highly oriented pyrolytic graphite (HOPG). Furthermore, the formation of PC-solvated lithium-GICs, $Li(PC)_yC_n$, was confirmed by *in situ* X-ray diffraction measurement (XRD) [16]. Based on these results, the co-intercalation of PC is the most plausible cause of the exfoliation of graphite. Therefore, we consider that the solvation structure of lithium-ion should strongly influence the charge-discharge behavior of natural graphite.

The main purpose of this work was to clarify the effect of the solvation number of PC molecules per lithium-ion on the charge-discharge behavior of natural graphite in PC-containing solutions. We studied the charge-discharge properties of natural graphite in mixed solutions of PC and dimethyl carbonate (DMC). The solvation numbers of PC molecules per lithium-ion were investigated by Raman spectroscopy and found to vary in different PC:DMC solutions. We examined the correlation between the solvation number of PC molecules and the charge-discharge behavior of natural graphite and discuss the mechanism of the exfoliation of a graphite electrode.

1.2. Experimental Methods

Natural graphite powder (NG-7, Kansai Coke and Chemicals, Co. Ltd.,) was used as an active material. A composite electrode was prepared by coating copper foil with a slurry (containing NG-7 and polyvinylidene difluoride (PVdF)). The weight ratio of NG-7 to PVdF was 9:1. The electrolyte components were all battery-grade chemicals purchased from Kishida Chemical. The water contents in the electrolytes were guaranteed to be less than 20 ppm.

Electrolytes consisting of 1 mol dm^{-3} $LiClO_4$ dissolved in EC:DMC (1:1 by vol.), pure PC and PC:DMC (1:1–1:9 by vol.) were used for charge-discharge tests with a natural graphite electrode.

The charge-discharge tests were carried out using a three-electrode cell, in which lithium foil was used as both the counter and reference electrodes. Unless otherwise noted, the potentials in this paper are referenced to Li/Li^+. The constant current is set at 37.2 mA g^{-1}, corresponding to the rate of C/10. To make the SEI compositions constant in various PC:DMC solutions, a charge-discharge measurement of graphite electrode was conducted for two cycles in an EC-based electrolyte. After that, the EC-based electrolyte was replaced by various PC:DMC electrolytes, in which a charge-discharge measurement of a graphite electrode was conducted. All of the electrochemical measurements were conducted in an argon-filled dry box at 30 ^oC.

Raman spectra were recorded with a triple monochromator (Jobin-Yvon, T-64000) with a 514.5 nm line (50 mW) from an argon ion laser (NEC, GLG3260). A quartz cell was used for Raman spectroscopy of solutions.

The solvation ability of the solvents toward lithium-ion was studied by a theoretical calculation with the density functional theory using Gaussian 98W [20]. The reaction enthalpies of a lithium-ion and a solvent molecule were calculated at 298.15 K. Molecular structures were fully optimized in advance with B3LYP/6-31G (d). Single-point energies were calculated at the B3LYP/6-311 + G(3df, 3pd) level by using the optimized geometries obtained.

1.3. Results

1.3.1. Charge-discharge behaviors in PC:DMC mixed solutions.

Figure 1.1 shows charge-discharge curves for natural graphite in an electrolyte consisting of 1 mol dm^{-3} $LiClO_4$ PC and PC:DMC (1:1 by vol.) after being cycled in 1 mol dm^{-3} $LiClO_4$ EC:DMC (1:1 by vol.). The electrode potential remained constant at around 0.8 V during the charge process and the exfoliation of graphite was observed. These behaviors suggest that the decomposition of PC occurred continuously instead of the reversible intercalation and de-intercalation of lithium-ion at a graphite electrode. Note that the SEI film was derived from the EC-based electrolyte, which is generally stable and enables us to suppress the further decomposition of electrolyte solutions. In this case, however, PC molecules continuously decompose even in the presence of the EC-derived SEI. Based on these results, the EC-derived SEI did not prevent the co-intercalation of PC molecules, resulting in the decomposition of PC and the exfoliation of graphite. Although the amount of PC molecules is relatively small in an

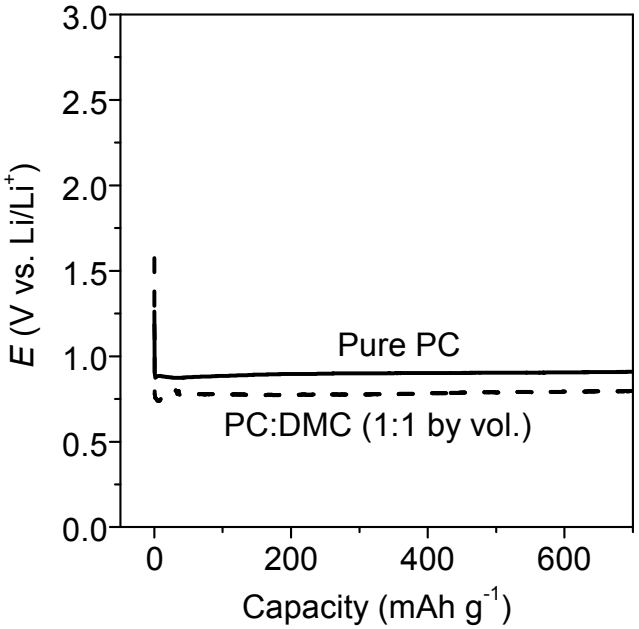

Fig. 1.1 Potential curves of natural graphite in 1 mol dm^{-3} $LiClO_4$ / pure PC (solid line) and PC:DMC (1:1 by vol.) (broken line) after being cycled in 1 mol dm^{-3} $LiClO_4$ / EC:DMC (1:1 by vol.).

electrolyte consisting of PC:DMC (1:1 by vol.), the potential curve in the electrolyte is the same as that in pure PC solution, except that the plateau potential is different. A PC molecule has relatively high solvation ability and interacts strongly with lithium-ion [21]. Due to the high solvation ability of PC, lithium-ion would be preferentially solvated by PC molecules in PC:DMC (1:1 by vol.) solution. Therefore, the solvation structure of lithium-ion might differ slightly between PC:DMC (1:1 by vol.) and pure PC. This point will be discussed in detail later. The results in the present study disagree with a previous report [17] in which an electrolyte consisting of $LiPF_6$ / PC:DEC:DMC (1:1:1 by vol.) enabled the intercalation of lithium-ion into spheroidal natural graphite, although there was a large amount of electrolyte decomposition. However, the other report [22] clearly indicated that the charge-discharge behavior in PC-containing electrolytes greatly depended on the type of graphite used. Therefore, the discrepancy in the results may be attributed to the difference in the type of graphite.

Figure 1.2 shows charge-discharge curves for natural graphite in an electrolyte composed of 1 mol dm^{-3} $LiClO_4$ PC:DMC (1:7 by vol.) after being cycled in 1 mol dm^{-3} $LiClO_4$ EC:DMC (1:1 by vol.). Natural graphite in $LiClO_4$ / PC:DMC (1:7 by vol.) showed an entirely different behavior from that in $LiClO_4$ / PC or PC:DMC (1:1 by vol.). At the 1st charge in $LiClO_4$ /

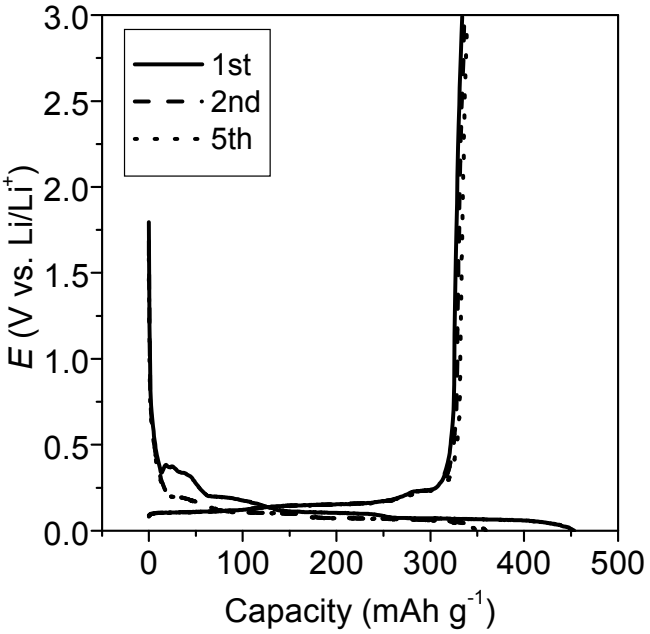

Fig. 1.2 Charge and discharge curves of natural graphite in 1 mol dm^{-3} $LiClO_4$ / PC:DMC (1:7 by vol.) after being cycled in 1 mol dm^{-3} $LiClO_4$ / EC:DMC (1:1 by vol.).

PC:DMC (1:7 by vol.), the potential plateau appeared at around 0.4 V and was followed by a potential decrease to 0 V. The initial charge capacity was about 450 mAh g^{-1} and therefore the irreversible capacity was relatively large. This plateau and irreversible capacity may be attributed to electrolyte decomposition. These results indicate that electrolyte decomposition on graphite could occur in the 1st cycle in $LiClO_4$ / PC:DMC (1:7 by vol.) even in the presence of an EC-based SEI. However, the exfoliation of graphite was not observed and the subsequent charge-discharge tests were successful. The discharge capacities at the 1st to 5th cycles were about 330–340 mAh g^{-1}, which are close to the theoretical capacity of 372 mAh g^{-1}. Therefore, the charge-discharge behaviors of graphite in PC:DMC mixed solutions depend on the PC contents, and electrolytes with low PC contents allow successful charge and discharge without the exfoliation of graphite. One possible factor in these behaviors is the solvation structure of lithium-ion, which is greatly influenced by the PC contents, as will be discussed later.

The behaviors of natural graphite in charge-discharge tests under various mixing ratios of PC and DMC containing 1 mol dm^{-3} $LiClO_4$ are summarized in Table 1.1. The use of pure PC and PC:DMC (1:1 – 1:3 by vol.) led to the exfoliation of graphite and the potential curves were almost the same as those in Fig. 1.1. On the other hand, the charge-discharge tests of natural

graphite were successful, as shown in Fig. 1.2, when electrolytes consisting of PC:DMC (1:7–1:9 by vol.) were used. In an electrolyte of an intermediate composition, PC:DMC (1:4–1:6 by vol.), the results showed poor reproducibility. One example is shown in Fig. 1.3. The electrode potential gradually decreased from ca. 0.8 V to 0 V and subsequent cycles failed. In another case, the 1st charge-discharge cycle was successful but the 2nd or 3rd cycle was unsuccessful. Thus, electrolytes composed of PC:DMC (1:4–1:6 by vol.) showed complicated results.

There is at least one possible hypothesis to explain the successful charge-discharge behaviors in electrolytes with low PC contents. The thermodynamic stability of solvated lithium-ion, $Li(solv)_x^+$, is different in various PC:DMC solutions because of the different solvation structures of lithium-ion. We consider that the stability of solvated lithium-ion should influence both the intercalation chemistry of solvated lithium-ion and the charge-discharge behavior of graphite in PC-containing electrolytes. To confirm this hypothesis, we investigated the solvation structures of lithium-ion in various PC:DMC solutions. Raman spectra of PC:DMC solutions were used to evaluate the solvation numbers of PC molecules per lithium-ion.

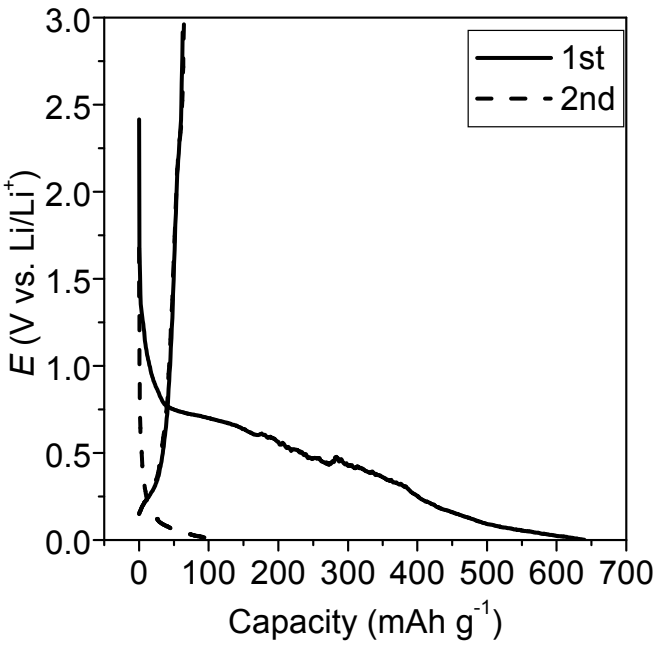

Fig. 1.3 Charge and discharge curves of natural graphite in 1 mol dm^{-3} $LiClO_4$ / PC:DMC (1:4 by vol.) after being cycled in 1 mol dm^{-3} $LiClO_4$ / EC:DMC (1:1 by vol.).

1.3.2. Solvation numbers of PC molecules per lithium-ion.

Figure 1.4 shows Raman spectra of 1 mol dm^{-3} $LiClO_4$ / PC:DMC (1:1, 1:4 and 1:7 by vol.) in the range of 675–745 cm^{-1}. The band at around 712 cm^{-1} is assigned to the symmetric ring deformation mode of PC molecules [23]. Deconvolution using a Lorentzian function shows that the band consists of two components at 712 cm^{-1} and 722 cm^{-1}. The bands at 712 cm^{-1} and 722 cm^{-1} are attributed to PC molecules free of Li^+ and solvating Li^+, respectively [23–26]. The same assignment was performed for the bands of EC molecules in $LiClO_4$ / EC [27] and LiTFSI / EC:DMC [28] solutions. Based on the intensity of the bands at 712 cm^{-1} (I_{free}, PC free of Li^+) and at 722 cm^{-1} (I_{solv}, PC solvating Li^+), the concentration ratio (c_{free}/c_{solv}) of PC free of Li^+ and solvating Li^+ can be calculated by using the following equation [27,29],

$$\frac{c_{free}}{c_{solv}} = \frac{I_{free}}{I_{solv}} \frac{\Gamma^*_{solv}}{\Gamma^*_{free}} \tag{1}$$

where Γ_{free}^* and Γ_{solv}^* denote the Raman intensities per unit concentration of PC free of Li^+ (I_{free} / c_{free}) and solvating Li^+ (I_{solv} / c_{solv}), respectively. To obtain c_{free}/c_{solv}, we need to know the value of $\Gamma_{solv}^*/\Gamma_{free}^*$ which can be evaluated from the slope of I_{free} *vs* I_{solv} plots (Fig. 1.5) for different salt concentrations (0.8–1.4 mol dm^{-3}) of pure PC solutions by using the following equation[27];

$$I_{solv} = -\frac{\Gamma^*_{solv}}{\Gamma^*_{free}} I_{free} + c_{PC,tot}\Gamma^*_{solv} \tag{2}$$

Here, we assume that the total concentration of PC ($c_{PC,tot} = c_{free} + c_{solv}$) is almost the same in the concentration range of 0.8–1.4 mol dm^{-3}. The total intensity (I_{v1}) of totally symmetric bands (v_1) [23] of ClO_4^- (933 cm^{-1} for free anions and 939 cm^{-1} for ion pairs [30]) was used as an internal standard and the obtained Raman intensity values of PC molecules, I_{free} and I_{solv}, were normalized by the Raman intensity per unit concentration (I_{v1} / c_{LiClO4}) for the v_1 mode. The I_{free} *vs* I_{solv} plots show a linear correlation and the value of $\Gamma_{solv}^*/\Gamma_{free}^*$ in this measurement system is evaluated to be 0.14 from the slope. This $\Gamma_{solv}^*/\Gamma_{free}^*$ value of PC is small compared to that of EC (1.09) [27]. In fact, the Raman band of EC solvating Li^+ is large enough to appear as an isolated peak [27,28]. In the case of PC, however, the Raman band of PC solvating Li^+ (722 cm^{-1}) is much smaller than that of PC free of Li^+ (712 cm^{-1}) and appears as a small shoulder in salt concentrations of around 1 mol dm^{-3}, as shown in the present study (Fig. 1.4) and in previous reports [23,26]. Hence, the $\Gamma_{solv}^*/\Gamma_{free}^*$ value of PC, 0.14, would be reasonable, although the

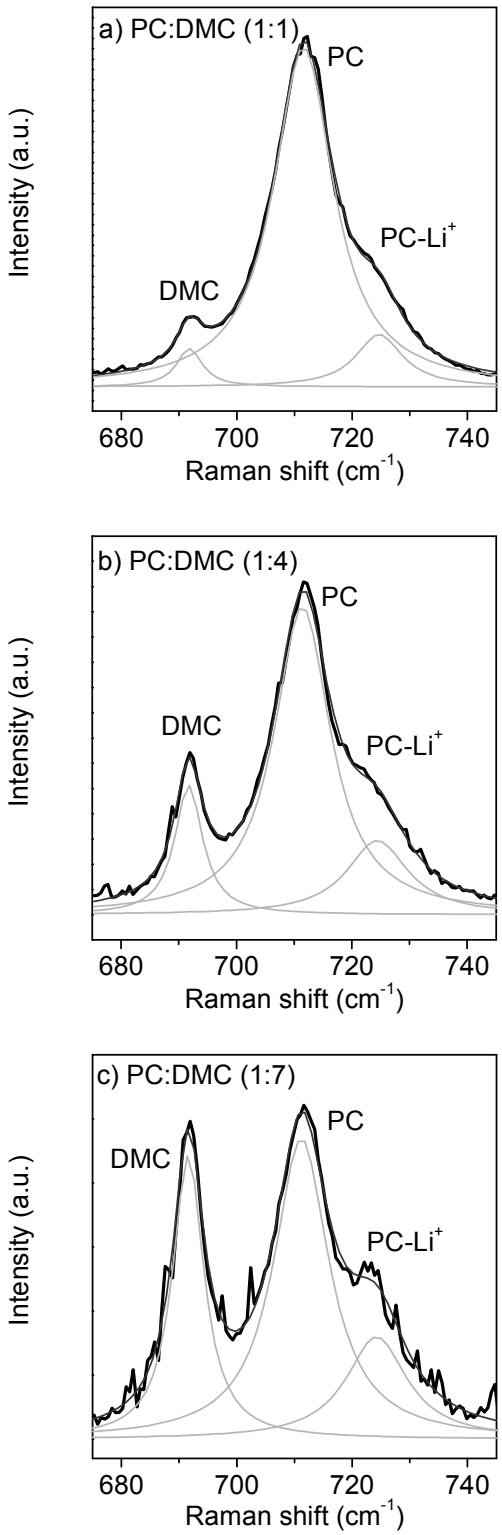

Fig. 1.4 Raman spectra of 1 mol dm^{-3} $LiClO_4$ dissolved in a) PC:DMC (1:1 by vol.), b) PC:DMC (1:4 by vol.) and c) PC:DMC (1:7 by vol.).

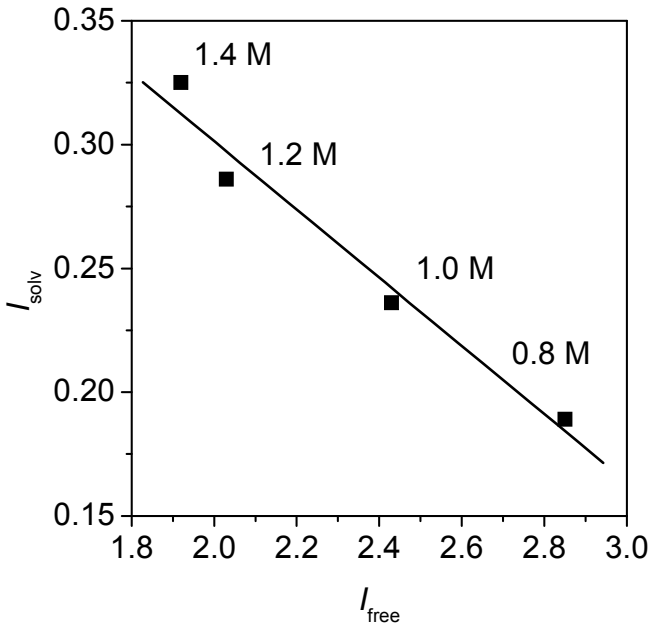

Fig. 1.5 Relation between intensities of PC free of Li^+ (I_{free}) and PC solvating Li^+ (I_{solv}) in 0.8–1.4 mol dm^{-3} $LiClO_4$ / pure PC solutions. I_{free} and I_{solv} were normalized by Raman intensity per unit concentration of the totally symmetric bands (v_1) of ClO_4^-.

reason for the small value is not clear. We can then obtain c_{free}/c_{solv} values for various mixing ratios of PC:DMC solutions from eq. 1. By using c_{free}/c_{solv} values, we evaluated the average solvation numbers ($N_{PC,ave}$) of PC molecules per lithium-ion from the following equation:

$$N_{PC,ave} = \frac{c_{solv}}{c_{Li,tot}} = \frac{c_{PC,tot}}{c_{Li,tot}\left(1 + c_{free}/c_{solv}\right)} \quad (3).$$

$c_{Li,tot}$ and $c_{PC,tot}$ denote the total concentrations of lithium-ion and PC in $LiClO_4$ / PC:DMC solutions, respectively. Note that $N_{PC,ave}$ is an average value. At lithium-ion concentrations around 1 mol dm^{-3}, lithium-ion exists in two forms: dissociated lithium-ions and solvent-shared ion pairs [23]. Based only on the Raman spectra, we could not distinguish between the solvation numbers of PC associated with these two forms of lithium-ions. Therefore, $N_{PC,ave}$ values are an average of these two solvation numbers. To obtain these two solvation numbers separately, we need to know the degree of dissociation (α) of $LiClO_4$. The value of α can be evaluated from Raman bands for the v_1 mode of ClO_4^- free of Li^+ and pairing with Li^+, but deconvolution of the bands is difficult and the resultant α values are not reliable. Therefore, we used the average values, $N_{PC,ave}$, although it would be desirable for a clear discussion to know the solvation numbers of both dissociated lithium-ions and solvent-shared ion pairs.

$N_{PC,ave}$ values in PC:DMC solutions of various mixing ratios containing 1 mol dm^{-3} $LiClO_4$ are shown in Table 1.1. The $N_{PC,ave}$ values vary from 3.7 in pure PC to 0.9 in PC:DMC (1:9 by vol.). In the literature, the total solvation numbers of lithium-ion in organic solutions of salt concentrations around 1 mol dm^{-3} were reported to be 4.1 – 4.3 in $LiClO_4$ / EC [27], 3.9 – 4.6 in $LiAsF_6$ / acetone [31], 2.8 – 3.7 in $LiCF_3SO_3$ / EC:DMC [28], 3.9 – 4.4 in $LiPF_6$ / EC:DMC [28] and 3.6 – 4.4 in $LiClO_4$ / PC [26]. Therefore, the $N_{PC,ave}$ value of 3.7 in pure PC in the present study is quite reasonable and the results of the Raman measurement would be accurate and reliable. If we assume that the total solvation number is 3.7, the $N_{PC,ave}$ value of 0.9 in PC:DMC (1:9 by vol.) means that, on average, 0.9 molecules of PC and 2.8 molecules of DMC solvate one lithium-ion.

Table 1.1. Average solvation numbers ($N_{PC,ave}$) of PC per lithium-ion and charge-discharge behaviors of graphite in PC:DMC solutions.

PC:DMC	**Charge-discharge**	$N_{PC,ave}$
Pure PC	Failure	3.7
1:1	Failure	2.7
1:2	Failure	2.1
1:3	Failure	1.9
1:4	Intermediate	1.5
1:5	Intermediate	1.4
1:6	Intermediate	1.2
1:7	Success	1.1
1:8	Success	0.9
1:9	Success	0.9

1.4. Discussion

The relation between $N_{PC,ave}$ and PC volume% in PC:DMC solutions is shown in Fig. 1.6. Naturally, $N_{PC,ave}$ decreases with decreasing PC volume% in PC:DMC solutions. As reported previously [21], PC molecules preferentially solvate lithium-ion because PC molecules have a higher solvation ability than DMC molecules. Therefore, $N_{PC,ave}$ shows a small change (from 2.7 to 3.7) in electrolytes with high PC contents (> 50 vol%) and lithium-ion is mainly solvated by PC molecules. On the other hand, $N_{PC,ave}$ changes drastically in electrolytes with low PC contents (<50 vol%). The charge-discharge results in various PC:DMC solutions containing 1 mol dm^{-3} $LiClO_4$ are also shown in Fig. 1.6. When $N_{PC,ave}$ was larger than 1.9, the charge-discharge tests for natural graphite failed, as shown in Fig. 1.1, and the exfoliation of graphite was observed. On the other hand, natural graphite in electrolytes with $N_{PC,ave} < 1.1$ showed successful charge and discharge (Fig. 1.2). These results indicate that a lithium-ion solvated by more than two PC molecules causes the exfoliation of graphite and the decomposition of PC when it intercalates into graphite, while a lithium-ion solvated by one or no PC molecules can intercalate into graphite without damaging graphite. In the case of electrolytes with $1.2 < N_{PC,ave}$

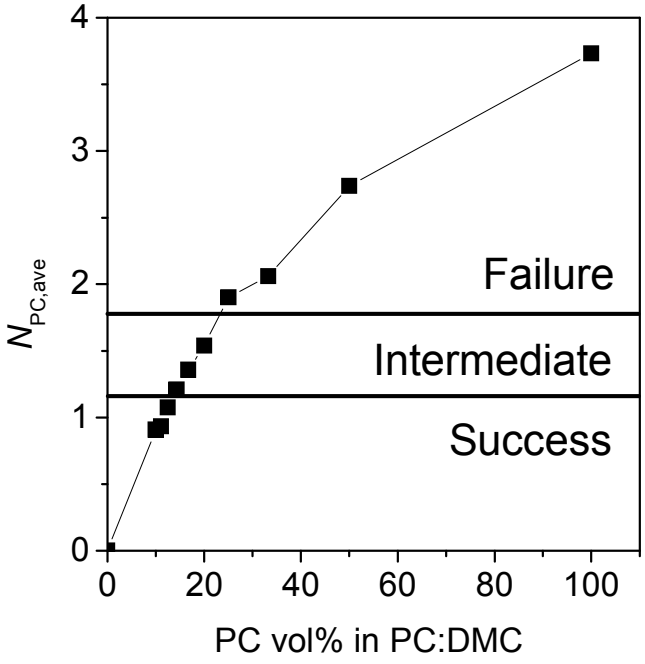

Fig. 1.6 Relation between PC volume% in PC:DMC solutions and average solvation numbers ($N_{PC,ave}$) of PC per lithium-ion. The charge-discharge results for natural graphite in PC:DMC solutions are also shown.

< 1.5, complicated results were obtained, as noted previously. These $N_{PC,ave}$ values are averages and an electrolyte composed of PC:DMC (1:4 by vol.) ($N_{PC,ave}$ = 1.5), for example, contains both lithium-ion solvated by more than two PC molecules and that solvated by one or no PC molecules. Therefore, the charge-discharge curves would show intermediate behavior between success and failure, although the detailed mechanism is not clear.

In the present study, an EC-derived SEI was formed on graphite before charge-discharge tests in PC:DMC solutions. We also conducted charge-discharge tests for natural graphite in PC:DMC (1:7 by vol.) solution without an EC-derived SEI, but the tests failed resulting in the exfoliation of graphite. Hence, the existence of a highly stable SEI (i.e., EC-derived one) is the first prerequisite for successful charge and discharge in this system, and PC:DMC-derived SEI is not stable. Even in the presence of an EC-derived SEI, however, the charge-discharge behaviors of natural graphite depended on the mixing ratios of PC:DMC solutions. So, why does a lithium-ion solvated by 1.9 or more PC molecules cause the decomposition of PC and the exfoliation of graphite, while a lithium-ion solvated by 1.1 or less PC molecules can successfully intercalate into graphite?

The hypothesis presented here is that the thermodynamical stabilities of solvated lithium-ion influence the intercalation chemistry of solvated lithium-ion and the charge-discharge behaviors of graphite in PC-containing electrolytes. The stability of solvated lithium-ion is determined by the solvation abilities of solvents. To know the solvation abilities of PC and DMC, the enthalpy change (ΔH) in the following reaction was calculated with the density functional theory using Gaussian98W [20]:

$Li^+ + solvent = Li(solvent)^+$ ΔH.

The calculated ΔH values are –217.1 kJ mol^{-1} for PC and –185.8 kJ mol^{-1} for DMC. Therefore, the solvation ability of PC is higher than that of DMC. The same tendency was reported in a previous paper [21]. Based on these results, lithium-ion solvated by PC molecules is thermodynamically more stable than that solvated by DMC molecules. In electrolytes of PC:DMC (1:7–1:9 by vol.), solvated lithium-ion is relatively unstable because of the small $N_{PC,ave}$ values. Hence, the intercalation of PC-solvated lithium-ion is unlikely to occur because it promptly decomposes at the surface before it intercalates deep into graphite. The decomposition of solvated lithium-ion can be confirmed from the potential plateau at around 0.4 V in the 1st charge of graphite in PC:DMC (1:7 by vol.) (Fig. 1.2). On the other hand, solvated lithium-ion is relatively stable in electrolytes with large $N_{PC,ave}$ (PC:DMC (1:1 – 1:3 by vol.)) and thus, it

intercalates deep into graphite at around 1 V. This intercalation of PC-solvated lithium-ion would cause the exfoliation of graphite.

This relation between the stability of solvated lithium-ion and the electrochemical properties of graphite can also be applied to other electrolyte systems. In EC-based electrolytes, a charge-discharge test of graphite is successful without the exfoliation of graphite. EC molecules have a slightly lower solvation ability (ΔH = –210.3 kJ mol^{-1}) than PC molecules and thus the EC-solvated lithium-ion promptly decomposes after it intercalates into graphite. These phenomena were previously observed by *in situ* STM [1,10] and AFM [15,19] methods. The intercalation of solvated lithium-ion was clearly observed in electrolytes composed of dimethylsulfoxide (DMSO, ΔH = –235.2 kJ mol^{-1}) or dimethoxyethane (DME, ΔH = –254.0 kJ mol^{-1}), which have high solvation abilities [14]. These results are compatible with the present hypothesis. However, no exfoliation of graphite is observed in electrolyte composed of DMSO or DME. Therefore, the stability of solvated lithium-ion is not the only reason for the difference in the charge-discharge behaviors of graphite in PC:DMC solutions.

Another potential cause of the different charge-discharge behaviors is the stability of Li-(solvent)$_x$-GIC, i.e., the stress of graphene layers induced by the intercalation of solvated lithium-ion [32]. One of the factors in the stress of graphite layers is the size of solvated lithium-ion. A DMC molecule is linear and small, while a PC molecule is large and rigid because of the ring. Hence, a lithium-ion solvated mainly by PC molecules (large $N_{PC,ave}$) has a larger solvation structure than that solvated mainly by DMC molecules (small $N_{PC,ave}$). Therefore, when electrolytes with large $N_{PC,ave}$ (PC:DMC (1:1–1:3 by vol.)) are used, the intercalation of large solvated lithium-ion would induce stress in graphene layers, leading to the exfoliation of graphite. On the other hand, a solvated lithium-ion is small in electrolytes with small $N_{PC,ave}$ (PC:DMC (1:7–1:9 by vol.)). Therefore, graphite would not be damaged even under intercalation of the solvated lithium-ion. This hypothesis can explain the intercalation of DMSO- or DME-solvated lithium-ion without the exfoliation of graphite, since both DMSO and DME molecules are smaller than PC.

The two hypotheses presented here can explain some previous results. Our group reported that salt-concentrated PC solutions (i.e., 2.72 mol dm^{-3} LiBETI / PC) enabled the successful charge and discharge of natural graphite [33]. In this solution (2.72 mol dm^{-3}), the $N_{PC,ave}$ value should be below 2 because the molar ratio of lithium-ion and PC is 1:2. Therefore, intercalation of the solvated lithium-ion hardly occurs because the solvated lithium-ion is unstable and

decomposes before it intercalates deep into graphite. In another report [32], our group used an *in situ* STM method to clarify that the exfoliation of graphite is less vigorous in trifluoropropylene carbonate (TFPC) than in PC. The size of a TFPC molecule is almost the same as that of PC, but the solvation ability of TFPC is much lower than that of PC [34] due to the electron-withdrawing fluorine group. The instability of TFPC-solvated lithium-ion prevents it from intercalating deep into graphite, leading to the small extent of exfoliation. Furthermore, our group reported that the intercalation of lithium-ion occurs successfully in $LiClO_4$ / PC solutions containing DMSO [14]. Lithium-ion is preferentially solvated by DMSO molecules in these solutions because the solvation ability of DMSO is much higher than that of PC. Therefore, the solvated lithium-ion is relatively small and stable, resulting in intercalation of the solvated lithium-ion without the exfoliation of graphite. The DMSO-solvated lithium-ion then decomposes between graphene layers to form a stable SEI.

These results support the validity of the hypothesis that the thermodynamical stabilities of both the solvated lithium-ion and Li-(solvent)$_x$-GIC influence the intercalation chemistry of solvated lithium-ion. Therefore, the charge-discharge behavior of graphite in PC-containing electrolytes greatly depends on the solvation structure of lithium-ion. The present results may be useful for optimizing the electrolyte compositions for the successful charge and discharge of a graphite electrode.

1.5. Conclusions

The mixing ratios of PC:DMC solutions determine the Li^+-intercalation behavior of natural graphite in the presence of an EC-derived SEI. Raman spectra show that the solvation numbers ($N_{PC,ave}$) of PC molecules per lithium-ion vary in different PC:DMC solutions. The following associations were found between the charge-discharge behavior of natural graphite and $N_{PC,ave}$ in $LiClO_4$ / PC:DMC solutions:

1. Electrolytes with high $N_{PC,ave}$ (> 1.9) cause the exfoliation of graphite and the decomposition of solvents.
2. Electrolytes with low $N_{PC,ave}$ (< 1.1) lead to the reversible intercalation / de-intercalation of lithium-ion into/from graphite without exfoliation.

These results indicate that charge-discharge behaviors of natural graphite depend on $N_{PC,ave}$ values. One possible hypothesis is that the thermodynamical stabilities of both solvated lithium-ion and Li-(solvent)$_x$-GIC influence the intercalation chemistry of solvated lithium-ion.

Therefore, the charge-discharge behavior of graphite in PC-containing electrolytes greatly depends on the solvation structure of lithium-ion.

References

[1] Ogumi, Z.; Inaba, M. *Bull. Chem. Soc. Jpn.* **1998**, *71*, 521.

[2] Peled, E. *J. Electrochem. Soc.* **1979**, *126*, 2047.

[3] Aurbach, D.; Levi, M. D.; Levi, E.; Schechter, A.; Granot, E. *J. Power Sources* **1997**, *68*, 91.

[4] Aurbach, D.; Markovsky, B.; Weissman, I.; Levi, E.; Ein-Eli, Y. *Electrochim. Acta* **1999**, *45*, 67.

[5] Aurbach, D. *J. Power Sources* **2000**, *89*, 206.

[6] Yazami, R. *Electrochim. Acta* **1999**, *45*, 87.

[7] Dey, A. N.; Sullivan, B. P. *J. Electrochem. Soc.* **1970**, *117*, 222.

[8] Arakawa, M.; Yamaki, J. I. *J. Electroanal. Chem.* **1987**, *219*, 273.

[9] Dudley, J. T.; Wilkinson, D. P.; Thomas, G.; LeVae, R.; Woo, S.; Blom, H.; Horvath, C.; Juzkow, M. W.; Denis, B.; Juric, P.; Aghakian, P.; Dahn, J. R. *J. Power Sources* **1991**, *35*, 59.

[10] Inaba, M.; Siroma, Z.; Kawatate, Y.; Funabiki, A.; Z. Ogumi, Z. *J. Power Sources* **1997**, *68*, 221.

[11] Naji, A.; Ghanbaja, J.; Willmann, P.; Billaud, D. *Carbon* **1997**, *35*, 845.

[12] Chung, G. C.; Kim, H. J.; Yu, S.I.; Jun, S. H.; Choi, J. W.; Kim, M. H. *J. Electrochem. Soc.* **2000**, *147*, 4391.

[13] Aurbach, D.; Zinigrad, E.; Cohen, Y.; Teller, H. *Solid State Ionics* **2002**, *148*, 405.

[14] Abe, T.; Kawabata, N.; Mizutani, Y.; Inaba, M.; Ogumi, Z. *J. Electrochem. Soc.* **2003**, *150*, A257.

[15] Jeong, S. K.; Inaba, M.; Iriyama, Y.; Abe, T.; Ogumi, Z. *J. Power Sources* **2003**, *119–121*, 555.

[16] Wagner, M. R.; Albering, J. H.; Moeller, K. C.; Besenhard, J. O.; Winter, M. *Electrochem. Commun.* **2005**, *7*, 947.

[17] Gnanaraj, J. S.; Thompson, R. W.; DiCarlo, J. F.; Abraham, K. M. *J. Electrochem. Soc.* **2007**, *154*, A185.

[18] Hardwick, L. J.; Buqa, H.; Holzapfel, M.; Scheifele, W.; Krumeich, F.; Novak, P. *Electrochim. Acta* **2007**, *52*, 4884.

[19] Jeong, S. K.; Inaba, M.; Iriyama, Y.; Abe, T.; Ogumi, Z. *J. Power Sources* **2008**, *175*, 540.

[20] Frisch, M. J.; Trucks, G. W.; Schlegel, H. B.; Scuseria, G. E.; Robb, M. A.; Cheeseman, J. R.; Zakrzewski, V. G.; Montgomery, J. A., Jr.; Stratmann, R. E.; Burant, J. C.; Dapprich, S.; Millam, J. M.; Daniels, A. D.; Kudin, K. N.; Strain, O. F. M. C.; Tomasi, J.; Barone, B.; Cossi, M.; Cammi, R.; Mennucci, B.; Pomelli, C.; Adamo, C.; Clifford, S.; Ochterski, J.; Petersson, G. A.; Ayala, P. Y.; Cui, Q.; Morokuma, K.; Malick, D. K.; Rabuck, A. D.; Raghavachari, K.; Foresman, J. B.; Ciolovski, J.; Ortiz, J. V.; Stefanov, V. V.; Liu, G.; Liashensko, A.; Piskorz, P.; Komaroni, I.; Gomperts, R.; Martin, R. L.; Fox, D. J.; Keith, T.; Al-Laham, M. A.; Peng, C. Y.; Nanayakkara, A.; Gonzalez, C.; Challacombe, M.; Gill, P. M. W.; Johnson, B.; Chen, W.; Wong, M. W.; Andres, J. L.; Head-Gordon, M.; Replogle, E. S.; Pople, J. A. *Gaussian 98*; Gaussian Inc.: Pittsburgh, PA, 1998.

[21] Arai, J.; Nishimura, K.; Muranaka, Y.; Ito, Y. *J. Power Sources* **1997**, *68***,** 304.

[22] Chung, G. C.; Jun, S. H.; Lee, K. Y.; Kim, M. H. *J. Electrochem. Soc.* **1999**, *146*, 1664.

[23] Battisti, D.; Nazri, G. A.; Klassen, B.; Aroca, R. *J. Phys. Chem.* **1993**, *97*, 5826.

[24] Kondo, K.; Sano, M.; Hiwara, A.; Omi, T.; Fujita, M.; Kuwae, A.; Iida, M.; Mogi, K.; Yokoyama, H. *J. Phys. Chem. B* **2000**, *104*, 5040.

[25] Tsunekawa, H.; Narumi, A.; Sano, M.; Hiwara, A.; Fujita, M.; Yokoyama, H. *J. Phys. Chem. B* **2003**, *107*, 10962.

[26] Xuan, X.; Wang, J.; Tang, J.; Qu, G.; Lu, J. *Phys. Chem. Liq.* **2001**, *39*, 327.

[27] Hyodo, S.; Okabayashi, K. *Electrochim. Acta* **1989**, *34*, 1551.

[28] Morita, M.; Asai, Y.; Yoshimoto, N.; Ishikawa, M. *J. Chem. Soc., Faraday Trans.* **1998**, *94*, 3451.

[29] Hyodo, S.; Okabayashi, K. *Electrochim. Acta* **1989**, *34*, 1557.

[30] Frost, R. L.; James, D. W.; Appleby, R.; Mayes, R. E. *J. Phys. Chem.* **1982**, *86*, 3840.

[31] Deng, Z.; Irish, D. E. *J. Chem. Soc., Faraday Trans.* **1992**, *88*, 2891.

[32] Inaba, M.; Kawatate, Y.; Funabiki, A.; Jeong, S. K.; Abe, T.; Ogumi, Z. *Electrochim. Acta* **1999**, *45*, 99.

[33] Jeong, S. K.; Inaba, M.; Iriyama, Y.; Abe, T.; Ogumi, Z. *Electrochem. Solid-State Lett*. **2003**, *6*, A13.

[34] Arai, J.; Katayama, H.; Akahoshi, H. *J. Electrochem. Soc.* **2002**, *149*, A217.

Chapter 2

Electrochemical Lithium Intercalation into Graphite in Dimethyl-Sulfoxide-Based Electrolytes: Effect of Solvation Structure of Lithium-Ion

2.1. Introduction

Electrochemical intercalation of lithium-ion into graphite is an essential reaction of the negative electrode in lithium-ion batteries. The resultant lithium-graphite intercalation compound (Li-GIC) exhibits an extremely low potential (~ 0 V vs. Li/Li^+), which endows lithium-ion batteries with prominently high energy density compared to other secondary batteries. The high energy density has pushed lithium-ion batteries up to the strong position as power sources for portable electronic devices and next-generation electric vehicles. Despite the growing importance of lithium-ion batteries, fundamental study on the graphite negative electrode is inadequate, and our knowledge has not reached a complete understanding of the reaction mechanism.

One of the questions about the reaction mechanism is the compatibility of a graphite electrode and electrolyte solvents. Ethylene carbonate (EC)-based electrolytes allow for reversible intercalation and deintercalation of lithium-ion at a graphite electrode, whereas in dimethyl sulfoxide (DMSO) or 1,2-dimethoxy ethane (DME), for example, solvated lithium-ion intercalates into graphite, which is referred to as cointercalation of solvents [1–4]. In addition, propylene carbonate (PC) causes the exfoliation of graphite layers, which is related with the cointercalation of solvents in a generally-accepted notion [5–8]. Due to such phenomena, lithium-ion batteries have no options of electrolyte solvents but EC. However, EC-based electrolytes have a disadvantage in lithium-ion conductivity at low temperature, driving researchers to seek alternative solvents. To open up the options of electrolyte solvents, we need to present a clear guideline for the suppression of the cointercalation of solvents.

The cointercalation of solvents was reported in the syntheses of various alkali-metal-GIC's by chemical and electrochemical methods [9–14]. In the case of the chemical synthesis, it is generally accepted that one of the determining factors for the cointercalation of solvents is the

strength of solvation toward cation; the stronger the solvation is, the more favorable the cointercalation of solvents is [13,14]. These results in a chemical synthesis of GIC's led us to conceive of a new approach for the suppression of the cointercalation of solvents during electrochemical intercalation of lithium-ion into graphite: a deliberate change in the solvation structure of lithium-ion in a solution. Our recent studies have clarified that the exfoliation of graphite can be avoided by changing the solvation structure of lithium-ion in PC-based electrolytes [15,16]. These results imply a relationship between the cointercalation of solvents and the solvation structure of lithium-ion in a solution.

This work sheds light on the influence of solvation structure of lithium-ion on the cointercalation of solvents into graphite. We used DMSO as an electrolyte solvent which tends to cointercalate with lithium-ion into graphite. The solvation structure of lithium-ion was changed with two kinds of solution: 1) lithium-salt-concentrated solutions and 2) binary solutions with dimethyl carbonate (DMC). The solvation number of DMSO toward lithium-ion in these solutions was evaluated by Raman spectroscopy of the solution. A charge-discharge test of graphite was conducted in these DMSO-based solutions, and the relationship between the behaviors of graphite and the solvation number of DMSO toward lithium-ion was discussed.

2.2. Experimental Methods

Natural graphite powder (NG-7, Kansai Coke and Chemicals Co., Ltd.) was used as an active material. A composite electrode was prepared by coating slurry containing NG-7 on a copper foil. The slurry composed of NG-7 and polyvinylidene difluoride (PVdF) in *N*-methylpyrrolidone (NMP). The weight ratio of NG-7 and PVdF was 9:1. Electrolyte components were lithium bis(trifluoro methanesulfonyl)imide ($LiN(SO_2CF_3)_2$, LiTFSI), lithium perchlorate ($LiClO_4$), DMSO, EC, and/or DMC. The electrolyte components were purchased from Kishida Chemical Co., Ltd. They were all lithium-battery grade chemicals and the water contents in the electrolyte solutions were guaranteed to be less than 20 ppm.

Charge-discharge tests were conducted with a three-electrode cell. Lithium foil was used as both counter and reference electrodes. The potential in the present paper were referenced to Li/Li^+. The constant current was set at 37.2 mA g^{-1}, which corresponds to the rate of C/10. Electrolyte solutions consisting of 3.2 mol dm^{-3} LiTFSI/DMSO and 1.0 mol dm^{-3} LiTFSI/DMSO:DMC (1:x by vol., x = 0, 1.3, 4.8, 10.7) were used for the charge-discharge tests of natural graphite. In the binary solutions of DMSO and DMC, the nature of a surface film (i.e.,

solid electrolyte interphase, SEI [17]) on graphite is expected to vary significantly, because the SEI composition depends on the solution used. Therefore, pre-cycling tests were conducted in 1.0 mol dm^{-3} $LiClO_4$/EC:DMC (1:1 by vol.) and an EC-based SEI was formed on graphite. After the pre-cycling, the EC-based electrolyte was replaced by a given DMSO:DMC solution, in which the charge-discharge test was carried out. All of the electrochemical measurements were conducted in an argon-filled drybox in which the temperature was kept at 30 ^{o}C.

Raman spectra were recorded with a triple monochromator (Jobin-Yvon, T-64000) with a 514.5 nm line (50 mW) from an argon ion laser (NEC, GLG3260). A quartz cell was used for the Raman spectroscopy of solutions.

The enthalpy change in a complexation reaction of lithium-ion and a solvent molecule was calculated with the density functional theory by using Gaussian98W [18]. A molecular structure was fully optimized at the B3LYP/6-31G (d) level and its thermal energy was calculated at 298.15 K. Single-point energy was calculated at the B3LYP/6-311 + G (3df, 3pd) level by using the optimized geometry. The reaction enthalpy was evaluated from the changes in single-point energy and thermal energy at 298.15 K.

2.3. Results and Discussion

2.3.1. Electrochemical Behavior of Natural Graphite in Lithium-Salt-Concentrated DMSO Solutions.

One way to change the solvation structure of lithium-ion in a solution is the addition of excess amount of lithium salt to the solution. In a salt-concentrated solution, the solvation number toward lithium-ion is expected to be smaller than that in a solution with normal concentration (e.g., 1 mol dm^{-3} solution). This section describes the electrochemical behavior of graphite in LiTFSI/DMSO solutions with different salt concentrations.

Figure 2.1 shows potential curves of natural graphite in 1.0, 2.0, and 3.2 mol dm^{-3} LiTFSI/DMSO solutions. In 1.0 mol dm^{-3} LiTFSI/DMSO solution, the electrode potential gradually decreased from 1.5 V to 1.1 V, followed by a potential plateau at 1.1 V. In our previous study, such capacity at the potential over 1 V was attributed to the intercalation of DMSO-solvated lithium-ion (i.e., the cointercalation of DMSO) into graphite [2,3]. Therefore, the product at the potential over 1 V was a ternary GIC, that is, Li-$(DMSO)_x$-GIC. The intercalation of DMSO-solvated lithium-ion increases the interlayer spacing of graphite from 0.335 nm to 1.16 nm [2]. Therefore, the resultant Li-$(DMSO)_x$-GIC is unstable to cause the

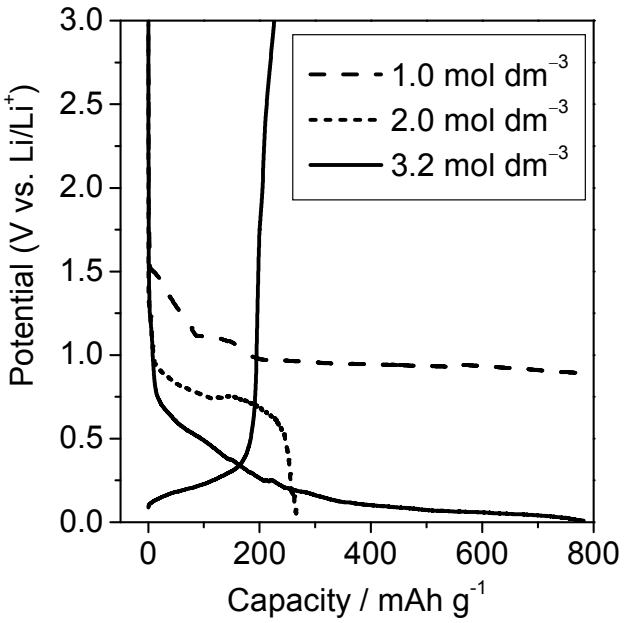

Fig. 2.1 Potential curves of natural graphite (NG-7) in LiTFSI/DMSO solutions with different salt concentrations: 1.0, 2.0, and 3.2 mol dm^{-3}.

deterioration of graphite layers. A potential plateau at 0.9–0.8 V should be attributed to continuous decomposition of DMSO accompanied by the deterioration of graphite layers. Eventually, the electrode potential dropped to 0 V after prolonged charge, and the following discharge capacity was almost nothing.

A natural graphite electrode showed a different behavior in 2.0 mol dm^{-3} LiTFSI/DMSO solution. No capacity was observed over 1 V, indicating that the cointercalation of DMSO did not occur. However, a potential plateau appeared at 0.8–0.7 V, followed by a sharp plunge to 0 V, and the discharge capacity was not obtained. Therefore, severe decomposition of DMSO occurred, which hindered the intercalation of lithium-ion into graphite.

The behavior of a natural graphite electrode in 3.0 mol dm^{-3} LiTFSI/DMSO was completely different from those in the former two solutions. A plateau was observed at 0.2–0 V during charge, which was attributed to the intercalation of lithium-ion into graphite [19]. The following discharge capacity was around 200 mAh g^{-1}. Therefore, although the irreversible capacity was large, both intercalation and deintercalation of lithium-ion were possible in this electrolyte. With the large irreversible capacity considered, the decomposition of the solution did occur. However, no capacity was observed at around 0.7 V during charge, indicating that the decomposition of DMSO was less severe than that in 2.0 mol dm^{-3} LiTFSI/DMSO solution. It is also important

that there was no capacity over 1 V, suggesting that this electrolyte suppressed the cointercalation of DMSO into graphite. Such a behavior was also observed in salt-concentrated PC solutions.[8,15] As a result, it is obvious that the behavior of graphite depends on the salt concentration of LiTFSI/DMSO solutions.

2.3.2. Electrochemical Behavior of Natural Graphite in DMSO:DMC Binary Solutions.

Another way to change the solvation structure of lithium-ion is to use DMSO:DMC binary solutions. In such solutions, the solvation number of DMSO molecules toward lithium-ion is expected to be small, because some DMC molecules should solvate lithium-ion. In this section, we discuss the behavior of graphite in DMSO:DMC binary solutions with different mixing ratios.

Figure 2.2 shows potential curves of natural graphite in 1.0 mol dm^{-3} LiTFSI/DMSO:DMC (1:*x* by vol., *x* = 0, 1.3, and 4.8) after being pre-cycled in 1.0 mol dm^{-3} $LiClO_4$/EC:DMC (1:1 by vol.). In 1.0 mol dm^{-3} LiTFSI/DMSO solution, potential plateaus were observed over 1 V, which were attributed to the cointercalation of DMSO [2,3]. Therefore, the cointercalation of DMSO into graphite did occur even after the pre-cycling in the EC-based solution. A potential plateau below 1 V should be attributed to continuous decomposition of DMSO accompanied by

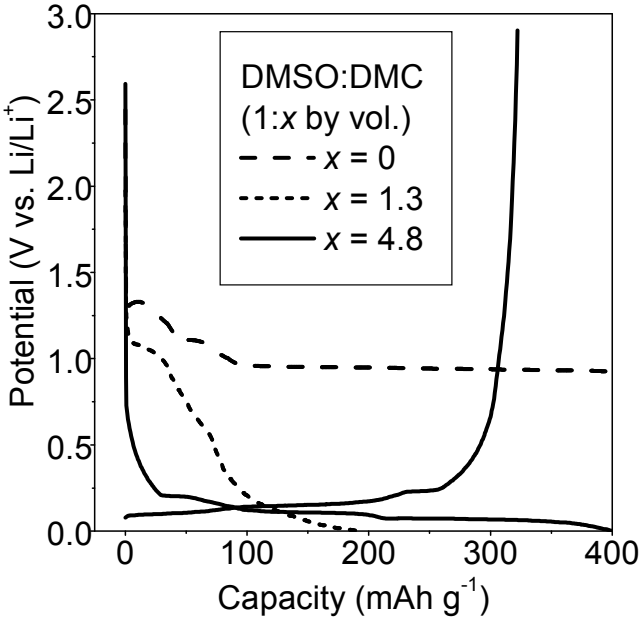

Fig. 2.2 Potential curves of natural graphite (NG-7) in 1.0 mol dm^{-3} LiTFSI/DMSO:DMC (1:*x* by vol., *x* = 0, 1.3, and 4.8) after being pre-cycled in 1.0 mol dm^{-3} $LiClO_4$/EC:DMC (1:1 by vol.).

the deterioration of graphite layers, as is discussed in the previous section.

A behavior of a natural graphite electrode in 1.0 mol dm^{-3} LiTFSI/DMSO:DMC (1:1.3 by vol.) showed poor reproducibility. In one case, severe decomposition of the solution was observed, and in another case, the intercalation and deintercalation of lithium-ion occurred. One result of the most frequent occurrence is shown in Fig. 2.2. The potential curve exhibited a gradual decrease from 1.1 V to 0 V during charge. Therefore, the cointercalation of DMSO and its decomposition did occur, but were less severe than those in 1.0 mol dm^{-3} LiTFSI/DMSO solution. However, the discharge capacity was almost nothing, indicating that the intercalation and deintercalation of lithium-ion did not occur.

In 1.0 mol dm^{-3} LiTFSI / DMSO:DMC (1:4.8 by vol), a natural graphite electrode showed a completely different behavior (Fig. 2.2). A potential curve showed no capacity over 0.5 V and thus, the cointercalation of DMSO and its decomposition were suppressed in this electrolyte. In addition, there were potential plateaus below 0.25 V during charge and discharge, indicating that the intercalation and deintercalation of lithium-ion occurred at graphite [19]. The discharge capacity was more than 300 mAh g^{-1}, which is close to the theoretical capacity of graphite (372 mAh g^{-1}). The same behavior of graphite was observed in 1.0 mol dm^{-3} LiTFSI / DMSO:DMC (1:10.7 by vol). These results suggest that the intercalation behavior of lithium-ion into graphite depends on the DMSO content in electrolytes, and that an electrolyte with low DMSO content allows for the intercalation and deintercalation of lithium-ion without the cointercalation and decomposition of DMSO.

It should be noted that an EC-derived SEI was formed on the surface of graphite in advance to the cycling in DMSO:DMC solutions. Therefore, we have to discuss the effect of the EC-derived SEI on the behavior of a graphite electrode. The intent of this treatment was to conduct the charge-discharge tests under the same condition of the SEI. However, the nature of the SEI film might be different in various electrolyte solutions. The irreversible capacity was relatively large in LiTFSI/DMSO:DMC (1:4.8 by vol.) (Fig. 2.2), indicating that a small amount of solvent decomposition occurred in the solution. This behavior means that the EC-derived SEI was partially decomposed in the presence of strong base, DMSO, and some components in the SEI were re-created in the DMSO:DMC solution. Therefore, the composition of the SEI was not completely constant in various DMSO-based solutions despite our intent. However, an important point is that the cointercalation of DMSO was suppressed in DMSO:DMC (1:4.8 by

vol.) solution during the re-creation of the SEI. Therefore, although the composition of the SEI would also be important, there should be another factor which determines the behavior of a graphite electrode.

2.3.3. Solvation Structure of Lithium-Ion in DMSO-Based Solution.

It is worthwhile to investigate the solvation structure of lithium-ion in the DMSO-based solutions used in this work, because the solvation structure should vary significantly in the salt-concentrated solution and the DMSO:DMC binary solution. A Raman spectrum of a given solution provides us with information about the states of DMSO in the solution. In this section, we evaluated the solvation number of DMSO molecules toward lithium-ion in the salt-concentrated solution and the DMSO:DMC binary solution.

Figure 2.3 shows the Raman spectra of pure DMSO, 1.0, 2.0, and 3.2 mol dm^{-3} LiTFSI/DMSO

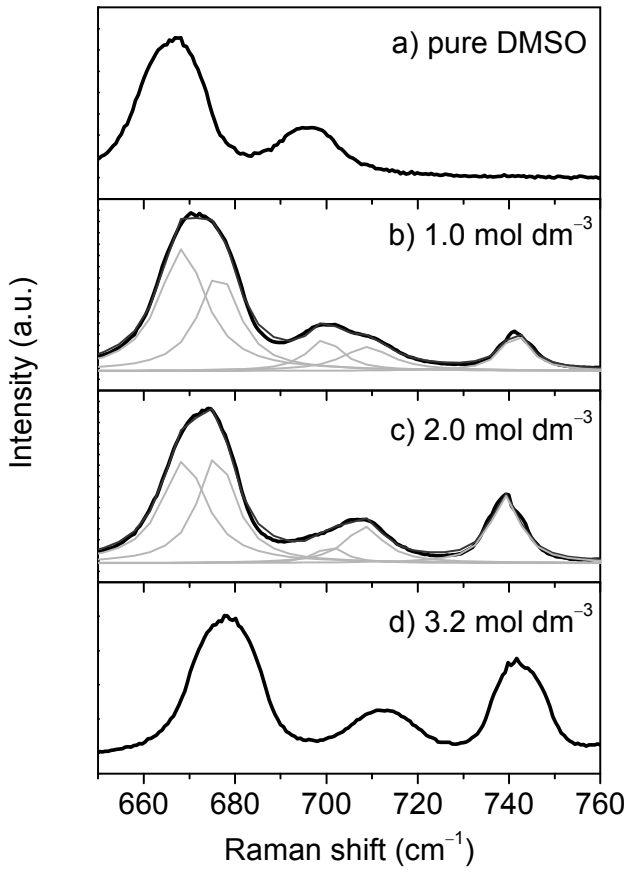

Fig. 2.3 Raman spectra of LiTFSI/DMSO solutions with different salt concentrations: a) pure DMSO, b) 1.0, c) 2.0, and d) 3.2 mol dm^{-3}.

in a range of 650–760 cm^{-1}. The Raman spectrum of pure DMSO (Fig. 2.3a) showed two bands at 667 and 697 cm^{-1}, which were assigned to the C–S symmetric and asymmetric stretching modes of DMSO molecules, respectively [20–22]. In the Raman spectra of 1.0 mol dm^{-3} and 2.0 mol dm^{-3} LiTFSI/DMSO (Figs. 2.3b and 2.3c), another band appeared at 742 cm^{-1}, which derived from several modes of $TFSI^-$ anion [23]. Furthermore, the deconvolution using a Lorentizian function indicated that each of the bands at 667 and 697 cm^{-1} composed of two bands. The newly-observed bands at 676 and 708 cm^{-1} were assigned to the C–S symmetric and asymmetric stretching modes of DMSO molecules that solvate lithium-ion [21,22]. Hence, there are two states of DMSO molecules in 1.0 mol dm^{-3} LiTFSI/DMSO solution: free and solvating DMSO. On the other hand, the Raman spectrum of 3.2 mol dm^{-3} LiTFSI/DMSO (Fig. 2.3d) was quite different from the former two spectra. There were no bands at 667 and 697 cm^{-1} which were attributed to free DMSO molecules. The absence of these bands indicates that all the DMSO molecules are in a solvating state in 3.2 mol dm^{-3} LiTFSI/DMSO. Such significant decrease in free solvents was reported in various salt-concentrated solutions of DMSO [21,22] and other solvents [15,23,24]. On the basis of Raman spectra, Kondo *et al.* implied the presence of some clustering structures in salt-concentrated PC solutions [23]. In the present study, the Raman bands from solvating DMSO molecules showed a small upward shift compared to those in other solutions. This upward shift of the Raman bands suggests a more complicated solvation state of DMSO molecules. In addition, the viscosity of the salt-concentrated solution was very high compared to the solution with lower salt concentration. These results support the formation of clustering structures, but the details are not clear.

Figure 2.4 shows the Raman spectra of 1.0 mol dm^{-3} LiTFSI/DMSO:DMC (1:x by vol., x = 0, 1.3, 4.8, 10.7) in a range of 650–760 cm^{-1}. There were five bands observed in this range of wave number, the attribution of which is shown in the previous paragraph. Although a DMC molecule does have a vibration mode in this range of wave number, the Raman scattering intensity of the mode is small enough to be neglected. In the Raman spectrum of 1.0 mol dm^{-3} LiTFSI/DMSO:DMC (1:1.3 by vol.) (Fig. 2.4b), there were four bands deriving from the C–S symmetric and asymmetric stretching modes of DMSO molecules: the bands at 667 and 697 cm^{-1} from free DMSO and the bands at 676 and 708 cm^{-1} from solvating DMSO. Therefore, both free and solvating DMSO molecules exist in 1.0 mol dm^{-3} LiTFSI/DMSO:DMC (1:1.3 by

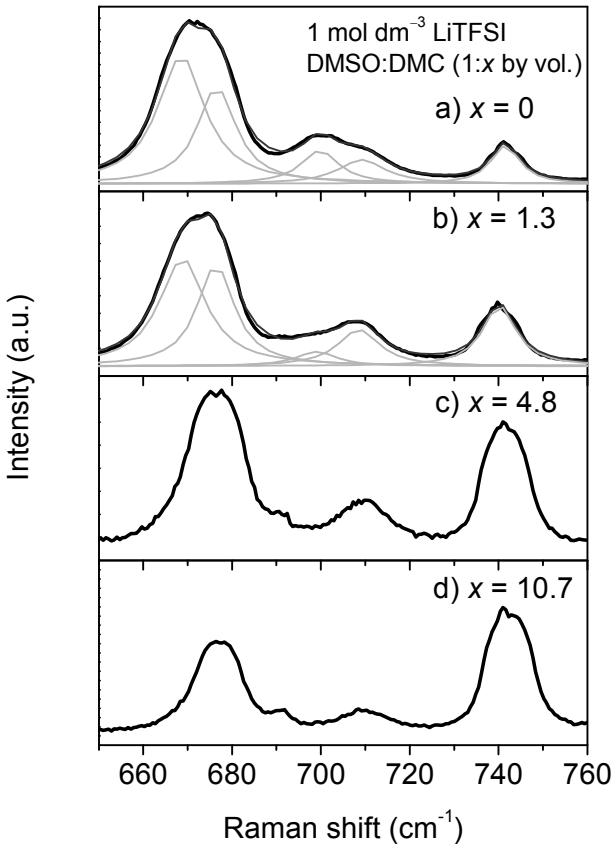

Fig. 2.4 Raman spectra of 1.0 mol dm^{-3} LiTFSI/DMSO:DMC (1:x by vol.): x = a) 0, b) 1.3, c) 4.8, and d) 10.7.

vol.). In contrast, the Raman spectra of 1.0 mol dm^{-3} LiTFSI/DMSO:DMC (1:4.8 and 1:10.7 by vol.) (Figs. 2.4c and 2.4d) did not show the bands from free DMSO molecules (667 and 697 cm^{-1}), indicating that almost all the DMSO molecules solvate lithium-ion in these solutions. Such a behavior is usually referred to as selective solvation. Lithium-ion is preferentially solvated by DMSO over DMC in DMSO:DMC binary solutions, because the interaction of DMSO and lithium-ion is much stronger than that of DMC and lithium-ion, as described in the next section.

The solvation number of DMSO molecules toward lithium-ion can be evaluated from the intensity ratio of the bands from free and solvating DMSO [26,27]. In the present paper, we used the bands at 697 and 708 cm^{-1} (i.e., the C-S asymmetric stretching mode of free and solvating DMSO, respectively) to evaluate the solvation number of DMSO. This is because these two bands are well-separated compared to those from the C–S symmetric stretching mode at 667 and

676 cm^{-1} [21]. The Raman intensity of the bands at 697 cm^{-1} (I_{free}) and 708 cm^{-1} (I_{solv}) is determined by the concentration of free DMSO molecules ($[DMSO]_{free}$) and solvating DMSO molecules ($[DMSO]_{solv}$),

$$I_{free} = \Gamma^*_{free}[DMSO]_{free} \quad (1)$$

$$I_{solv} = \Gamma^*_{solv}[DMSO]_{solv} \quad (2)$$

$$[DMSO] = [DMSO]_{free} + [DMSO]_{solv} \quad (3)$$

where [DMSO] denotes the total concentration of DMSO molecules, and Γ_{free}* and Γ_{solv}* denote the Raman scattering intensities per unit concentration of free and solvating DMSO molecules, respectively. From Eqs. 1 and 2, the following equation is given:

$$\frac{[DMSO]_{free}}{[DMSO]_{solv}} = \frac{I_{free}}{I_{solv}} \frac{\Gamma^*_{solv}}{\Gamma^*_{free}} \quad (4).$$

Consequently, as long as we know the Γ_{solv}*/Γ_{free}* value, the concentration ratio of free and solvating DMSO ($[DMSO]_{free}/[DMSO]_{solv}$) can be obtained from Eq. 4. The substitution of $[DMSO]_{free}$ and $[DMSO]_{solv}$ in Eq. 3 using Eqs. 1 and 2 derives the following equation:

$$\frac{I_{solv}}{[DMSO]} = -\frac{\Gamma^*_{solv}}{\Gamma^*_{free}} \frac{I_{free}}{[DMSO]} + \Gamma^*_{solv} \quad (5).$$

Therefore, the Γ_{solv}*/Γ_{free}* value can be evaluated from the slope of I_{solv}/[DMSO] vs. I_{free}/[DMSO] plot. Figure 2.5 shows the I_{solv}/[DMSO] vs. I_{free}/[DMSO] plot in LiTFSI/DMSO solutions with various salt concentrations. Here, the intensities, I_{solv} and I_{free}, were normalized by the intensity of the band at 3000 cm^{-1}, that is, C–H antisymmetric stretching mode of DMSO [22]. The I_{solv}/[DMSO] vs. I_{free}/[DMSO] plot was linear and its slope gave the Γ_{solv}*/Γ_{free}* value of 1.6 in the present experimental condition. The use of this value enables us to obtain the $[DMSO]_{free}/[DMSO]_{solv}$ value from Eq. 4. The solvation number of DMSO molecules toward lithium-ion (N_{DMSO}) is shown in the following equation,

$$N_{DMSO} = \frac{[DMSO]_{solv}}{[Li^+]} = \frac{[DMSO]}{[Li^+]\left(1 + [DMSO]_{free}/[DMSO]_{solv}\right)} \quad (6)$$

where $[Li^+]$ denotes the concentration of lithium salt in a given solution. Using Eq. 6, the N_{DMSO} value can be evaluated from the $[DMSO]_{free}/[DMSO]_{solv}$ value. In 3.2 mol dm^{-3} LiTFSI/DMSO and 1.0 mol dm^{-3} LiTFSI/DMSO:DMC (1:4.8 and 1:10.7 by vol.), almost all the DMSO

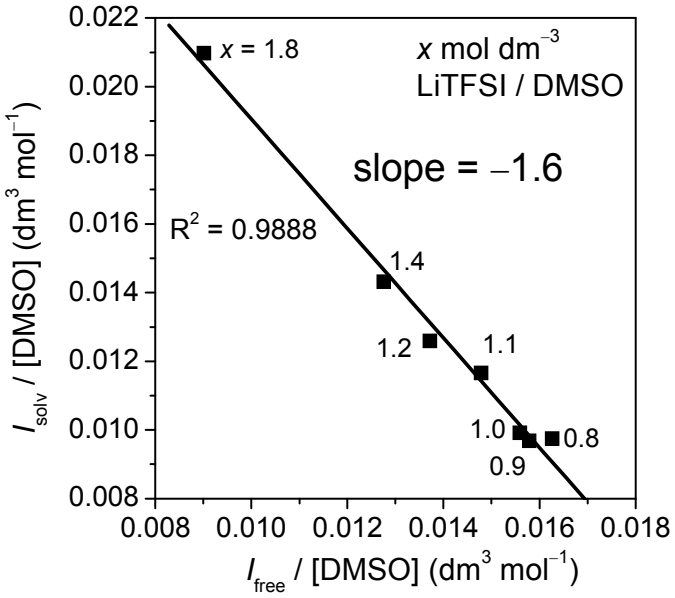

Fig. 2.5 I_{free}/[DMSO] vs. I_{solv}/[DMSO] plot of the C–S asymmetric stretching band of DMSO molecules in LiTFSI / DMSO with various salt-concentrations. The intensities, I_{free} and I_{solv}, were normalized by the intensity of the band at 3000 cm^{-1}.

molecules solvate lithium-ion, as shown in Figs. 3 and 4. Therefore, the N_{DMSO} value is obtained from the following equation:

$$N_{DMSO} = \frac{[DMSO]_{solv}}{[Li^+]} \approx \frac{[DMSO]}{[Li^+]} \quad (7).$$

The obtained N_{DMSO} values in various DMSO-based solutions are shown in Tables 2.1 and 2.2. In 1.0 mol dm^{-3} LiTFSI/DMSO, the N_{DMSO} value was evaluated to be 4.2, which was in good agreement with the previous reports by experiments [21,22] and theoretical calculations [28]. It is generally accepted that the solvation number of lithium-ion is around 4 in organic solutions [26,29,30]. Hence, the N_{DMSO} value of 4.2 is reasonable, suggesting that this experiment was accurate and reliable. It is clear from Tables 1 and 2 that the N_{DMSO} values drastically decreased in the salt-concentrated solution (e.g., 3.2 mol dm^{-3} LiTFSI/DMSO) and DMSO:DMC binary solution (e.g., 1.0 mol dm^{-3} LiTFSI/DMSO:DMC (1:4.8 by vol.)). The N_{DMSO} values in these solutions were approximately half of that in 1.0 mol dm^{-3} LiTFSI/DMSO.

Table 2.1: Relation between Electrochemical Behavior of Natural Graphite and Solvation Number of DMSO toward Lithium ion (N_{DMSO}) in LiTFSI/DMSO Solutions with Different Conentrations

$[Li^+]$ (mol dm^{-3})	[DMSO] (mol dm^{-3})	$[DMSO]_{solv}$ (mol dm^{-3})	N_{DMSO}	Behavior of graphite
1.0	11.5	4.2	4.2	cointercalation
2.0	10.2	6.6	3.3	intermediate
3.2	6.6	6.6	2.1	Li^+ intercalation

Table 2.2: Relation between Electrochemical Behavior of Natural Graphite and Solvation Number of DMSO toward Lithium-Ion (N_{DMSO}) in 1.0 mol dm^{-3} LiTFSI/DMSO:DMC (1:*x* by vol.) Solutions with Different Mixing Ratios

$[Li^+]$ (mol dm^{-3})	Mixing ratio by volume	[DMSO] (mol dm^{-3})	$[DMSO]_{solv}$ (mol dm^{-3})	N_{DMSO}	Behavior of graphite
1.0	DMSO	11.5	4.2	4.2	cointercalation
1.0	1:1.3	5.0	3.1	3.1	intermediate
1.0	1:4.8	2.0	2	2	Li^+ intercalation
1.0	1:10.7	1.0	1	1	Li^+ intercalation

2.3.4 Correlation between Electrochemical Behavior of Graphite and Solvation Structure of Lithium-Ion in DMSO-Based Electrolytes.

Tables 2.1 and 2.2 summarize a relation between electrochemical behaviors of natural graphite and N_{DMSO} values in DMSO-based solutions. In this paper, we deliberately changed the N_{DMSO} value by using two methods: 1) addition of excess amount of lithium salt and 2) addition of DMC to a DMSO solution. It is clear from Tables 1 and 2 that the N_{DMSO} value gradually decreased from 4.2 to 2 or 1 with an increase in the lithium salt or DMC. Interestingly, natural graphite in these two kinds of solution, salt-concentrated and DMC-added solutions, showed similar behaviors, as long as the N_{DMSO} value was the same. In 1.0 mol dm^{-3} LiTFSI/DMSO solution (N_{DMSO} = 4.2), the intercalation of DMSO-solvated lithium-ion (i.e., cointercalation of

DMSO) occurred instead of the intercalation of lithium-ion. When the N_{DMSO} value decreased to around 3 in 2.0 mol dm^{-3} LiTFSI/DMSO and 1.0 mol dm^{-3} LiTFSI/DMSO:DMC (1:1.3 by vol.), natural graphite showed an intermediate behavior; the cointercalation of DMSO was less vigorous but the intercalation and deintercalation of lithium-ion were not observed. On the contrary, the intercalation and deintercalation of lithium-ion took place without the cointercalation of DMSO in 3.2 mol dm^{-3} LiTFSI/DMSO and 1.0 mol dm^{-3} LiTFSI/DMSO:DMC (1:4.8 and 1:10.7 by vol.) , in which the N_{DMSO} value was around 2 or less. Although we cannot rule out the effect of a complicated solvation structure (e.g., clustering structure) in the case of the salt-concentrated solution, a series of our results indicate that the N_{DMSO} value in DMSO based solutions does influence the behavior of electrochemical lithium intercalation into natural graphite. The N_{DMSO} value of around 3 is a criterion for determining whether the intercalation of lithium-ion or solvated lithium-ion occurs; lithium-ion solvated by four DMSO molecules intercalates into graphite without desolvation, whereas lithium-ion solvated by two or less DMSO molecules does after desolvation.

Our question here is why the behavior of graphite is related with the solvation number of DMSO. One reasonable answer to this question is the difference in thermodynamical stability of solvated lithium-ion in a solution, as discussed in the case of PC-based solutions [16]. The stability of solvated lithium-ion should drastically vary depending on the N_{DMSO} value, because the solvation of DMSO toward lithium-ion is quite strong among various organic solvents. To know the strength of solvation toward lithium-ion in various organic solvents, we calculated the enthalpy change (ΔH) in the following complexation reaction with density functional theory:

$$Li^+ + \text{solvent} = Li(\text{solvent})^+ \quad (8).$$

Calculated ΔH values are shown in Table 2.3. Lithium-ion is highly stabilized by the interaction with DMSO, the ΔH value of which is even comparable with that of a bidentate solvent, DME. It is interesting to note the relation between the behavior of graphite and ΔH. A solvent with large ΔH (e.g., DMSO and DME) tends to cointercalate into graphite, whereas a solvent with small ΔH (e.g., EC and DMC) does not cause cointercalation. These results clearly indicate a relationship between the stability of solvated lithium-ion and the intercalation behavior of lithium-ion into graphite. Such a relationship was also reported in a chemical synthesis of alkali-metal-GIC's by a solution method [13,14]. This correlation reasonably accounts for our results of graphite in DMSO-based solutions. In the present study, the use of salt-concentrated DMSO

Table 2.3: Relation between Electrochemical Behavior of Natural Graphite and Enthalpy Changes in Complexation Reaction of Lithium-Ion and a Solvent Molecule

solvent	ΔH^a (kJ mol^{-1})	Behavior of graphite
1,2-dimethoxy ethane (DME)	–254.0	cointercalation
dimethyl sulfoxide (DMSO)	–235.2	cointercalation
propylene carbonate (PC)	–217.1	exfoliation
ethylene carbonate (EC)	–210.3	Li^+ intercalation
dimethyl carbonate (DMC)	–185.8	Li^+ intercalation

[a] Enthalpy change of the complexation reaction (Li^+ + solvent = Li^+-solvent) calculated with B3LYP/6-311+G (3df, 3pd)//B3LYP/6-31G (d).

solutions and DMSO:DMC binary solutions greatly decreased the N_{DMSO} value and thus, the sta bility of solvated lithium-ion should be much lower in these solutions than that in 1.0 mol dm^{-3} LiTFSI/DMSO. This destabilization of solvated lithium-ion suppressed the cointercalation of solvents and allowed for the intercalation of lithium-ion after desolvation.

Our next question is why the intercalation behavior of lithium-ion into graphite is related with the stability of solvated lithium-ion. To answer this question, we need to take into consideration a reaction at the near-surface of graphite. The first step of the electrochemical reaction of graphite with a solution is the intercalation of solvated lithium-ion at the near-surface of graphite, which does occur also in an EC-based solution [5–7]. After the intercalation, the solvated lithium-ion promptly decomposes to form an SEI film at the near-surface of graphite. As a result, a bulk of the Li-(solvent)$_x$-GIC cannot be found in an EC-based electrolyte, and instead Li-GIC is formed. These results suggest that EC-solvated lithium-ion is too unstable to exist in the interlayer of graphite. On the contrary, the formation of Li-(DMSO)$_x$-GIC in a DMSO-based solution was confirmed, although the x value was not identified [2,3]. Therefore, the DMSO-solvated lithium-ion, Li(DMSO)$_x$, intercalates deep inside graphite without decomposition at the near-surface of graphite, suggesting that Li(DMSO)$_x$ is stable in the interlayer of graphite. As a result, a relationship arises between the behavior of lithium intercalation and the stability of solvated lithium-ion. The present study showed that the cointercalation of DMSO occurred in a solution with N_{DMSO} = 4.2 even though an EC-based SEI

existed, but that it was suppressed in solutions where the N_{DMSO} value was 2 or less. An interpretation of these behaviors is that lithium-ion solvated by four DMSO molecules, $Li(DMSO)_4^+$, is stable enough to break through the SEI and exist in the interlayer of graphite without decomposition, resulting in the cointercalation of DMSO. The stability of lithium-ion solvated by three DMSO molecules, $Li(DMSO)_3^+$ or $Li(DMSO)_3(DMC)_y^+$, is intermediate and causes a complicated behavior, the mechanism of which is not clear. On the contrary, lithium-ion solvated by two or less DMSO molecules, $Li(DMSO)_2^+$ or $Li(DMSO)_2(DMC)_y^+$, is too unstable to intercalate without desolvation, leading to the formation of a Li-GIC.

The discussion above provides us a new approach toward the suppression of solvent cointercalation: the decrease in the solvation number of the relevant solvents toward lithium-ion. This approach is applicable to the suppression of exfoliation of graphite in PC-based solution [15,16]. The results in the present study allow us to further understand the mechanism of electrochemical lithium intercalation into graphite. In a practical application, our argument will help with the optimization of electrolyte components and the quest for a new electrolyte solvent in lithium-ion batteries.

2.4. Conclusions

The electrochemical intercalation behavior of lithium-ion into natural graphite depended on the solvation number of DMSO toward lithium-ion (N_{DMSO}) in DMSO-based solutions: 1) salt-concentrated solutions and 2) DMSO:DMC binary solutions. The intercalation of DMSO-solvated lithium-ion (i.e., cointercalation of DMSO) occurred in a solution with N_{DMSO} = 4.2 (e.g., 1.0 mol dm^{-3} LiTFSI/DMSO). On the contrary, the intercalation and deintercalation of lithium-ion were observed in solutions where N_{DMSO} was 2 or less (e.g., 3.2 mol dm^{-3} LiTFSI/DMSO and 1.0 mol dm^{-3} LiTFSI/DMSO:DMC (1:4.8 by vol.)). These results suggest that the cointercalation of solvents can be suppressed by decreasing the solvation number of the relevant solvents toward lithium-ion.

References

[1] Besenhard, J. O. *Carbon* **1976**, *14*, 111–115.

[2] Abe, T.; Kawabata, N.; Mizutani, Y.; Inaba, M.; Ogumi, Z. *J. Electrochem. Soc.* **2003**, *150*, A257−A261.

[3] Abe, T.; Fukuda, H.; Iriyama, Y.; Ogumi, Z. *J. Electrochem. Soc.* **2004**, *151*, A1120−A1123.

[4] Schoderböck, P.; Boehm, H. P. *Synth. Met.* **1991**, *44*, 239−246.

[5] Besenhard, J. O.; Winter, M.; Yang, J.; Biberacher, W. *J. Power Sources* **1995**, *54*, 228−231.

[6] Inaba, M.; Siroma, Z.; Kawatate, Y.; Funabiki, A.; Ogumi, Z. *J. Power Sources* **1997**, *68*, 221−226.

[7] Jeong, S. K.; Inaba, M.; Iriyama, Y.; Abe, T.; Ogumi, Z. *J. Power Sources* **2003**, *119−121*, 555−560.

[8] Jeong, S. K.; Inaba, M.; Iriyama, Y.; Abe, T.; Ogumi, Z. *J. Power Sources* **2008**, *175*, 540−546.

[9] Besenhard, J. O.; Möhwald, H.; Nickl, J. J. *Carbon* **1980**, *18*, 399−405.

[10] Okuyama, N; Takahashi, T.; Kanayama, S.; Yasunaga, H. *Physica B+C* **1981**, *105*, 298−301.

[11] Beguin, F.; Gonzalez, B.; Conard, J.; Estrade-Szwarckopf, H.; Guerard, D. *Synth. Met.* **1985**, *12*, 187−193.

[12] Mizutani, Y.; Ihara, E.; Abe, T.; Asano, M.; Harada, T.; Ogumi, Z.; Inaba, M. *J. Phys. Chem. Solids* **1996**, *57*, 799−803.

[13] Abe, T.; Mizutani, Y.; Tabuchi, T.; Ikeda, K.; Asano, M.; Harada, T.; Inaba, M.; Ogumi, Z. *J. Power Sources* **1997**, *68*, 216−220.

[14] Inagaki, M.; Tanaike, O. *Carbon* **2001**, *39*, 1083−1090.

[15] Jeong, S. K.; Inaba, M.; Iriyama, Y.; Abe, T.; Ogumi, Z. *Electrochem. Solid-State Lett.* **2003**, *6*, A13−A15.

[16] Yamada, Y.; Koyama, Y.; Abe, T.; Ogumi, Z. *J. Phys. Chem. C* **2009**, *113*, 8948−8953.

[17] Peled, E. *J. Electrochem. Soc.* **1979**, *126*, 2047−2051.

[18] Frisch, M. J.; Trucks, G. W.; Schlegel, H. B.; Scuseria, G. E.; Robb, M. A.; Cheeseman, J. R.; Zakrzewski, V. G.; Montgomery, J. A., Jr.; Stratmann, R. E.; Burant, J. C.; Dapprich, S.; Millam, J. M.; Daniels, A. D.; Kudin, K. N.; Strain, O. F. M. C.; Tomasi, J.; Barone, B.;

Cossi, M.; Cammi, R.; Mennucci, B.; Pomelli, C.; Adamo, C.; Clifford, S.; Ochterski, J.; Petersson, G. A.; Ayala, P. Y.; Cui, Q.; Morokuma, K.; Malick, D. K.; Rabuck, A. D.; Raghavachari, K.; Foresman, J. B.; Ciolovski, J.; Ortiz, J. V.; Stefanov, V. V.; Liu, G.; Liashensko, A.; Piskorz, P.; Komaroni, I.; Gomperts, R.; Martin, R. L.; Fox, D. J.; Keith, T.; Al-Laham, M. A.; Peng, C. Y.; Nanayakkara, A.; Gonzalez, C.; Challacombe, M.; Gill, P. M. W.; Johnson, B.; Chen, W.; Wong, M. W.; Andres, J. L.; Head-Gordon, M.; Replogle, E. S.; Pople, J. A. *Gaussian 98*; Gaussian Inc.: Pittsburgh, PA, 1998.

[19] Dahn, J. R. *Phys. Rev. B* **1991**, *44*, 9170–9177.

[20] Emons, H. H.; Birkeneder, F.; Pollmer, K. *Z. Anorg. Allg. Chem.* **1986**, *534*, 175–187.

[21] Alia, J. M.; Edwards, H. G. M. *Vib. Spectrosc.* **2000**, *24*, 185–200.

[22] Xuan, X. P.; Wang, J. J.; Zhao, Y.; Zhu, J. J. *J. Raman spectrosc.* **2007**, *38*, 865–872.

[23] Kondo, K.; Sano, M.; Hiwara, A.; Omi, T.; Fujita, M.; Kuwae, A.; Iida, M.; Mogi, K.; Yokoyama, H. *J. Phys. Chem. B* **2000**, *104*, 5040.

[24] Wang, Z. X.; Huang, B. Y.; Xue, R. J.; Chen, L.Q.; Huang, X. J. *J. Electrochem. Soc.* **1998**, *145*, 3346.

[25] Brouillette, D.; Irish, D. E.; Taylor, N. J.; Perron, G.; Odziemkowski, M.; Desnoyers, J. E. *Phys. Chem. Chem. Phys.* **2002**, *4*, 6063–6071.

[26] Hyodo, S.; Okabayashi, K. *Electrochim. Acta* **1989**, *34*, 1551–1556.

[27] Hyodo, S.; Okabayashi, K. *Electrochim. Acta* **1989**, *34*, 1557–1561.

[28] Frolov, Y. L.; Guchik, I. V.; Shagun, V. A.; Vaschenko, A. V.; Trofimov, B. A. *J. Struct. Chem.* **2003**, *44*, 927–931.

[29] Morita, M.; Asai, Y.; Yoshimoto, N.; Ishikawa, M. *J. Chem. Soc., Faraday Trans.* **1998**, *94*, 3451–3456.

[30] Deng, Z.; Irish, D. E. *J. Chem. Soc., Faraday Trans.* **1992**, *88*, 2891–2896.

Part 2

Activation Energy of Electrochemical Lithium Intercalation into Graphite

Chapter 3

Kinetics of Lithium-Ion Transfer at the Interface between $Li_{0.35}La_{0.55}TiO_3$ and Binary Electrolytes

3.1. Introduction

Lithium-ion batteries have attracted much attention as a power source for hybrid electric vehicles (HEVs), plug-in hybrid electric vehicles (PHEVs) and electric vehicles (EVs) due to their high energy density and cycling stability. However, there are some barriers to be overcome for automobile applications. One such barrier is the rate performance of these batteries. Therefore, it is important to focus on the kinetic aspects of charge-discharge reactions in lithium-ion batteries.

The charge-discharge mechanism of lithium-ion batteries is simple. Lithium-ion is transferred from a positive (negative) electrode to a negative (positive) electrode during charge (discharge). Therefore, rapid lithium-ion transfer is required for high rate performance of lithium-ion batteries. In lithium-ion batteries, several processes play a role in lithium-ion and electron transfer, as follows: *i*) electron transport at the positive and negative electrodes, *ii*) electron transport at a current collector / electrode interface, *iii*) lithium-ion diffusion in active materials, *iv*) lithium-ion (charge) transfer at an electrode / electrolyte interface, *v*) lithium-ion transport in an electrolyte that has penetrated a composite electrode, and *vi*) lithium-ion transport in an electrolyte (separator). Among these processes, the electron-transport processes (*i* and *ii*) are generally fast compared to ion-transport processes because conductive agents are added to composite electrodes. The resistance in lithium-ion transport processes (*iii*, *v* and *vi*) has been widely studied and can be reduced by adopting a smaller size for the active material and a thinner composite electrode and separator. On the other hand, less attention has been paid to the interfacial lithium-ion transfer process (*iv*), and the mechanism of this interfacial process is not clear.

We previously reported the kinetics of interfacial lithium-ion transfer at carbonaceous materials [1–5], lithium titanate [6] and lithium cobalt oxide [7]. We also investigated lithium-ion transfer at an ideal interfacial system consisting of solid electrolyte / liquid or polymer electrolytes, in which only interfacial lithium-ion transfer can occur without any redox reactions

at the interface or structural changes in solid phases [8–10]. The activation energies of interfacial lithium-ion transfer are large (around 50 kJ mol^{-1} or more) compared to those of lithium-ion transport in solid [11–14] or liquid [15–17] electrolytes. Furthermore, the activation energies of the interfacial process depend on the solvation abilities of the electrolyte solvents. Based on these results, we concluded that the desolvation process of lithium-ion can be a rate-determining step of interfacial lithium-ion transfer.

In general, a binary solution consisting of a cyclic carbonate (i.e., ethylene carbonate (EC) or propylene carbonate (PC)) and a linear carbonate (i.e., dimethyl carbonate (DMC), diethyl carbonate (DEC) or ethyl methyl carbonate (EMC)) is used as an electrolyte in lithium-ion batteries. The mixing ratio of the two kinds of carbonate is determined to balance the ionic conductivity and viscosity of the electrolytes. However, it is not yet clear how the mixing ratios of solvents influence the kinetics of interfacial lithium-ion transfer, i.e., the desolvation process of lithium-ion. Xu *et al.* investigated the kinetics of interfacial lithium-ion transfer at a graphite composite electrode in EC:DMC binary electrolytes [18,19]. They reported that the composition of a surface film (solid electrolyte interphase, SEI) on graphite varied with the mixing ratios of EC:DMC binary electrolytes and that the surface film influenced the activation energies of interfacial lithium-ion transfer. However, the influence of the solvent itself (i.e., desolvation process) on the kinetics of interfacial lithium-ion transfer was not clear in their report.

In the present study, we used a model system consisting of solid electrolyte / liquid electrolyte to study the kinetics of interfacial lithium-ion transfer in EC:DMC binary electrolytes by four-probe ac impedance spectroscopy. This system is ideal for studying interfacial lithium-ion transfer because there is no redox reaction, structural changes, or surface films. To clarify the relation between the kinetics of interfacial lithium-ion transfer and solvent molecules in EC:DMC binary electrolytes, the solvation structures of lithium-ion in EC:DMC electrolytes were investigated by Raman spectroscopy.

3.2. Experimental Methods

$Li_{0.35}La_{0.55}TiO_3$ (LLT) (diameter: 10 mm, thickness: 1 mm) was used as a solid electrolyte due to its high lithium-ion conductivity. Binary solutions consisting of 1 mol dm^{-3} $LiClO_4$ dissolved in EC:DMC (1:1, 1:9, 1:14 by vol.) were used as an electrolyte. An electrolyte consisting of 0.7 mol dm^{-3} $LiClO_4$ / DMC was used as a reference. All electrolytes were

purchased from Kishida Chemical Co., Ltd. and the water content of the electrolytes was less than 20 ppm.

A four-probe cell (Fig. 3.1) was used for ac impedance spectroscopy. The four electrodes were all lithium metal. The contact area of solid and liquid electrolytes was kept constant at 0.20 cm^2. The ac impedance measurement was conducted over a frequency region of 100 kHz – 100 mHz with an applied ac voltage amplitude of 10 mV in an argon atmosphere.

Raman spectra were recorded with a triple monochromator (Jobin-Yvon, T-64000) with a 514.5 nm line (50 mW) from an argon ion laser (NEC, GLG3260). A quartz cell was used for Raman spectroscopy of solutions.

The solvation ability of solvents toward lithium-ion was evaluated with the density functional theory using Gaussian 98W [20]. The reaction enthalpies of a lithium-ion and a solvent molecule were calculated at 298.15 K. Molecular structures were fully optimized with B3LYP/6-31G (d) in advance. Single-point energies were calculated at the B3LYP/6-311 + G(3df, 3pd) level by using the resulting optimized geometries.

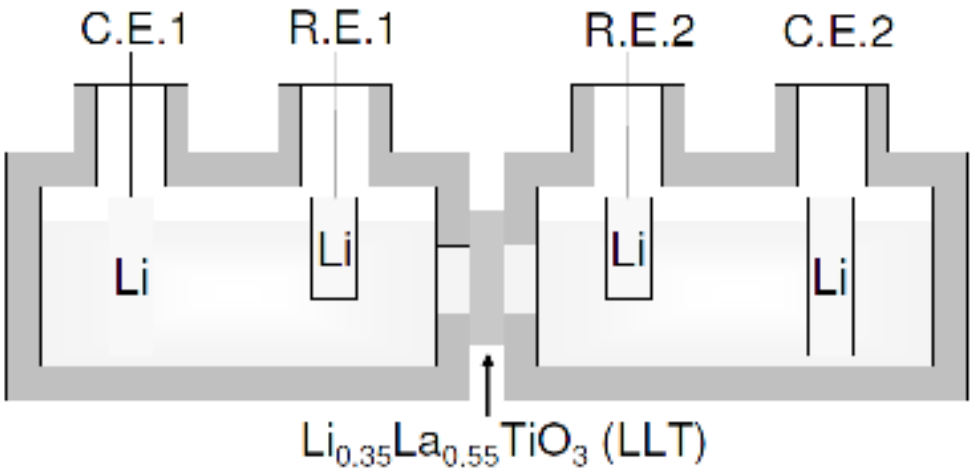

Fig. 3.1 Schematic diagram of a four-probe cell.

3.3. Results

3.3.1. AC impedance measurement of a system consisting of Li / electrolyte / LLT / electrolyte / Li.

To study the kinetics of interfacial lithium-ion transfer, we first carried out ac impedance measurements of LLT to clarify the resistance derived from LLT. Since the LLT prepared in the present study is a polycrystal, there should be two components of resistance in LLT: bulk and grain-boundary resistance. Figure 3.2 shows a Nyquist plot of a two-electrode system consisting of Au / LLT / Au. Two resistances were observed as a *Z'* intercept and a semicircle with a characteristic frequency of ca. 1 kHz. Inaguma *et al.* reported that the resistances at the higher frequency region (*Z'* intercept) and lower frequency region (the semicircle with a characteristic frequency of ca. 1 kHz) could be attributed to bulk and grain-boundary resistance, respectively [12]. These results show that the bulk resistance does not give a semicircle in the present frequency region and grain-boundary resistance appears as a semicircle with a characteristic frequency of ca. 1 kHz.

Figure 3.3 shows a Nyquist plot for a four-probe system consisting of Li / electrolyte / LLT / electrolyte / Li. The electrolyte used here was 1 mol dm^{-3} $LiClO_4$ / EC:DMC (1:14 by vol.). There were three components of resistance: a *Z'* intercept and two semicircles with characteristic frequencies of 1 kHz and 10 Hz. Since a four-probe cell was used in the present study, the resistances from the counter electrodes (lithium metal) can be neglected and those between the two reference electrodes should be observed by ac impedance spectroscopy. Therefore, the following four resistances can appear in Nyquist plots: 1) lithium-ion-transport resistance in the electrolyte (R_{sol}), 2) grain-boundary resistance of LLT (R_{gb}), 3) bulk resistance of LLT (R_b) and 4) interfacial lithium-ion-transfer resistance at LLT / liquid electrolyte (charge-transfer resistance, R_{ct}). In the Nyquist plot for Au / LLT / Au (Fig. 3.2), the semicircle with a characteristic frequency of 1 kHz can be assigned to R_{gb} of LLT and the *Z'* intercept should include R_b of LLT. The *Z'* intercept also contains R_{sol} because lithium-ion transport in electrolytes is generally fast and does not give a semicircle. Hence, the semicircle with a characteristic frequency of 10 Hz was attributed to the interfacial resistance, R_{ct}. This assignment is consistent with our previous studies [8–10]. When electrolytes with other mixing ratios were used, the assignment of the two semicircles was the same as that discussed above.

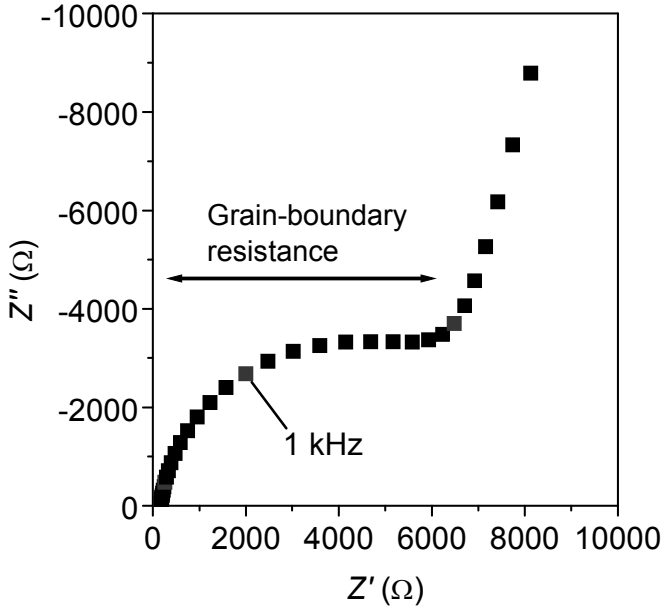

Fig. 3.2 Nyquist plot for a two-electrode system consisting of Au / LLT / Au.

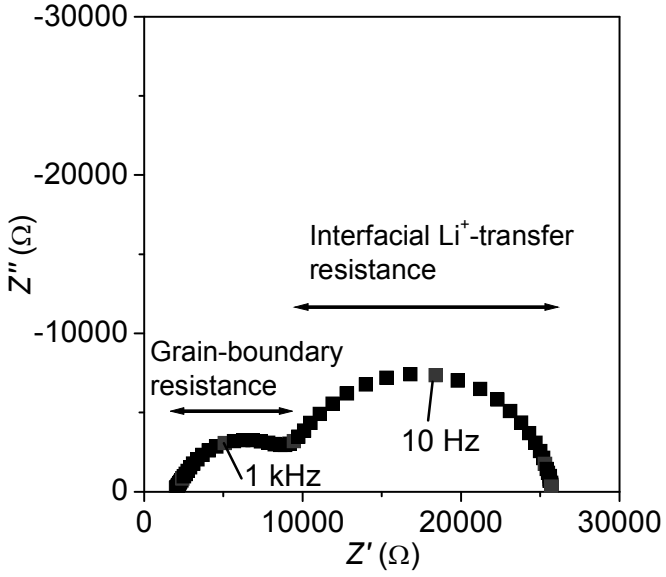

Fig. 3.3 Nyquist plot for a four-probe system consisting of Li / electrolyte / LLT / electrolyte / Li. The electrolyte used here was 1 mol dm^{-3} $LiClO_4$ dissolved in EC:DMC (1:14 by vol.).

3.3.2. Activation energies of interfacial lithium-ion transfer at LLT / EC:DMC binary electrolytes.

We used activation energies to discuss the kinetics of interfacial lithium-ion transfer at LLT / liquid electrolytes. Studies on activation energies are useful for clarifying the discussion because the activation energy values indicate the essential kinetics of an interfacial process without the effects of lithium-ion activity or the effective surface area (i.e., wettability of solvents on LLT).

Figure 3.4 shows the temperature-dependence (Arrhenius plots) of interfacial conductivities ($1 / R_{ct}$) at LLT / liquid electrolytes. Activation energies were evaluated from the slopes of the Arrhenius plots according to the Arrhenius equation, $1/R_{ct} = A\exp(-E_a/RT)$. A, E_a, R and T denote the frequency factor, activation energy, gas constant and absolute temperature, respectively. When a binary electrolyte consisting of $LiClO_4$ / EC:DMC (1:1 by vol.) was used, the activation energy was evaluated to be 51 kJ mol^{-1}. As discussed in a previous report [8], this activation energy is much larger than those of lithium-ion conduction in LLT [11,12] and electrolytes [14–16]. These results mean that a large activation barrier exists in lithium-ion transfer at an LLT / liquid electrolyte interface. We ascribed this large activation barrier to the energy for the desolvation of lithium-ion [8]. In the case of $LiClO_4$ / DMC, however, the activation energy was 32 kJ mol^{-1}, which was much smaller than that in $LiClO_4$ / EC:DMC (1:1

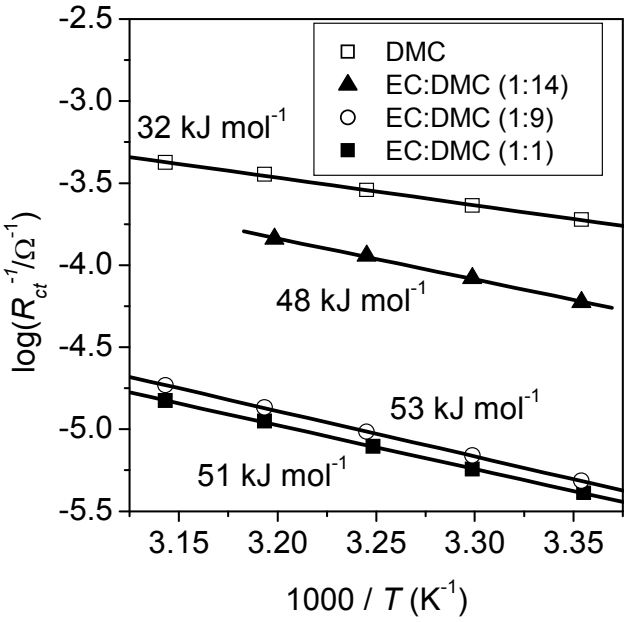

Fig. 3.4 Arrhenius plots of conductivities ($1 / R_{ct}$) at LLT / liquid electrolyte interfaces. Activation energies were evaluated from the slopes of the Arrhenius plots.

by vol.). Although the salt concentration is low in this electrolyte (0.7 mol dm^{-3}), due to the low solubility of the lithium salt in DMC, the salt concentration does not affect activation energies and does not cause the small activation energy. These results indicate that the desolvation of lithium-ion in $LiClO_4$ / DMC is fast compared to that in $LiClO_4$ / EC:DMC (1:1 by vol.).

We also examined the effect of the mixing ratios of EC:DMC binary electrolytes on the activation energies of interfacial lithium-ion transfer. We used 1 mol dm^{-3} $LiClO_4$ / EC:DMC (1:9 or 1:14 by vol.) as an electrolyte. The activation energies of interfacial lithium-ion transfer in these electrolytes were around 50 kJ mol^{-1}, which was as large as that in 1 mol dm^{-3} $LiClO_4$ / EC:DMC (1:1 by vol.). Based on these results, EC molecules are involved in the desolvation process of lithium-ion even in electrolytes containing a small amount of EC. Therefore, the solvation structures of lithium-ion in various EC:DMC binary electrolytes should be studied.

3.3.3. Solvation structures of lithium-ion in EC:DMC binary electrolytes.

Raman spectra were used to investigate the solvation structures of lithium-ion in various EC:DMC binary electrolytes. Figure 3.5 shows Raman spectra of 1 mol dm^{-3} $LiClO_4$ dissolved in EC:DMC (1:1 by vol.) and EC:DMC (1:9 by vol.) in a range of 680–760 cm^{-1}. The bands at 718 cm^{-1} and 731 cm^{-1} are assigned to the symmetric ring deformation mode of EC molecules free of Li^+ and solvating Li^+, respectively [21,22]. The band at 695 cm^{-1} is derived from both EC and DMC molecules. The intensities of the bands at 718 cm^{-1} (I_{free}, EC free of Li^+) and at 731 cm^{-1} (I_{solv}, EC solvating Li^+) are related to the concentrations of EC free of Li^+ (c_{free}) and solvating Li^+ (c_{solv}), as shown in the following equations:

$$I_{free} = \Gamma^*_{free} c_{free} \quad (1)$$

$$I_{solv} = \Gamma^*_{solv} c_{solv} \quad (2)$$

where Γ_{free}^* and Γ_{solv}^* denote Raman intensities per unit concentration of EC free of Li^+ and solvating Li^+, respectively. The concentration ratio (c_{free}/c_{solv}) of EC free of Li^+ and solvating Li^+ can be calculated as [21,23],

$$\frac{c_{free}}{c_{solv}} = \frac{I_{free}}{I_{solv}} \frac{\Gamma^*_{solv}}{\Gamma^*_{free}} \quad (3)$$

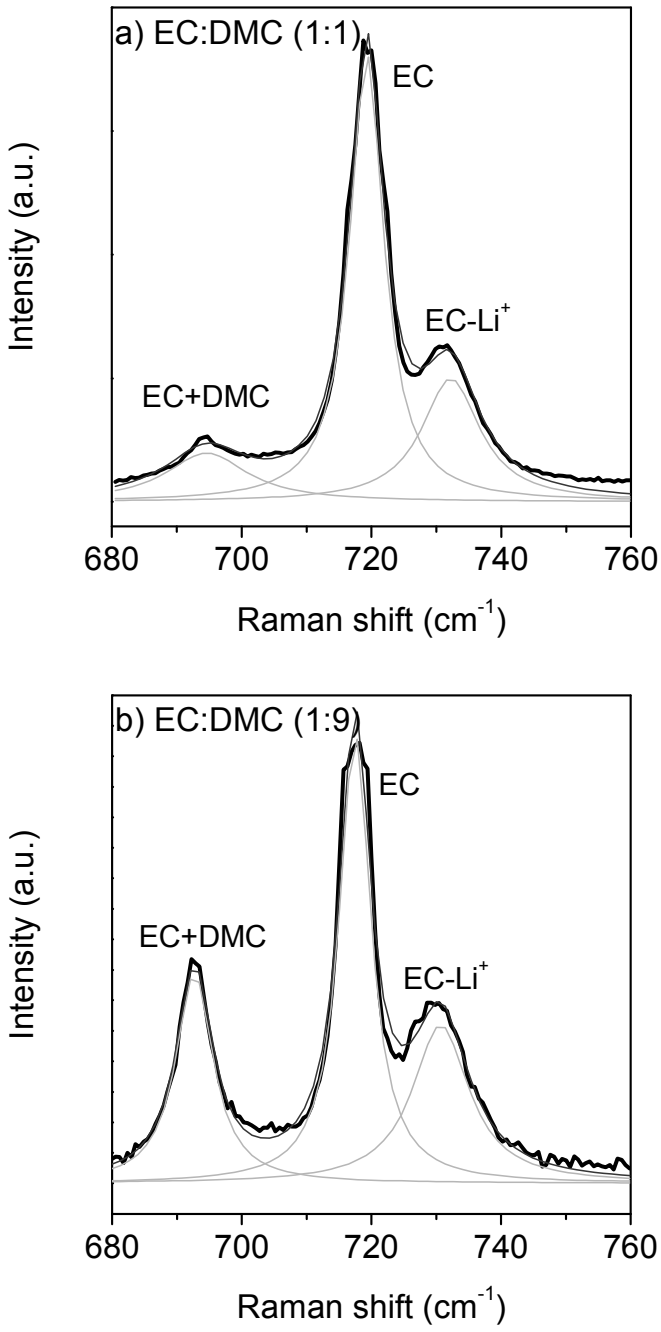

Fig. 3.5 Raman spectra of 1 mol dm^{-3} $LiClO_4$ dissolved in a) EC:DMC (1:1 by vol.) and b) EC:DMC (1:9 by vol.).

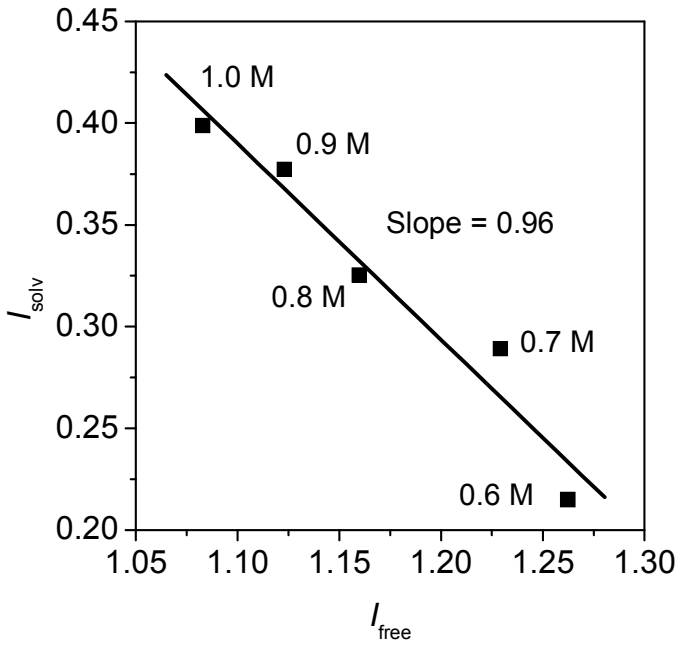

Fig. 3.6 Relation between the Raman intensities of EC free of Li^+ (I_{free}) and EC solvating Li^+ (I_{solv}) in 0.6–1.0 mol dm^{-3} $LiClO_4$ / EC:DMC (1:1 by vol.). The values of I_{free} and I_{solv} were normalized by the Raman intensity of a DMC-derived band at 519 cm^{-1}.

The value of $\Gamma_{solv}^*/\Gamma_{free}^*$ can be obtained from the slope of I_{free} vs I_{solv} plots (Fig. 3.6) for EC:DMC (1:1 by vol.) solutions with different salt concentrations (0.6–1.0 mol dm^{-3}) by the following equation [21]:

$$I_{solv} = -\frac{\Gamma_{solv}^*}{\Gamma_{free}^*} I_{free} + c_{EC,tot}\Gamma_{solv}^* \quad (4).$$

We assumed that the total concentration of EC ($c_{EC,tot} = c_{free} + c_{solv}$) was constant in a concentration range of 0.6–1.0 mol dm^{-3}. The intensity (I_{DMC}) of a DMC-derived band at 519 cm^{-1} was used as an internal standard and the obtained Raman intensity values of EC molecules, I_{free} and I_{solv}, were normalized by I_{DMC}. The I_{free} vs. I_{solv} plots showed a linear correlation and the value of $\Gamma_{solv}^*/\Gamma_{free}^*$ in this measuring system was evaluated to be 0.96 from the slope. This value is compatible with a previous report [21]. We can obtain c_{free}/c_{solv} values for EC:DMC solutions with various mixing ratios from eq. 3. With the c_{free}/c_{solv} values, we evaluated the average solvation numbers ($N_{EC,ave}$) of EC molecules per lithium-ion with the following equation:

$$N_{EC,ave} = \frac{c_{solv}}{c_{Li,tot}} = \frac{c_{EC,tot}}{c_{Li,tot}\left(1 + c_{free}/c_{solv}\right)} \quad (5)$$

Here, $c_{Li,tot}$ and $c_{EC,tot}$ denote the total concentrations of lithium-ion and EC molecules in $LiClO_4$ / EC:DMC solutions, respectively. Table 3.1 shows $N_{EC,ave}$ values in EC:DMC solutions with various mixing ratios containing 1 mol dm^{-3} $LiClO_4$. The value of $N_{EC,ave}$ was 3.5 in pure EC, and it decreased to 0.4 in EC:DMC (1:14 by vol.). The total solvation numbers of lithium-ion in organic solutions with salt concentrations of around 1 mol dm^{-3} have been previously reported to be 4.1 – 4.3 in $LiClO_4$ / EC [21], 3.9 – 4.6 in $LiAsF_6$ / acetone [24], 2.8 – 3.7 in $LiCF_3SO_3$ / EC:DMC [22] and 3.9 – 4.4 in $LiPF_6$ / EC:DMC [22]. The $N_{EC,ave}$ value of 3.5 in pure EC in the present study is slightly small compared to these results. This is because there are several kinds of ion pairs in the electrolyte. Based on the Raman spectra, we could not distinguish between the solvation numbers of EC toward dissociated lithium-ion and ion pairs. Therefore, we used the average values, $N_{EC,ave}$, although it would be preferable to know the actual solvation numbers of dissociated lithium-ion and ion pairs.

3.4. Discussion

Table 3.1 shows the relation between the activation energies of interfacial lithium-ion transfer and $N_{EC,ave}$ in EC:DMC binary electrolytes. The activation energy of interfacial lithium-ion transfer in pure EC could not be evaluated because of the high viscosity of the electrolyte. The activation energies in electrolytes containing EC molecules were around 50 kJ mol^{-1}, while an electrolyte consisting of $LiClO_4$ / DMC gave an activation energy of 30 kJ mol^{-1}. These results mean that the energies for the desolvation process of lithium-ion are different in these

Table 3.1. Average solvation numbers ($N_{EC,ave}$) of EC molecules per lithium-ion and activation energies (E_a) of interfacial lithium-ion transfer in EC:DMC binary electrolytes containing 1 mol dm^{-3} $LiClO_4$

EC:DMC	$N_{EC,ave}$	E_a (kJ mol^{-1})
pure EC	3.5	-
1:1	2.5	51
1:9	0.6	53
1:14	0.4	48
pure DMC	0	32

solutions. We can evaluate the energies for desolvation by the density functional theory. We calculated the enthalpy change (ΔH) of the following reaction using Gaussian 98W [20]:

$Li^+ + solvent = Li(solvent)^+$ ΔH

The calculated ΔH values were -210.3 kJ mol^{-1} for EC and -185.8 kJ mol^{-1} for DMC. These results indicate that the solvation ability of EC is higher than that of DMC. Therefore, the desolvation of lithium-ion from an EC molecule requires much more energy than that from a DMC molecule. In electrolytes containing EC molecules, EC selectively solvates lithium-ion due to the high solvation ability of EC. In fact, $N_{EC,ave}$ values are 0.6 in EC:DMC (1:9 by vol.) and 0.4 in EC:DMC (1:14 by vol.), and many EC molecules solvate lithium-ion, even though there exists only a small amount of EC molecules in the electrolytes. Hence, the desolvation of lithium-ion requires much more energy in EC-containing electrolytes than in those without EC. These results clearly indicate that the activation energies of interfacial lithium-ion transfer depend on the solvation ability of solvents, and the desolvation process of lithium-ion is the rate-determining step.

A comparison of activation energies in EC:DMC (1:1, 1:9 and 1:14 by vol.) suggests another important hypothesis. In these electrolytes, the activation energies of interfacial lithium-ion transfer were almost unchanged (ca. 50 kJ mol^{-1}). These results suggest that the energies for desolvation from 2.5, 0.6 and 0.4 molecules of EC are almost the same. One possible hypothesis is that desolvation from the last solvent molecule ($Li^+(solvent) = Li^+ + solvent$) is the rate-determining step, and earlier desolvation has little effect on the kinetics of interfacial lithium-ion transfer. The results of the theoretical calculation support this hypothesis. The difference in the activation energies in EC:DMC and DMC electrolytes was about 20 kJ mol^{-1}, which was consistent with the difference in ΔH of EC and DMC molecules (24.5 kJ mol^{-1}). Since the values of ΔH were calculated from the reaction of one lithium-ion with one solvent molecule, these results imply that the activation energies reflect the energies for desolvation from the last solvent molecule. To verify this hypothesis of the stepwise desolvation, we need to investigate the solvation structure of lithium-ion near the electrode, i.e., at around the outer Helmholtz plane (OHP). However, it is difficult to know the solvation structures of ion near the interface, and no one has experimentally investigated them as far as we know. Therefore, there is only a theoretical approach for obtaining the information on the solvation structures near the interface. Matsui *et al.* used Monte Carlo statistical mechanics simulations to evaluate the solvation

numbers of lithium-ion in organic solvents [25]. They reported that the solvation number of lithium-ion gradually decreased inside the OHP with decreasing distances between the lithium-ion and the electrode surface. A similar tendency was reported in the case of sodium-ion in an organic solvent and water [26]. Based on the simulations and our results on the activation energies and the enthalpy changes, it is reasonable to consider that the desolvation occurs in a stepwise way and the desolvation from the last solvent molecule is the rate-determining step.

The LLT / liquid electrolyte system in the present study is a model for electrode / electrolyte interfaces in lithium-ion batteries. The present results suggest that there is a large activation barrier in lithium-ion transfer (charge transfer) at electrode / electrolyte interfaces and that the kinetics of interfacial lithium-ion transfer depend on the electrolyte solvents. To achieve fast charge transfer at such interfaces, we must consider the interaction between lithium-ion and solvent molecules and identify a solvent with low solvation ability as well as a high dielectric constant. The kinetics of lithium-ion transfer at graphite electrode / EC:DMC binary electrolyte interfaces are now under investigation and will be reported elsewhere.

3.5. Conclusions

The activation energies of lithium-ion transfer at LLT / liquid electrolyte interfaces depended on the solvation ability of the electrolyte solvents. Based on these results, the activation energies of interfacial lithium-ion transfer reflect the energies for the desolvation of lithium-ion from solvent molecules. Raman spectra clarified that there was a dramatic difference in the solvation numbers of EC molecules per lithium-ion between EC:DMC (1:1 by vol.) and EC:DMC (1:9 by vol.). However, the activation energies of interfacial lithium-ion transfer were almost the same (ca. 50 kJ mol^{-1}) in these EC:DMC binary electrolytes. These results indicate that the desolvation of lithium-ion from the last solvent molecule is the rate-determining step of interfacial lithium-ion transfer and earlier desolvation processes have almost no effect on the kinetics of interfacial lithium-ion transfer.

References

[1] Abe, T.; Fukuda, H.; Iriyama, Y.; Ogumi, Z. *J. Electrochem. Soc.* **2004**, *151*, A1120.

[2] Doi, T.; Takeda, K.; Fukutsuka, T.; Iriyama, Y.; Abe, T.; Ogumi, Z. *Carbon* **2005**, *43*, 2352.

[3] Doi, T.; Iriyama, Y.; Abe, T.; Ogumi, Z. *J. Electrochem. Soc.* **2005**, *152*, A1521.

[4] Ogumi, Z.; Abe, T.; Fukutsuka, T.; Yamate, S.; Iriyama, Y. *J. Power Sources* **2004**, *127*, 72.

[5] Doi, T.; Miyatake, K.; Iriyama, Y.; Abe, T.; Ogumi, Z.; Nishizawa, T. *Carbon* **2004**, *42*, 3183.

[6] Doi, T.; Iriyama, Y.; Abe, T.; Ogumi, Z. *Anal. Chem.* **2005**, *77*, 1696.

[7] Yamada, I.; Iriyama, Y.; Abe, T.; Ogumi, Z. *J. Power Sources* **2007**, *172*, 933.

[8] Abe, T.; Sagane, F.; Ohtsuka, M.; Iriyama, Y.; Ogumi, Z. *J. Electrochem. Soc.* **2005**, *152*, A2151.

[9] Abe, T.; Ohtsuka, M.; Sagane, F.; Iriyama, Y.; Ogumi, Z. *J. Electrochem. Soc.* **2004**, *151*, A1950.

[10] Sagane, F.; Abe, T.; Iriyama, Y.; Ogumi, Z. *J. Power Sources* **2005**, *146*, 749.

[11] Inaguma, Y.; Chen, L. Q.; Itoh, M.; Nakamura, T *Solid State Ionics* **1994**, *70/71***,** 196.

[12] Inaguma, Y.; Chen, L. Q.; Itoh, M.; Nakamura, T.; Uchida, T.; Ikuta, H.; Wakihara, M. *Solid State Commun.* **1993**, *86***,** 689.

[13] Bohnke, O.; Bohnke, C.; Fourquet, J. L. *Solid State Ionics* **1996**, *91***,** 21.

[14] Fu, J. *Solid State Ionics* **1997**, *96*, 195.

[15] Ding, M. S.; Jow, T. R. *J. Electrochem. Soc.* **2003**, *150*, A620.

[16] Ding, M. S.; Xu, K.; Jow, T. R. *J. Electrochem. Soc.* **2005**, *152*, A132.

[17] Ding, M. S. *J. Electrochem. Soc.* **2004**, *151*, A40.

[18] Xu, K.; Lam, Y.; Zhang, S. S.; Jow, T. R.; Curtis, T. B. *J. Phys. Chem. C* **2007**, *111*, 7411.

[19] Xu, K. *J. Electrochem. Soc.* **2007**, *154*, A162.

[20] Frisch, M. J.; Trucks, G. W.; Schlegel, H. B.; Scuseria, G. E.; Robb, M. A.; Cheeseman, J. R.; Zakrzewski, V. G.; Montgomery, J. A., Jr.; Stratmann, R. E.; Burant, J. C.; Dapprich, S.; Millam, J. M.; Daniels, A. D.; Kudin, K. N.; Strain, O. F. M. C.; Tomasi, J.; Barone, B.; Cossi, M.; Cammi, R.; Mennucci, B.; Pomelli, C.; Adamo, C.; Clifford, S.; Ochterski, J.; Petersson, G. A.; Ayala, P. Y.; Cui, Q.; Morokuma, K.; Malick, D. K.; Rabuck, A. D.; Raghavachari, K.; Foresman, J. B.; Ciolovski, J.; Ortiz, J. V.; Stefanov, V. V.; Liu, G.; Liashensko, A.; Piskorz, P.; Komaroni, I.; Gomperts, R.; Martin, R. L.; Fox, D. J.; Keith, T.; Al-Laham, M. A.; Peng, C. Y.; Nanayakkara, A.; Gonzalez, C.; Challacombe, M.; Gill, P. M. W.; Johnson, B.; Chen, W.; Wong, M. W.; Andres, J. L.; Head-Gordon, M.; Replogle, E. S.; Pople, J. A. *Gaussian 98*; Gaussian Inc.: Pittsburgh, PA, 1998.

[21] Hyodo, S.; Okabayashi, K. *Electrochim. Acta* **1989**, *34*, 1551.

[22] Morita, M.; Asai, Y.; Yoshimoto, N.; Ishikawa, M. *J. Chem. Soc., Faraday Trans.* **1998**, *94*, 3451.

[23] Hyodo, S.; Okabayashi, K. *Electrochim. Acta* **1989**, *34*, 1557.

[24] Deng, Z.; Irish, D. E. *J. Chem. Soc., Faraday Trans.* **1992**, *88*, 2891.

[25] Matsui, T.; Takeyama, K. *Electrochim. Acta* **1998**, *43*, 1355.

[26] Matsui, T.; Jorgensen, W. L. *J. Am. Chem. Soc.* **1992**, *114*, 3220.

Chapter 4

Kinetics of Lithium Ion Transfer at the Interface between Graphite and Liquid Electrolytes: Effects of Solvent and Surface Film

4.1. Introduction

Graphite has been used as a negative electrode of lithium-ion batteries because it meets the requirements for energy densities and cycling stabilities. Recently, lithium-ion batteries have attracted much attention as a power source of automobiles such as hybrid electric vehicles (HEVs), plug-in hybrid electric vehicles (PHEVs) and electric vehicles (EVs). The application of lithium-ion batteries for the automobiles gives new requirements for electrode materials. One of such requirements is the rate performance, i.e., fast charge and discharge.

To achieve the high rate performance of lithium-ion batteries, an internal resistance consisting of lithium-ion and electron transport must be reduced. Among several processes of lithium-ion and electron transport, the lithium-ion (charge) transfer at an electrode / electrolyte interface is an essential process of the charge-discharge reaction of lithium-ion batteries. However, little attention was paid to the interfacial lithium-ion transfer. We studied the kinetics of the interfacial lithium-ion transfer and reported that a large activation barrier existed in lithium-ion transfer at a graphite / electrolyte interface [1] and other interfaces [2–8]. The activation energies of the interfacial lithium-ion transfer were around 50 kJ mol^{-1} or more, which were high compared to those of lithium-ion transport in solid [9–12] or liquid [13–15] electrolytes. On the other hand, the activation energy of solvated lithium-ion transfer [1] (i.e., intercalation of dimethyl sulfoxide (DMSO)-solvated lithium-ion into graphite) was an exceptionally small value of around 25 kJ mol^{-1}. Based on these results, we concluded that the desolvation of lithium-ion is the rate-determining step of the interfacial lithium-ion transfer at graphite [1] and that the choice of electrolyte solvents is crucial for faster interfacial lithium-ion transfer [7,8].

In general, a binary solution consisting of a cyclic carbonate (i.e., ethylene carbonate (EC) or propylene carbonate (PC)) and a linear carbonate (i.e., dimethyl carbonate (DMC), diethyl carbonate (DEC) or ethyl methyl carbonate (EMC)) is used as an electrolyte of lithium-ion batteries. A mixing ratio of the two kinds of carbonate is determined to balance the ionic

conductivity and viscosity of the electrolytes. Xu *et al.* used EC:DMC binary electrolytes to investigate the kinetics of the interfacial lithium-ion transfer at graphite composite electrode [16,17]. They reported that the composition of a surface film (solid electrolyte interphase, SEI) on graphite varied with the mixing ratios of EC:DMC binary electrolytes and that the SEI influenced the activation energies of the interfacial lithium-ion transfer. On the other hand, we built an ideal interface consisting of a solid electrolyte and a binary liquid electrolyte to clarify that the kinetics of the interfacial lithium-ion transfer reflected the energies for the desolvation of lithium-ion from the solvent molecule [8]. Therefore, we need to consider the two factors, electrolyte solvents and SEI films, to further understand the kinetics of the interfacial lithium-ion transfer at graphite.

In the present study, we used highly oriented pyrolytic graphite (HOPG) as a model electrode to investigate the kinetics of the interfacial lithium-ion transfer in EC:DMC binary solutions by ac impedance spectroscopy. The HOPG model electrode is useful for evaluating accurate charge-transfer resistances and activation energies because it gives a clear Nyquist plot due to its flat surface and absence of binders. To consider separately the effects of electrolyte solvents and SEI films, different solutions were used for the formation of SEI films and ac impedance spectroscopy. We evaluated activation energies of the interfacial lithium-ion transfer at HOPG with various SEI films in various EC:DMC binary electrolytes, and discuss the effects of the two factors, electrolyte solvents and SEI films, on the kinetics of the interfacial lithium-ion transfer.

4.2. Experimental Methods

A basal plane of HOPG (Momentive Performance Materials Quartz, Inc., ZYH grade) was used as a model electrode. The surface of HOPG was cleaved with an adhesive tape in advance to electrochemical measurements. Binary solutions consisting of 1 mol dm^{-3} $LiClO_4$ dissolved in mixtures of EC and DMC (Kishida Chemical Co., Ltd.) were used as an electrolyte. Vinylene carbonate (VC, Kishida Chemical Co., Ltd.) and 2,3,4,5,6-pentafluorostyrene (PFS, Aldrich) (3 wt%) were used as an additive to the electrolytes. The water content of the electrolytes was less than 20 ppm.

Electrochemical measurements were carried out with a three-electrode cell (Fig. 4.1), which was made of polytetrafluoroethylene (PTFE) and SUS. An HOPG electrode was fixed between the PTFE component and the SUS current collector. The contact area between HOPG and electrolyte was kept at 0.38 cm^2 with an O ring. Lithium metal was used as both counter and

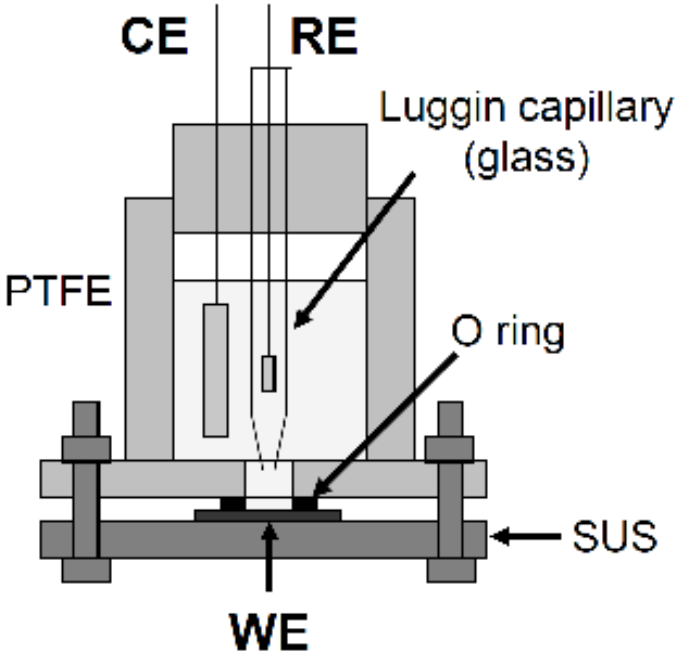

Fig. 4.1 Schematic diagram of a three-electrode cell.

reference electrodes. Unless otherwise noted, the potentials in this paper are referenced to Li/Li^+. We used Solartron 1480 MultiStat (Solartron Analyticlal) and SI 1255 Frequency Response Analyzer (EG&G Princeton Applied Research) for electrochemical measurements. Cyclic voltammetry was conducted in a potential range of 0–3 V with scan rate of 0.1 mV s^{-1} to form an SEI on HOPG. Electrolytes consisting of 1 mol dm^{-3} $LiClO_4$ dissolved in EC:DMC (1:1 by vol.) without additives, with VC and with PFS were used for the formation of SEI films on HOPG. After the cyclic voltammetry, the electrolyte was replaced by EC:DMC binary electrolytes with various mixing ratios. When we replaced the electrolyte, we washed the HOPG electrode with DMC and then with an EC:DMC solution with a given volume ratio. Since these processes were conducted promptly and carefully in an argon atmosphere, the state of the SEI on HOPG was retained after the replacement of electrolytes. AC impedance spectroscopy was carried out over a frequency range of 100 kHz – 10 mHz with an applied ac voltage of 5 mV. The analysis of resultant Nyquist plots was conducted with ZPlot software (Solartron Analytical). All the electrochemical measurements were conducted in an argon atmosphere.

The solvation ability of the solvents toward lithium-ion was evaluated with the density functional theory by using Gaussian 98W [18]. The reaction enthalpies of a lithium-ion and a solvent molecule were calculated at 298.15 K. Molecular structures were fully optimized with

B3LYP/6-31G (d) in advance. Single-point energies were calculated at the B3LYP/6-311 + G(3df, 3pd) level by using the resulting optimized geometries.

4.3. Results and Discussion

4.3.1. Cyclic voltammetry.

Figure 4.2 shows a cyclic voltammogram of HOPG in 1 mol dm^{-3} $LiClO_4$ / EC:DMC (1:1 by vol.) without additives, with 3 wt% of VC and with 3 wt% of PFS. Cathodic and anodic peaks were observed in a range of 0–0.6 V in all the cyclic voltammograms. These peaks were attributed to the electrochemical intercalation and deintercalation of lithium-ion at HOPG. The peak currents for the intercalation and deintercalation of lithium-ion were different in the cyclic voltammograms for the three electrolytes. The electrolytes containing VC or PFS gave large peak currents compared to those without additives. Therefore, VC and PFS formed an excellent SEI on HOPG and enabled the smooth intercalation/deintercalaion of lithium-ion. However, we cannot discuss the kinetics of interfacial lithium-ion transfer based only on the peak currents. The difference in the peak currents derived from several factors such as kinetics of interfacial lithium-ion transfer, amount of edge-plane sites, performance of SEI, and activity of lithium-ion in an electrolytes, etc. In the case of HOPG electrodes, the amount of edge-plane sites (reactive sites) on the basal plane varied depending on the cleaving process, which greatly influenced the peak currents of cyclic voltammograms. Therefore, we use AC impedance spectroscopy to discuss the kinetics of interfacial lithium-ion transfer at graphite in detail. In the cyclic voltammograms for electrolytes with VC or PFS, a cathodic peak clearly appeared at ca. 1.2 V. Since this cathodic peak was not observed in the cyclic voltammogram for the electrolyte without additives, it is clear that VC and PFS were reduced to form VC- and PFS-derived SEI films before the reductions of EC and DMC.

The formation mechanism of the VC-derived SEI was shown in several papers [19–21]. It is generally accepted that VC molecules are reduced on graphite to polymerize with a double bond. The VC-derived SEI is cohesive and flexible, and effectively protects further decomposition of electrolytes. PFS also serves as an SEI-forming additive, as shown in the cyclic voltammetry. A PFS molecule has a double bond and it would form a polymer-like SEI similar to VC-derived one.

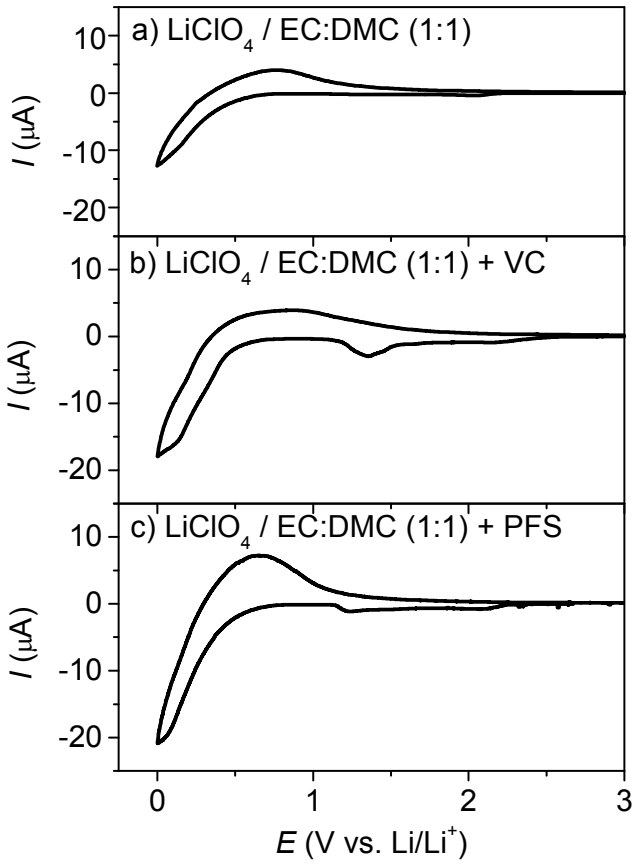

Fig. 4.2 Cyclic voltammogram of HOPG in a) 1 mol dm^{-3} $LiClO_4$ EC:DMC (1:1 by vol.) without additives, b) with VC and c) with PFS. The scan rate was set at 0.1 mV s^{-1}.

4.3.2. AC impedance spectroscopy.

Figure 4.3 shows the potential-dependence of Nyquist plots of HOPG in 1 mol dm^{-3} $LiClO_4$ / EC:DMC (1:1 by vol.). The ac impedance measurement was conducted after cyclic voltammetry to make sure that the formation of an EC-derived SEI was completed. In the Nyquist plots at 1.0 and 0.8 V, one small semicircle was observed at a characteristic frequency of 5 kHz. When the electrode potential was lowered to below 0.6 V, two semicircles clearly appeared at characteristic frequencies of 5 kHz and 4 Hz, and Warburg impedance was observed in a lower frequency region. Since a three-electrode cell was used, the resistance from the counter electrode (lithium metal) could be neglected. Hence, this system should give the following components of resistance: *i*) lithium-ion transport in an electrolyte (R_{sol}), *ii*) lithium-ion transport in an SEI (R_{SEI}), *iii*) lithium-ion (charge) transfer at an HOPG / electrolyte interface (R_{ct}), *iv*) lithium-ion diffusion in HOPG, and *v*) electron transport in HOPG and at an HOPG /

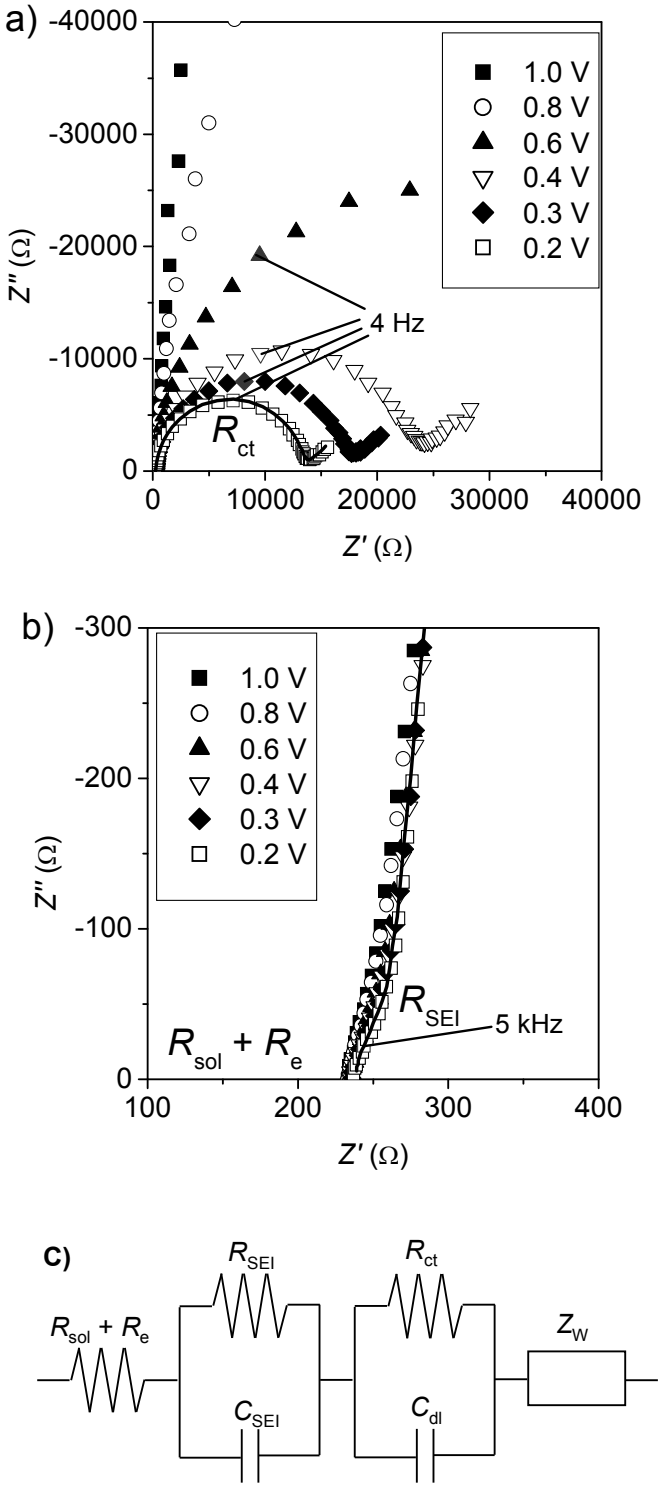

Fig. 4.3 a) Nyquist plots of HOPG in 1 mol dm^{-3} $LiClO_4$ / EC:DMC (1:1 by vol.). b) Enlarged figure of the Nyquist plots at a high frequency region. c) Equivalent circuit used for fitting the Nyquist plots.

current collector interface (R_e). Among these components of resistance, the electron transport (*v*) and lithium-ion transport in an electrolyte (*i*) usually give no semicircle in the present frequency region due to their high characteristic frequencies. These components of resistance appeared as a *Z'* intercept in the Nyquist plots. The lithium-ion diffusion in HOPG (*iv*) gave the Warburg impedance (Z_W), which was observed as a straight line with an angle of 45° from the *Z'* axis. The semicircle with a characteristic frequency of 5 kHz was observed at 1.0 V at which the charge-transfer reaction could not occur. Hence, this semicircle was attributed to the lithium-ion-transport resistance in the SEI (*ii*). The other semicircle with a characteristic frequency of 4 Hz appeared only at below 0.6 V and the diameter of the semicircle depended on the electrode potentials. Therefore, this semicircle was reasonably assigned to the lithium-ion-transfer resistance at the HOPG / electrolyte interface (*iii*). This assignment is in good agreement with previous reports [1,22,23].

We configured an equivalent circuit (Fig. 4.3c) to evaluate R_{ct} of the intercalation and deintercalation of lithium-ion at HOPG. A resistance, two RC-parallel circuits and a Warburg impedance were connected in series. The symbols C_{SEI} and C_{dl} denote a capacitance element in an SEI and a double-layer capacitance, respectively. Accurately, a capacitance element (i.e., the geometric capacitance of the cell) should be located in parallel with R_{sol} and R_e. However, the characteristic frequency of this element is out of the frequency range in the present study. Hence, we practically omitted the capacitance element in the equivalent circuit for the fitting of Nyquist plots. For better fitting, a constant phase element (CPE) was properly used as an alternative for C_{dl}. Since an SEI film is composed of several organic and inorganic layers [24], several RC-parallel circuits should be allocated for the lithium-ion transport in an SEI [22]. In the present paper, however, we allocated one RC-parallel circuit for the process because R_{SEI} was quite small in the case of HOPG electrodes and had almost no effect on R_{ct}. The fitting result for the Nyquist plot at 0.2 V is shown in Figs. 4.3a and 4.3b as a solid line. The best fit of the parameters in the equivalent circuit to experimental Nyquist plots gave R_{ct} values of the intercalation and deintercalation of lithium-ion at HOPG.

4.4.3. Effect of electrolyte solvents on kinetics of interfacial lithium-ion transfer at HOPG.

The conductivity of interfacial lithium-ion transfer ($1 / R_{ct}$) obeys the Arrhenius equation and depends on two factors, activation energy and frequency factor. We used the activation energy to discuss the kinetics of interfacial lithium-ion transfer because activation energy values indicate

the essential kinetics of the interfacial process without the effects of lithium-ion activity or effective surface area. Of course, the frequency factor is also important for the kinetics of interfacial lithium-ion transfer. However, the frequency factor is greatly influenced by the amount of edge-plane sites on HOPG. Therefore, the use of the activation energy is appropriate for the study on the influence of electrolyte solvents.

Figure 4.4 shows the temperature-dependences (Arrhenius plots) of the interfacial conductivities (1 / R_{ct}) at HOPG at 0.2 V in EC:DMC binary and DMC electrolytes. The activation energies were evaluated from the slopes of the Arrhenius plots with the Arrhenius equation, $1/R_{ct} = A\exp(-E_a/RT)$. The symbols A, E_a, R and T denote the frequency factor, activation energy, gas constant and absolute temperature, respectively. When an electrolyte consisting of $LiClO_4$ dissolved in EC:DMC (1:1 by vol.) was used, the activation energy was 58 kJ mol^{-1}. Such large activation energies were also reported for lithium-ion transfer at several solid / liquid interfaces [1–8]. We attributed these large activation energies to the energies for the desolvation of lithium-ion from the solvent [1,7,8]. However, an electrolyte consisting of

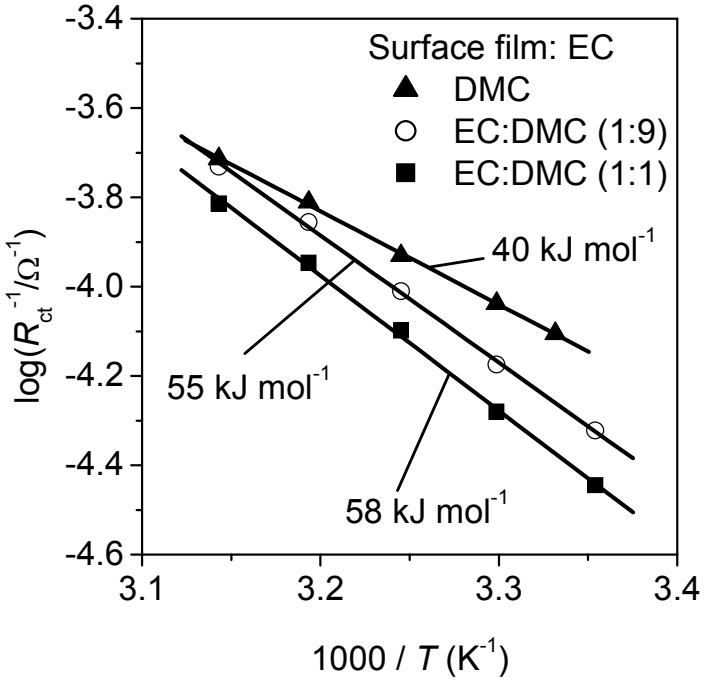

Fig. 4.4 Temperature-dependences of interfacial conductivities (1 / R_{ct}) at HOPG at 0.2 V in $LiClO_4$ / EC:DMC (1:1 and 1:9 by vol.) and $LiClO_4$ / DMC. The SEI film was in advance formed in an electrolyte consisting of 1 mol dm^{-3} $LiClO_4$ / EC:DMC (1:1 by vol.).

$LiClO_4$ dissolved in DMC gave a small activation energy of 40 kJ mol^{-1}. Since an EC-derived SEI was formed on HOPG in advance, the composition of the SEI would not be the reason for the small activation energy in $LiClO_4$ / DMC. Therefore, the small activation energy suggests that the energy for the desolvation of lithium-ion is small in $LiClO_4$ / DMC.

The energies for the desolvation of lithium-ion from EC and DMC can be evaluated with the density functional theory. We calculated the enthalpy change (ΔH) of the following reaction with Gaussian 98W [18].

$Li^+ + \text{solvent} = Li(\text{solvent})^+ \qquad \Delta H$

The calculated ΔH values are -210.3 kJ mol^{-1} and -185.8 kJ mol^{-1} for EC and DMC, respectively. These values indicate that the solvation ability of DMC is lower than that of EC. Therefore, the desolvation of lithium-ion from DMC needs much less energy than that from EC, resulting in the small activation energy of the interfacial lithium-ion transfer at graphite in $LiClO_4$ / DMC. Based on the ΔH and activation energies, we concluded again that the solvation ability of solvents determined the kinetics of the interfacial lithium-ion transfer at graphite, as reported in other interfaces [1,7,8].

Another interest of this paper is the comparison of the activation energies in EC:DMC (1:1 by vol.) and EC:DMC (1:9 by vol.). An electrolyte consisting of $LiClO_4$ dissolved in EC:DMC (1:9 by vol.) gave an activation energy of 55 kJ mol^{-1}, which was almost the same as that in $LiClO_4$ / EC:DMC (1:1 by vol.). The same behavior was observed at an ideal interface consisting of solid and liquid electrolytes [8]. As shown above, an EC molecule has the high solvation ability and gives high activation energies over 50 kJ mol^{-1}. However, there is only a small amount of EC molecules in $LiClO_4$ / EC:DMC (1:9 by vol.). In our previous study [8], the solvation numbers of EC molecules per lithium-ion were clarified to be 2.5 and 0.6 in EC:DMC (1:1 by vol.) and EC:DMC (1:9 by vol.), respectively. These results suggest that the energies for the desolvation of lithium-ion from 2.5 and 0.6 molecules of EC are almost the same. One hypothesis to explain these behaviors is that the desolvation of lithium-ion from the last solvent molecule ($Li^+(\text{solvent}) = Li^+ + \text{solvent}$) is the rate-determining step, and earlier desolvation has little effect on the kinetics of the interfacial lithium-ion transfer at graphite.

The results in the present study indicate that the kinetics of the interfacial lithium-ion transfer at graphite depends on the interaction between lithium-ion and solvent molecules. To

achieve the fast kinetics at graphite, we need to identify a solvent with low solvation ability as well as high dielectric constant.

4.3.4. Effect of SEI films on kinetics of interfacial lithium-ion transfer at HOPG.

Figure 4.5 shows the temperature-dependence of the interfacial conductivities (1 / R_{ct}) at HOPG in $LiClO_4$ / EC:DMC (1:1 by vol.). An SEI was formed in an electrolyte consisting of 1 mol dm^{-3} $LiClO_4$ dissolved in EC:DMC (1:1 by vol.) containing 3 wt% of VC. Since the Nyquist plot for HOPG in $LiClO_4$ / DMC gave poor reproducibility, the results were not shown here. The activation energies of the interfacial lithium-ion transfer at HOPG with the VC-derived SEI were evaluated to be 56 kJ mol^{-1}, which was almost the same as those at HOPG with an EC-derived SEI (Fig. 4.4). These results indicate that the existence of the VC-derived SEI does not change the kinetics of the interfacial lithium-ion transfer at graphite.

The presence of a PFS-derived SEI gave a different behavior. Figure 4.6 shows the temperature-dependences of the interfacial conductivities (1 / R_{ct}) at HOPG with a PFS-derived SEI in $LiClO_4$ / EC:DMC (1:1 by vol.) and $LiClO_4$ / DMC. The activation energy of the interfacial lithium-ion transfer in $LiClO_4$ / EC:DMC (1:1 by vol.) was 56 kJ mol^{-1}, which was

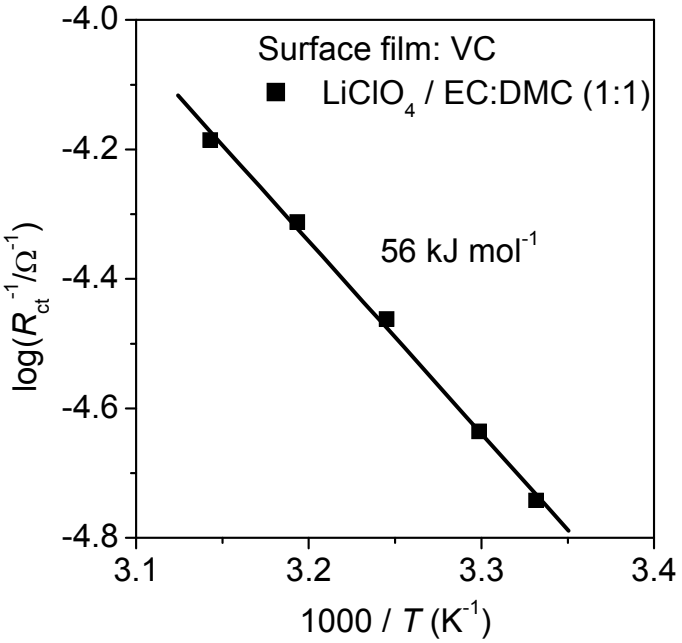

Fig. 4.5 Temperature-dependences of interfacial conductivities (1 / R_{ct}) at HOPG at 0.2 V in $LiClO_4$ / EC:DMC (1:1 by vol.). The SEI film was in advance formed in an electrolyte consisting of 1 mol dm^{-3} $LiClO_4$ / EC:DMC (1:1 by vol.) containing 3 wt% of VC.

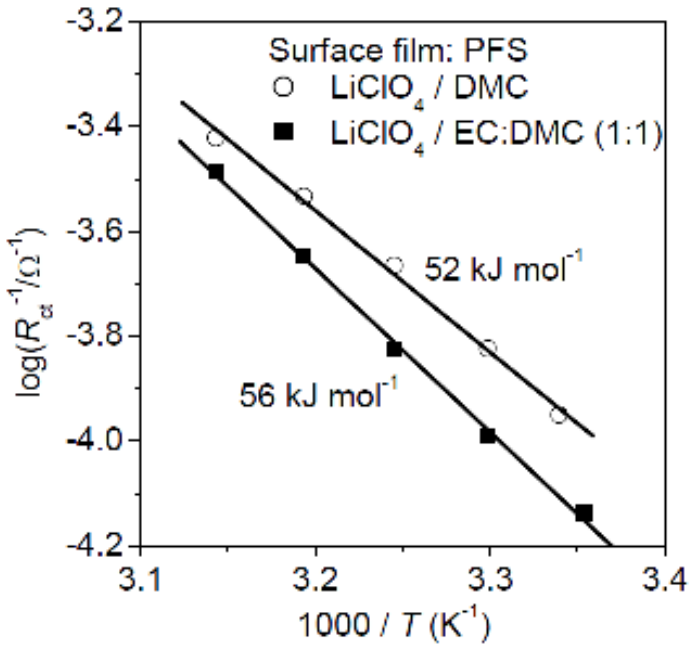

Fig. 4.6 Temperature-dependences of interfacial conductivities (1 / R_{ct}) at HOPG at 0.2 V in $LiClO_4$ / EC:DMC (1:1 by vol.) and $LiClO_4$ / DMC. The SEI film was in advance formed in an electrolyte consisting of 1 mol dm^{-3} $LiClO_4$ / EC:DMC (1:1 by vol.) containing 3 wt% of PFS.

close to those at HOPG with EC- and VC-derived SEI films. On the other hand, an electrolyte of $LiClO_4$ / DM C gave an activation energy of 52 kJ mol^{-1}, which was much larger than that at HOPG with an EC-derived SEI in the same electrolyte (40 kJ mol^{-1}, Fig. 4.4). Based on these results, it i s clear that the PFS-derived SEI influenced the kinetics of the interfacial lithium-ion transfer. Furthermore, the difference in the activation energies in EC:DMC (1:1 by vol.) and DMC was small (4 kJ mol^{-1}) in the presence of the PFS-derived SEI compared to that in the presence of the EC-derived SEI (18 kJ mol^{-1}). In the presence of the EC-derived SEI on HOPG, the activation energies depended on the solvation ability of the solvents, and this behavior was the same as that at an ideal interface consisting of solid and liquid electrolytes [7,8]. In the presence of the PFS-derived SEI, however, the solvation ability of the solvents had only a small effect on the activation energies of the interfacial lithium-ion transfer. These results suggest that the kinetics of the interfacial lithium-ion transfer is predominantly determined by the PFS-derived SEI, rather than the solvents.

The results in the present study imply that the kinetics of the interfacial lithium-ion transfer at graphite is influenced by the compositions of SEI films as well as the desolvation of lithium-

ion. The high activation energy at HOPG with the PFS-derived SEI in $LiClO_4$ / DMC implies that the desolvation of lithium-ion is impeded by the PFS-derived SEI. Therefore, the choice of additives as well as electrolyte solvents is important for the fast interfacial lithium-ion transfer at graphite. Although the relation between the compositions of SEI films and the activation energies of the interfacial lithium-ion transfer is not yet clear, these results indicate the possibility for controlling the kinetics of the lithium-ion transfer by an SEI.

In the present study, we used activation energies to discuss the kinetics of interfacial lithium-ion transfer at graphite, but frequency factors also determine the kinetics. Therefore, we need to consider the frequency factors as well as the activation energies to improve the kinetics of interfacial lithium-ion transfer at graphite. The frequency factors of interfacial lithium-ion transfer are now under investigation and will be presented elsewhere.

4.4. Conclusions

The kinetics of lithium-ion transfer at a graphite / electrolyte interface was influenced by the two factors; a solvent molecule in the electrolyte and an SEI film on graphite. As for the former one, the activation energies of the interfacial lithium-ion transfer depended on the solvation ability of solvents. Therefore, we concluded that the activation energies reflected the energies for the desolvation of lithium-ion from a solvent. Furthermore, the activation energies of the interfacial lithium-ion transfer were almost unchanged in EC:DMC (1:1 by vol.) and EC:DMC (1:9 by vol.), in which there was a drastic difference in the solvation numbers of EC molecules per lithium-ion. Based on these results, the desolvation of lithium-ion from the last solvent is the rate-determining step of the interfacial lithium-ion transfer at graphite. As for the latter one, the solvation ability of solvents had only a small effect on the activation energies of the interfacial lithium-ion transfer in the presence of a PFS-derived SEI on graphite. These results indicate that the kinetics of the interfacial lithium-ion transfer at graphite depends on the compositions of SEI films as well as the electrolyte solvents.

References

[1] Abe, T.; Fukuda, H.; Iriyama, Y.; Ogumi, Z. *J. Electrochem. Soc.* **2004**, *151*, A1120.

[2] Doi, T.; Takeda, K.; Fukutsuka, T.; Iriyama, Y.; Abe, T.; Ogumi, Z. *Carbon* **2005**, *43*, 2352.

[3] Ogumi, Z.; Abe, T.; Fukutsuka, T.; Yamate, S.; Iriyama, Y. *J. Power Sources* **2004**, *127*, 72.

[4] Doi, T.; Miyatake, K.; Iriyama, Y.; Abe, T.; Ogumi, Z.; Nishizawa, T. *Carbon* **2004**, *42*, 3183.

[5] Doi, T.; Iriyama, Y.; Abe, T.; Ogumi, Z. *Anal. Chem.* **2005**, *77*, 1696.

[6] Yamada, I.; Iriyama, Y.; Abe, T.; Ogumi, Z. *J. Power Sources* **2007**, *172*, 933.

[7] Abe, T.; Sagane, F.; Ohtsuka, M.; Iriyama, Y.; Ogumi, Z. *J. Electrochem. Soc.* **2005**, *152*, A2151.

[8] Yamada, Y.; Sagane, F.; Iriyama, Y.; Abe, T.; Ogumi, Z. *J. Phys. Chem. C, in press*.

[9] Inaguma, Y.; Chen, L. Q.; Itoh, M.; Nakamura, T. *Solid State Ionics* **1994**, *70/71*, 196.

[10] Inaguma, Y.; Chen, L. Q.; Itoh, M.; Nakamura, T.; Uchida, T.; Ikuta, H.; Wakihara, M. *Solid State Commun.* **1993**, *86*, 689.

[11] Bohnke, O.; Bohnke, C.; Fourquet, J. L. *Solid State Ionics* **1996**, *91*, 21.

[12] Fu, J. *Solid State Ionics* **1997**, *96*, 195.

[13] Ding, M. S.; Jow, T. R. *J. Electrochem. Soc.* **2003**, *150*, A620.

[14] Ding, M. S.; Xu, K.; Jow, T. R. *J. Electrochem. Soc.* **2005**, *152*, A132.

[15] Ding, M. S. *J. Electrochem. Soc*. **2004**, *151*, A40.

[16] Xu, K.; Lam, Y.; Zhang, S. S.; Jow, T. R.; Curtis, T. B. *J. Phys. Chem. C* **2007**, *111*, 7411.

[17] Xu, K. *J. Electrochem. Soc.* **2007**, *154*, A162.

[18] Frisch, M. J.; Trucks, G. W.; Schlegel, H. B.; Scuseria, G. E.; Robb, M. A.; Cheeseman, J. R.; Zakrzewski, V. G.; Montgomery, J. A., Jr.; Stratmann, R. E.; Burant, J. C.; Dapprich, S.; Millam, J. M.; Daniels, A. D.; Kudin, K. N.; Strain, O. F. M. C.; Tomasi, J.; Barone, B.; Cossi, M.; Cammi, R.; Mennucci, B.; Pomelli, C.; Adamo, C.; Clifford, S.; Ochterski, J.; Petersson, G. A.; Ayala, P. Y.; Cui, Q.; Morokuma, K.; Malick, D. K.; Rabuck, A. D.; Raghavachari, K.; Foresman, J. B.; Ciolovski, J.; Ortiz, J. V.; Stefanov, V. V.; Liu, G.; Liashensko, A.; Piskorz, P.; Komaroni, I.; Gomperts, R.; Martin, R. L.; Fox, D. J.; Keith, T.; Al-Laham, M. A.; Peng, C. Y.; Nanayakkara, A.; Gonzalez, C.; Challacombe, M.; Gill, P. M. W.; Johnson, B.; Chen, W.; Wong, M. W.; Andres, J. L.; Head-Gordon, M.; Replogle, E. S.; Pople, J. A. *Gaussian 98*; Gaussian Inc.: Pittsburgh, PA, 1998.

[19] Ota, H.; Sakata, Y.; Inoue, A.; Yamaguchi, S. *J. Electrochem. Soc.* **2004**, *151*, A1659.

[20] Wang, Y. X.; Nakamura, S.; Tasaki, K.; Balbuena, P. B. *J. Am. Chem. Soc*. **2002**, *124*, 4408.

[21] Aurbach, D.; Gamolsky, K.; Markovsky, B.; Gofer, Y.; Schmidt, M.; Heider, U. *Electrochim. Acta* **2002**, *47*, 1423.

[22] Levi, M. D.; Aurbach, D. *J. Phys. Chem. B* **1997**, *101*, 4630.

[23] Wagner, M. W. *Electrochim. Acta* **1997**, *42*, 1623.

[24] Yazami, R. *Electrochim. Acta* **1999**, *45*, 87.

Chapter 5

Kinetics of Electrochemical Insertion and Extraction of Lithium Ion at SiO

5.1. Introduction

Lithium-ion batteries have recently attracted much attention as a power source for electric vehicles (EVs) and plug-in hybrid electric vehicles (PHEVs). These applications of lithium-ion batteries give severe requirements to electrode materials. One of such requirements is a significant improvement of energy density of electrode materials. Therefore, an alternative electrode material has been explored for much higher energy density. One of the candidates for a new negative electrode is alloying materials such as Si and Sn [1,2]. These materials electrochemically react with lithium to form a lithium alloy which has an extremely high energy density compared to graphite. However, the alloying reaction shows a large volume change of the materials [3] which leads to capacity fade during charge-discharge cycles [4]. To overcome the problem, silicon monoxide (SiO) has recently attracted much attention as a next-generation negative electrode [5–13]. SiO shows a small volume change because it contains a relatively small amount of Si element which is active for the alloying reaction. The discharge capacity of SiO electrodes was reported to be over 600 mAh g^{-1} in several papers [9–12], which is much higher than that of a graphite electrode (372 mAh g^{-1}).

To commercialize the SiO electrode, we need to consider the rate performance in addition to the energy density. However, there are few reports on the kinetic aspect of alloying materials. Our group focused on the kinetics of charge (lithium-ion)-transfer reactions at a graphite / electrolyte interface [14,15] and other interfaces [16–19]. The activation energies of the charge-transfer reactions were around 50 kJ mol^{-1} or more, which were high compared to those of lithium-ion transport in solid [20–23] or liquid [24–26] electrolytes. This is because the desolvation of lithium-ion from solvents occurs during the charge transfer at the interfaces and the energy for the desolvation is large. In the case of SiO, however, the kinetics of the charge-transfer reaction might be quite different from those of graphite and other insertion materials.

In the present paper, the kinetics of the charge-transfer reaction at SiO were studied by ac impedance spectroscopy. At first, the assignment of semicircles in the resultant Nyquist plots was conducted and then, the activation energies of the charge-transfer reaction were investigated. One of the important points of this work is the effect of the desolvation process on the charge-transfer kinetics. Therefore, the activation energies of the charge-transfer reaction were measured in various solvents which have different solvation abilities.

5.2. Experimental Methods

An SiO electrode was provided by Sumitomo Titanium Corporation. The SiO electrode was prepared by the vapor deposition of SiO on a Cu foil. Electrolyte solutions were 1 mol dm^{-3} $LiClO_4$ dissolved in propylene carbonate (PC), dimethyl carbonate (DMC) and ethylene carbonate (EC) : DMC mixture (1:1 by vol.), and 1 mol dm^{-3} $LiCF_3SO_3$ dissolved in dimethyl sulfoxide (DMSO). All the electrolytes were purchased from Kishida Chemical Co., Ltd. and the water content of the electrolytes was less than 20 ppm.

Electrochemical measurements were carried out with a three-electrode cell [15]. Lithium metal was used as both counter and reference electrodes. Unless otherwise noted, the potentials in this paper are referenced to Li/Li^+. We used Solartron 1480 MultiStat (Solartron Analytical) and SI 1255 Frequency Response Analyzer (EG&G Princeton Applied Research) for electrochemical measurements. Cyclic voltammetry was conducted in a potential range of 0–3 V with scan rate of 1 mV s^{-1}. After cyclic voltammetry, ac impedance spectroscopy was carried out over a frequency region of 100 kHz – 10 mHz with an applied ac voltage of 5 mV. All the electrochemical measurements were conducted in an argon atmosphere.

The surface morphology of SiO was observed by scanning electron microscopy (SEM) using S-3000H (Hitachi). SiO was in advance charged from open circuit potential (OCP) to 0.2 V by a potential sweep method (1 mV s^{-1}) and then held at 0.2 V for 24 hours. After that, the SiO electrode was washed with DMC and dried in vacuum.

The solvation abilities of solvents toward lithium-ion were studied with the density functional theory by using Gaussian 98W [27]. Reaction enthalpies of a lithium-ion and a solvent molecule were calculated at 298.15 K. Molecular structures were fully optimized with B3LYP/6-31G (d) in advance. Single-point energies were calculated at the B3LYP/6-311 + G (3df, 3pd) by using the optimized geometries.

5.3. Results and Discussion

5.3.1. Electrochemical Reaction of SiO with Lithium.

Figure 5.1 shows cyclic voltammograms of SiO in an electrolyte consisting of 1 mol dm^{-3} $LiClO_4$ dissolved in EC:DMC (1:1 by vol.). Cathodic and anodic peaks were observed in a potential range of 0–0.6 V. These peaks were attributed to the insertion and extraction of lithium-ion at the SiO electrode. The anodic peak was small at the 1st cycle, and it gradually increased at the following cycles. These behaviors implied that the electrochemical reaction at SiO was complicated and that there would be side reactions at the early cycles. To investigate the kinetics of the charge transfer at SiO, we need to know the mechanism of the electrochemical reaction at SiO.

It is generally accepted that SiO consists of two phases: amorphous Si domains and amorphous SiO_2 domains (random mixture (RM) model) [28,29]. Both of these two domains electrochemically react with lithium. One of the most plausible reaction mechanisms is as follows.

Amorphous Si domains: $Si + xLi^+ + xe^- = Li_xSi$

Amorphous SiO_2 domains: $SiO_2 + yLi^+ + ye^- = Li_2O$ + Li-silicates

Nagao *et al.* reported the formation of Li-Si alloys and Li_2O after the electrochemical insertion of

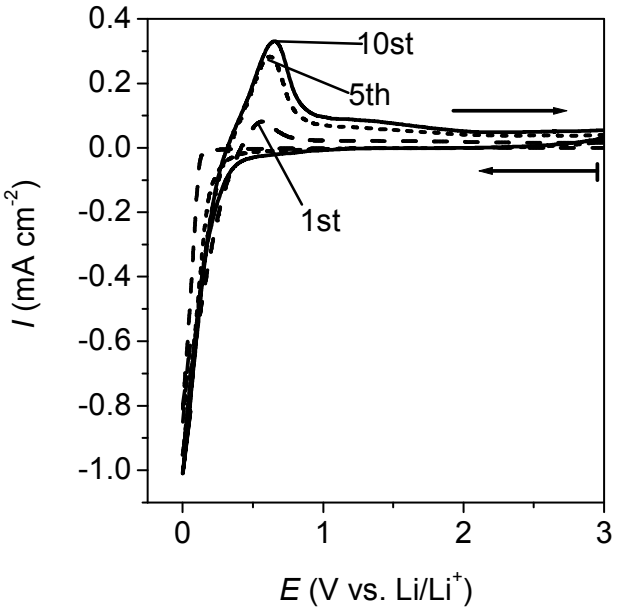

Fig. 5.1 Cyclic voltammograms of SiO in 1 mol dm^{-3} $LiClO_4$ EC:DMC (1:1 by vol.) at 30 ^oC. The scan rate was set at 1 mV s^{-1}.

lithium-ion by neutron elastic scattering measurements [8]. Miyachi *et al.* used X-ray photoelectron spectroscopy (XPS) to elucidate that Li-Si alloys, Li_2O and lithium silicates were formed after 1st charge [10,11]. Kim *et al.* verified the above reaction mechanism by solid-state ^{29}Si and ^{7}Li nuclear magnetic resonance (NMR) technique, electrochemical dilatometry, and charge-discharge measurement [12]. A reaction at amorphous Si domains is an alloying reaction which occurs reversibly to give the charge-discharge capacity. The cathodic and anodic peaks in a potential range of 0 – 0.6 V in the cyclic voltammogram were attributed to the alloying/dealloying reaction of amorphous Si domains. On the other hand, a reaction at amorphous SiO_2 domains is almost irreversible, which might be included in the cathodic peak at the early cycles of the cyclic voltammogram.

5.3.2. Surface Morphology of SiO.

An SEM image of an as-prepared SiO electrode is shown in Figs. 5.2a) and 5.2c). The surface of an SiO electrode was a particle- or needle-like structure with the size of 5–10 μm. To confirm that the morphology remained unchanged during ac impedance spectroscopy, we obtained SEM

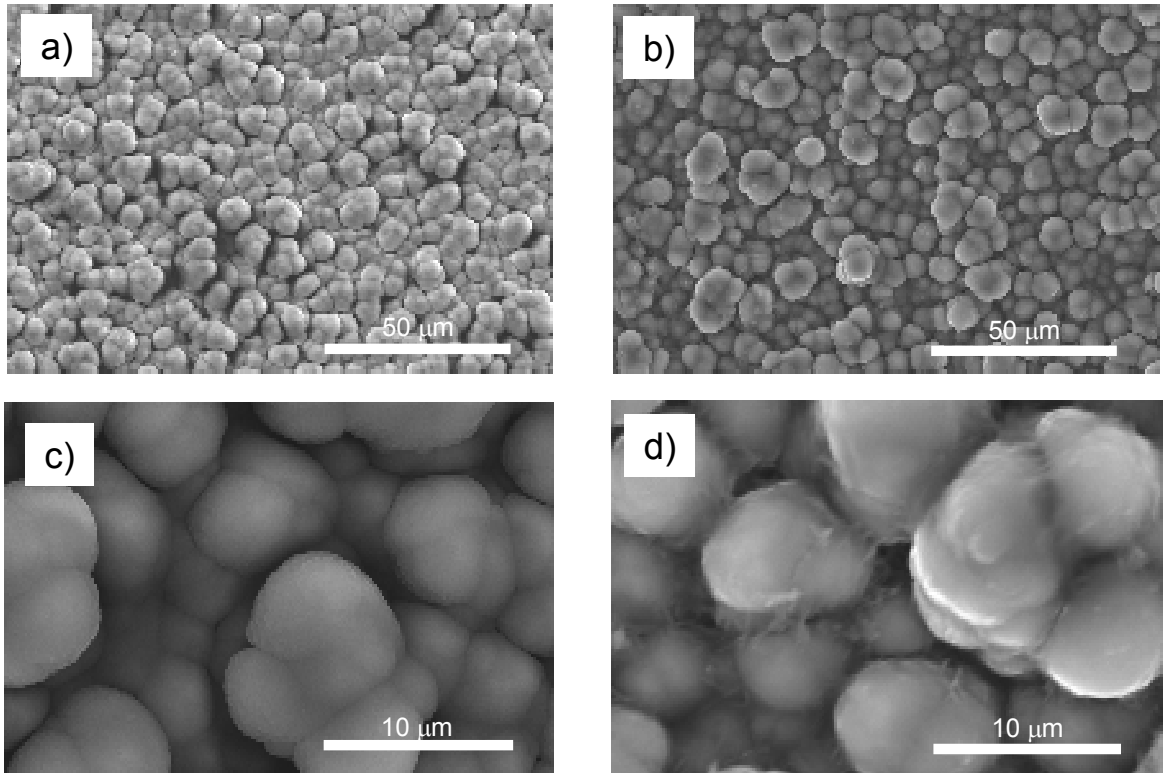

Fig. 5.2 SEM images of SiO a,c) as prepared and b, d) after being held at 0.2 V for 24 hours.

images of SiO which had been held at 0.2 V for 24 hours (Figs. 5.2b and 5.2d). There was no crack on the SiO electrode after being held at 0.2 V, and the surface morphology was almost the same as that of an as-prepared SiO electrode. As shown in Fig. 5.2d), there existed some precipitates on the SiO electrode after being held at 0.2 V. They were formed from the decomposition of electrolytes and would be a kind of solid electrolyte interphase (SEI).

5.5.3. AC Impedance Measurement of a System Consisting of Cu/SiO/Electrolyte/Li.

Figures 5.3 and 5.4 show Nyquist plots of an SiO electrode in an electrolyte consisting of 1 mol dm^{-3} $LiClO_4$ dissolved in EC:DMC (1:1 by vol.) at 303 K. The measurement was conducted after 10 cycles of cyclic voltammetry to make sure that the irreversible reactions (i.e., the reaction at amorphous SiO_2 domains and the decomposition of electrolytes) were terminated. Therefore, the kinetics of the alloying/dealloying reaction of the amorphous Si domains could be investigated by ac impedance spectroscopy. In the Nyquist plot at 1.7 V, one semicircle appeared at a characteristic frequency of 1 kHz. When the electrode potential was lowered to below 1.0 V, another semicircle was observed at a characteristic frequency of 1–0.1 Hz. Two semicircles and Warburg impedance were clearly observed in the Nyquist plot at 0.3 V. Since a three-electrode cell was used, the resistance from the counter electrode (lithium metal) could be neglected. Hence, this system should give the following components of resistance: (1) lithium-ion transport in an electrolyte (R_{sol}), (2) lithium-ion transport in an SEI film (R_{SEI}), (3) alloying reaction resistance at amorphous Si domains (charge-transfer resistance, R_{ct}), (4) lithium diffusion in an electrode, and (5) electron transport in an electrode and at an electrode / current collector interface (R_e). Among these components of resistance, the electron transport (5) and lithium-ion transport in the electrolyte solution (1) usually give no semicircle in the present frequency range due to their high characteristic frequencies. These components of resistance appeared as a Z' intercept in the Nyquist plot. The lithium diffusion in an electrode (4) gave the Warburg impedance (Z_W), which was observed as a straight line with an angle of 45^o from the Z' axis. The remaining two processes (2 and 3) give their own semicircles at each characteristic frequency. The semicircle with a characteristic frequency of 1 kHz was observed at 1.7 V at which the charge-transfer reaction could not occur. Therefore, we assigned this semicircle to the lithium-ion transport in the SEI film (2). The other semicircle with a characteristic frequency of 1 – 0.1 Hz appeared only at below 1.0 V. Hence, this semicircle was attributed to the charge transfer resistance at amorphous Si domains (3).

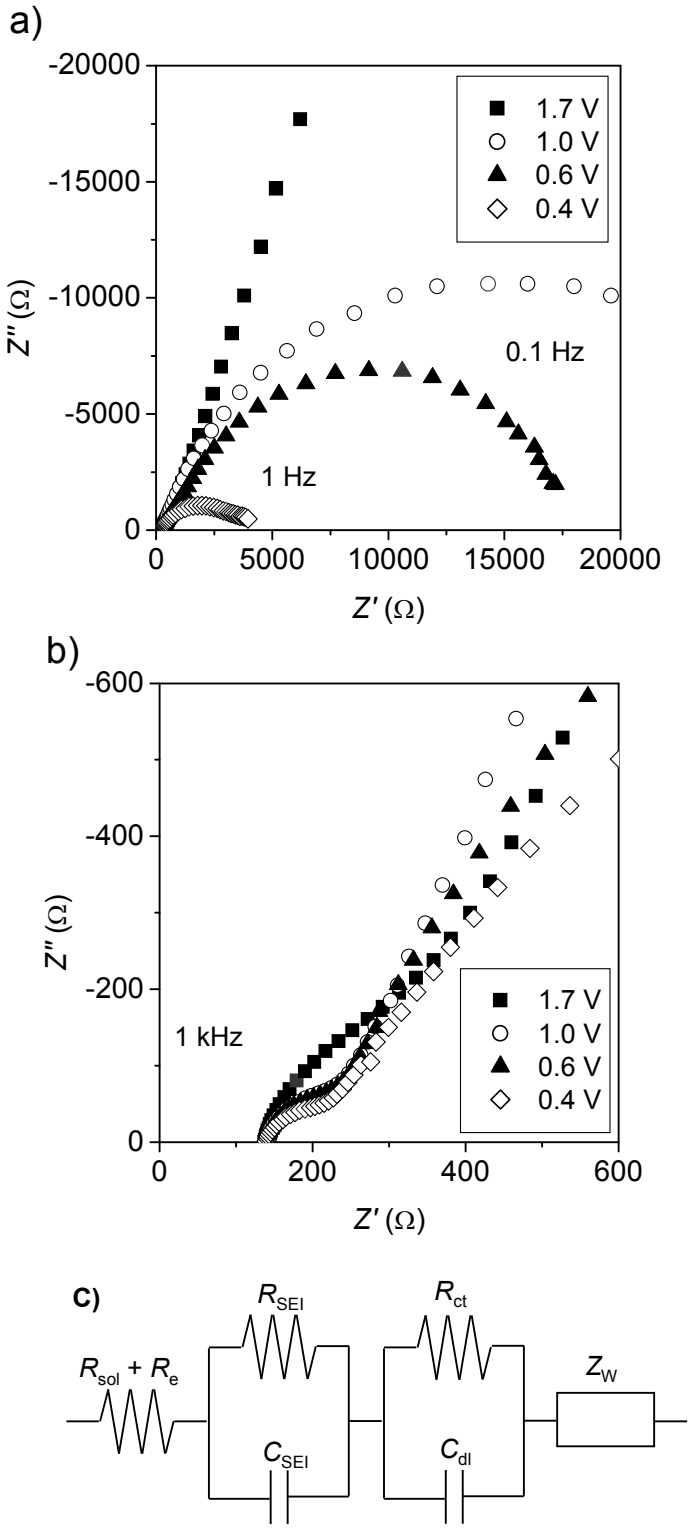

Fig. 5.3 a) Nyquist plots of SiO in 1 mol dm^{-3} $LiClO_4$ / EC:DMC (1:1 by vol.) at various potentials after 10 cycles. b) Enlarged figure of the Nyquist plots at high frequency region. c) Equivalent circuit used for fitting the Nyquist plots.

We configured an equivalent circuit (Fig. 5.3c) to evaluate the charge-transfer resistance and the ion-transport resistance in the SEI. A resistance, two RC-parallel circuits and a Warburg impedance were connected in series. The symbols, C_{SEI} and C_{dl}, denote a capacitance element in an SEI and a double-layer capacitance, respectively. Depending on the shape of the semicircle, a constant phase element (CPE) was properly used as an alternative for C_{dl}. The best fit of the parameters in the equivalent circuit to experimental Nyquist plots gave the values of charge-transfer resistance and the ion-transport resistance in the SEI.

The Nyquist plots showed a drastic change in a potential range of 0.30–0.20 V (Fig. 5.4).

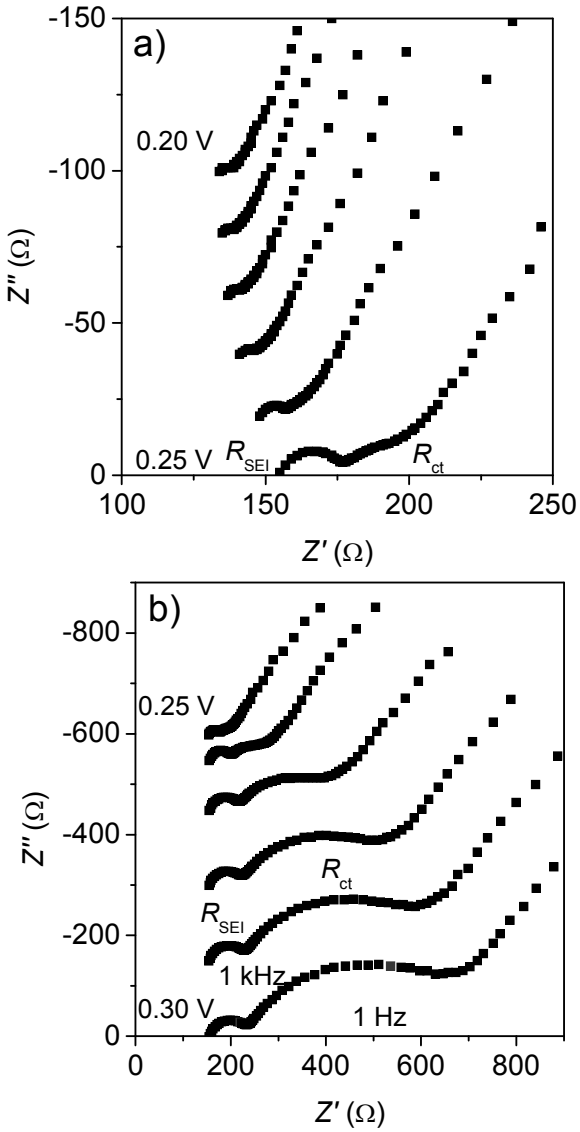

Fig. 5.4 Nyquist plots of SiO in 1 mol dm^{-3} $LiClO_4$ / EC:DMC (1:1 by vol.) after 10 cycles. The potential was changed by 10 mV in the ranges of a) 0.20–0.25 V and b) 0.25–0.30 V.

Figure 5.5 shows the potential dependence of the charge-transfer resistance *(*R_{ct}), the ion-transport resistance in the SEI (R_{SEI}), and the sum of electron-transport resistance (R_e) and lithium-ion transport resistance in the electrolyte (R_{sol}). The R_{ct} value significantly decreased in a potential range of 0.27–0.24 V and then disappeared at below 0.24 V. This variation of R_{ct} was attributed to the change in the activity of lithium in the Li-Si alloy. The $R_e + R_{sol}$ and R_{SEI} values also varied with decreasing potentials in a range of 0.26–0.22 V and these changes were reversible. The change in $R_e + R_{sol}$ was derived from the increasing electronic conductivity of amorphous Si domains due to the alloying with lithium. The reversible change in R_{SEI} would be caused by the volume changes of SiO. This hypothesis is supported by the report by Kim et al. [12]. They observed significant expansion of the SiO electrode below 0.25 V. In our study, the R_{SEI} value also changed significantly below 0.26 V, as shown in Figs. 5.4 and 5.5. Therefore, the volume change of SiO would be a major cause for the change in R_{SEI}, although the detailed mechanism was not clear in this work. An important result here is that R_{ct} was smaller than R_{SEI} at below 0.24 V. These results imply that the charge-transfer reaction at an SiO electrode is relatively fast.

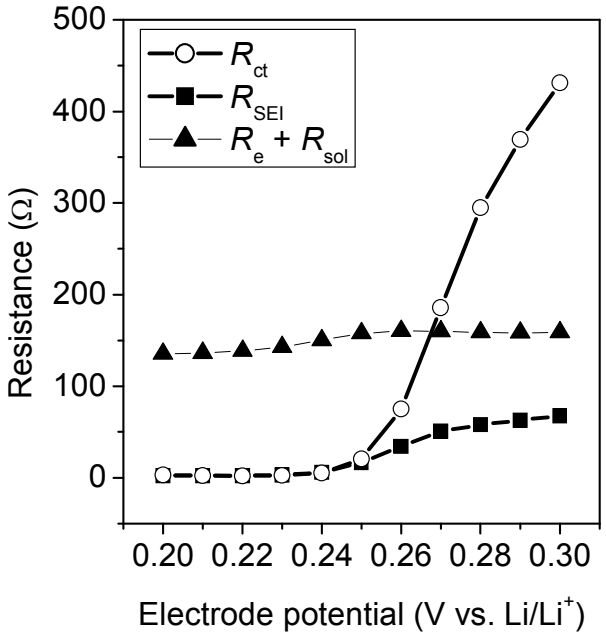

Fig. 5.5 Potential dependence of the charge-transfer resistance (R_{ct}), the ion-transport resistance in the SEI (R_{SEI}), and the sum of electron-transport resistance (R_e) and lithium-ion transport resistance in the electrolyte (R_{sol}).

5.3.4. Activation Energies of Charge Transfer at SiO.

The interfacial conductivity ($1/R_{ct}$) obeys the Arrhenius equation,

$$1/R_{ct} = A\exp(-E_a/RT) \quad (1)$$

where the symbols A, E_a, R and T denote a frequency factor, activation energy, gas constant and absolute temperature, respectively. Hence, the charge-transfer resistance depends on two factors, an activation energy and a frequency factor. We used the activation energy to discuss the kinetics of the charge-transfer reaction at SiO. A study on activation energies is useful for a clear discussion because the activation energy values indicate the essential kinetics of the reaction without the influences of effective surface area, activity of reactants and/or temperature.

Figure 5.6 shows the Arrhenius plots of the interfacial conductivities ($1 / R_{ct}$) at SiO at 0.4 V in various electrolytes. The activation energies of the charge-transfer reaction were evaluated from the slopes of the Arrhenius plots according to the Arrhenius equation (1). The activation energies were around 30 kJ mol^{-1} in the four electrolytes. These values are small compared to those at other electrodes: When a graphite electrode was used, the activation energy of the charge-transfer process was reported to be 53–59 kJ mol^{-1} in EC-based electrolytes [14,15]. In the case of positive electrode materials such as $LiMn_2O_4$ and $LiCoO_2$, the activation energies

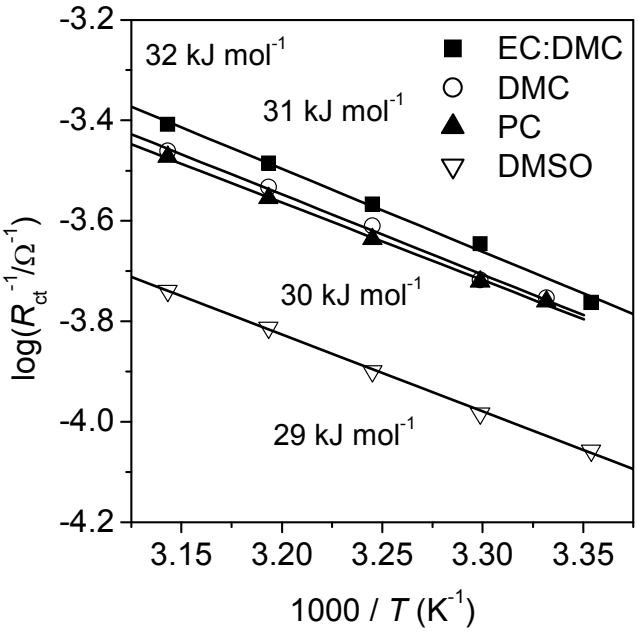

Fig. 5.6 Temperature-dependences of interfacial conductivities ($1 / R_{ct}$) at SiO in various electrolytes. The interfacial conductivities were obtained from the Nyquist plots at 0.4 V in the temperature range of 25–45 ^{o}C.

were evaluated to be around 50 kJ mol^{-1} in PC-based electrolytes [16,17]. Therefore, the small activation energies at SiO suggest that the charge-transfer reaction at SiO is much faster than those at other insertion electrodes.

One of the important points of the present paper is the effect of the desolvation of lithium-ion during the insertion of lithium-ion into the SiO electrode. Our group studied the kinetics of charge (lithium-ion) transfer at various interfaces and reported that the desolvation of lithium-ion was the rate-determining step of charge-transfer reactions, resulting in large activation energies (around 50 kJ mol^{-1} or more) [14,15,18,19]. In the case of the SiO electrode, however, the extremely small activation energies (around 30 kJ mol^{-1}) of the charge-transfer reaction suggest that the desolvation of lithium-ion does not influence the charge transfer at SiO.

A comparison of activation energies in various electrolytes supports this hypothesis about the effect of the desolvation of lithium-ion. Table 5.1 shows activation energies of charge (lithium-ion) transfer at interfaces consisting of various solid and liquid phases. The activation energies greatly varied at a graphite / liquid electrolyte interface [15] and ideal interfaces [17,18] consisting of solid electrolyte ($Li_{0.35}La_{0.55}TiO_3$ or Li-Al-Ti-phosphate-based glass) and liquid electrolyte. The activation energies of charge transfer at these interfaces depended on the enthalpy changes of the reaction (Li^+ + solvent = Li^+-solvent) calculated with the density

Table 5.1: Activation Energies of Charge (Lithium-Ion) Transfer at the Interfaces Consisting of Various Solid and Liquid Phases

Solvent	**Enthalpy change**	E_a **(kJ mol^{-1})**		
		Solid	**Graphite[14,15]**	**SiO**
DMSO	-235.5	70[b]	cointercalatio	29
PC	-217.1	57[b]	exfoliation	30
EC:DMC	-210.3 (EC)	51[c]	58	32
FEC[d]	-190.3	32[c]	-	-
DMC	-185.5	32[b]	40	31

[a] Reaction enthalpy of the reaction (Li^+ + solvent = Li^+-solvent).
[b] Solid electrolyte = Li-Al-Ti-phosphate-based glass electrolyte (OHARA glass).
[c] Solid electrolyte = $Li_{0.35}La_{0.55}$ TiO_3 (LLT).
[d] Fluoroethylene carbonate.

functional theory by Gaussian 98W [27]. Sinc

e the enthalpy changes indicate the solvation abilities of solvents, the correlation between the activation energies and the enthalpy changes suggests that the activation energies reflect the energy for desolvation of lithium-ion from the solvent. In the case of the SiO electrode, however, the activation energies of charge transfer remained unchanged at around 30 kJ mol^{-1} in the four electrolytes. Based on these results, it is sure that the kinetics of the charge transfer at SiO is not influenced by the compositions of electrolytes and that the desolvation of lithium-ion is not the rate-determining step of the charge transfer at SiO.

The results in the present study indicate that the kinetics of the electrochemical reaction at SiO is quite different from those at other insertion electrodes. As discussed in the previous part of this paper, the electrochemical reaction at SiO is the alloying/dealloying reaction at the amorphous Si domains. We consider that the absence of the effect of the desolvation is inherent in the alloying/dealloying reaction. Although the detailed mechanism is not yet clear, the small activation energies at SiO suggest that the SiO electrode has a kinetic advantage over other insertion electrodes such as graphite.

5.4. Conclusions

The activation energies of charge (lithium-ion) transfer at the SiO electrode were small compared to those at other insertion electrodes such as graphite. Therefore, the SiO electrode has an advantage in the kinetic aspect over other electrodes. Furthermore, the activation energies of charge transfer at SiO remained unchanged in various electrolytes. These results suggest that the charge-transfer kinetics at SiO is not influenced by the desolvation of lithium-ion which is the rate-determining step of charge transfer at other electrodes.

References

[1] Winter, M.; Besenhard, J. O. *Electrochim. Acta* **1999**, *45*, 31.

[2] Tarascon, J. M.; Armand, M. *NATURE* **2001**, *414*, 359.

[3] Boukamp, B. A.; Lesh, G. C.; Huggins, R. A. *J. Electrochem. Soc.* **1981**, *128*, 725.

[4] Besenhard, J. O.; Yang, J.; Winter, M. *J. Power Sources* **1997**, *68*, 87.

[5] Yang, J.; Takeda, Y.; Imanishi, N.; Capiglia, C.; Xie, J. Y.; Yamamoto, O. *Solid State Ionics* **2002**, *152–153*, 125.

[6] Netz, A.; Huggins, R. A.; Weppner, W. *J. Power Sources* **2003**, *119–121*, 95.

[7] Netz, A.; Huggins, R. A. *Solid State Ionics* **2004**, *175*, 215.

[8] Nagao, Y.; Sakaguchi, H.; Honda, H.; Fukunaga, T.; Esaka, T. *J. Electrochem. Soc.* **2004**, *151*, A1572.

[9] Tabuchi, T.; Yasuda, H.; Yamachi, M. *J. Power Sources* **2005**, *146*, 507.

[10] Miyachi, M.; Yamamoto, H.; Kawai, H.; Ohta, T.; Shirakata, M. *J. Electrochem. Soc.* **2005**, *152*, A2089.

[11] Miyachi, M.; Yamamoto, H.; Kawai, H. *J. Electrochem. Soc.* **2007**, *154*, A376.

[12] Kim, T.; Park, S.; Oh, S. M. *J. Electrochem. Soc.* **2007**, *154*, A1112.

[13] Yang, X.; Wen, Z.; Xu, X.; Lin, B.; Huang, S. *J. Power Sources* **2007**, *164*, 880.

[14] Abe, T.; Fukuda, H.; Iriyama, Y.; Ogumi, Z. *J. Electrochem. Soc.* **2004**, *151*, A1120.

[15] Yamada, Y.; Iriyama, Y.; Abe, T.; Ogumi, Z. *Langmuir* **2009**, *25*, 12766.

[16] Yamada, I.; Abe, T.; Iriyama, Y.; Ogumi, Z. *Electrochem. Commun.* **2003**, *5*, 502.

[17] Yamada, I.; Iriyama, Y.; Abe, T.; Ogumi, Z. *J. Power Sources* **2007**, *172*, 933.

[18] Abe, T.; Sagane, F.; Ohtsuka, M.; Iriyama, Y.; Ogumi, Z. *J. Electrochem. Soc.* **2005**, *152*, A2151.

[19] Yamada, Y.; Sagane, F.; Iriyama, Y.; Abe, T.; Ogumi, Z. *J. Phys. Chem. C* **2009**, *113*, 14528.

[20] Inaguma, Y.; Chen, L. Q.; Itoh, M.; Nakamura, T. *Solid State Ionics* **1994**, *70/71*, 196.

[21] Inaguma, Y.; Chen, L. Q.; Itoh, M.; Nakamura, T.; Uchida, T.; Ikuta, H.; Wakihara, M. *Solid State Commun.* **1993**, *86*, 689.

[22] Bohnke, O.; Bohnke, C.; Fourquet, J. L. *Solid State Ionics* **1996**, *91*, 21.

[23] Fu, J. *Solid State Ionics* **1997**, *96*, 195.

[24] Ding, M. S.; Jow, T. R. *J. Electrochem. Soc.* **2003**, *150*, A620.

[25] Ding, M. S.; Xu, K.; Jow, T. R. *J. Electrochem. Soc.* **2005**, *152*, A132.

[26] Ding, M. S. *J. Electrochem. Soc*. **2004**, *151*, A40.

[27] Frisch, M. J.; Trucks, G. W.; Schlegel, H. B.; Scuseria, G. E.; Robb, M. A.; Cheeseman, J. R.; Zakrzewski, V. G.; Montgomery, J. A., Jr.; Stratmann, R. E.; Burant, J. C.; Dapprich, S.; Millam, J. M.; Daniels, A. D.; Kudin, K. N.; Strain, O. F. M. C.; Tomasi, J.; Barone, B.; Cossi, M.; Cammi, R.; Mennucci, B.; Pomelli, C.; Adamo, C.; Clifford, S.; Ochterski, J.; Petersson, G. A.; Ayala, P. Y.; Cui, Q.; Morokuma, K.; Malick, D. K.; Rabuck, A. D.; Raghavachari, K.; Foresman, J. B.; Ciolovski, J.; Ortiz, J. V.; Stefanov, V. V.; Liu, G.;

Liashensko, A.; Piskorz, P.; Komaroni, I.; Gomperts, R.; Martin, R. L.; Fox, D. J.; Keith, T.; Al-Laham, M. A.; Peng, C. Y.; Nanayakkara, A.; Gonzalez, C.; Challacombe, M.; Gill, P. M. W.; Johnson, B.; Chen, W.; Wong, M. W.; Andres, J. L.; Head-Gordon, M.; Replogle, E. S.; Pople, J. A. *Gaussian 98*; Gaussian Inc.: Pittsburgh, PA, 1998.

[28] Brady, G. W. *J. Phys. Chem.* **1959**, *63*, 1119.

[29] Hohl, A.; Wieder, T.; Aken, P. A.; Weirich, T. E.; Denninger, G.; Vidal, M.; Osward, S.; Deneke, C.; Mayer, J.; Fuess, H. *J. Non-Cryst. Solids* **2003**, *320*, 255.

Part 3

Frequency Factor of Electrochemical Lithium Intercalation into Graphite

Chapter 6

Variation in Density of Electronic States at the Surface of Graphite and Its Influence on the Kinetics of Heterogeneous Electron Transfer

6.1. Introduction

The electrochemistry of graphite has long been of great interest to researchers in a wide variety of fields [1]. One of the factors drawing much attention is the expanding applicability of graphite electrodes. Graphite electrodes have been used not only in academic fields (e.g., electrochemical analysis), but also in industrial fields (e.g., iron and aluminum manufacturing). In addition, of recent interest are the applications to electrochemical energy storage/conversion devices such as lithium-ion batteries, electric-double-layer capacitors, and fuel cells. A growing demand for such devices puts ever-increasing importance on graphite electrodes, driving many researchers to vigorous studies on the electrochemistry of graphite.

Another driver for such intense researches is the uniqueness of the electrochemistry of graphite. Wightman *et al.* [2] and McCreery *et al*. [3–5] reported that the kinetics of heterogeneous electron transfer is different at the two planes, edge and basal planes, of graphite. A carefully-cleaved basal plane of highly oriented pyrolytic graphite (HOPG) is extremely inactive, retarding significantly the electron transfer of outer- and inner-sphere reactions, although the edge plane of HOPG is as active as glassy carbon or metal electrodes. Such a behavior is explained by the amount of edge orientations exposed on the surface of an HOPG basal plane. There are functional groups, e.g. carbonyl, hydroxyl, or carboxyl groups, at an edge orientation [1], which may facilitate inner-sphere electron transfer [6,7]. On a carefully-cleaved basal plane of HOPG, an edge orientation exists only at defects or grain boundaries. Therefore, the inner-sphere electron transfer is slow on an HOPG basal plane. As for the outer-sphere electron transfer, the density of electronic states (DOS) at the near-surface of graphite may play an important role in determining the kinetics, as pointed out by Cline *et al*. [4]. The basal plane of HOPG has considerably low DOS [8,9] compared to those at metal [10], resulting in the slow kinetics of outer-sphere electron transfer. An interesting point is that the kinetics of an outer-sphere redox couple varies depending on the amount of edge orientations on the basal planes of

HOPG [4]. These results led us to consider that there should be a variation in the surface DOS depending on the amount of edge orientations on an HOPG basal plane.

Surface DOS on an HOPG basal plane can be evaluated from a capacitance measurement. The electric double-layer capacitance on the basal plane of HOPG is exceptionally small due to the presence of a space-charge layer, an electric double layer formed inside graphite because of the small carrier density, i.e. small DOS, of graphite [11−13]. Gerischer *et al.* developed a theory that relates the space-charge-layer capacitance with DOS and demonstrated the evaluation of DOS on the basal plane of HOPG from a capacitance measurement [8,9]. DOS measured by this method is the one at the surface of an HOPG basal plane where a space-charge layer exists. Therefore, this method is useful to verify the variation in surface DOS on HOPG basal planes.

In the present study, we used the basal plane of HOPG as a model electrode for graphite and evaluated the surface DOS on it. We discuss a variation in the surface DOS on graphite, taking the amount of edge orientations into consideration. Furthermore, we evaluated the kinetics of an outer-sphere redox couple, $Ru(NH_3)_6^{3+/2+}$, on the basal plane of HOPG and discussed the relation between the surface DOS and the kinetics of the outer-sphere redox on HOPG basal planes.

6.2. Experimental Methods

A basal plane of HOPG (Momentive Performance Materials Quartz, Inc.) was used as a model electrode for graphite. The grade of HOPG was STM-1 and ZYH. The *c*-axis orientation of STM-1 is higher than that of ZYH, indicating less edge orientations on the basal plane of HOPG STM-1. The basal plane of HOPG was carefully cleaved with an adhesive tape so that the defect density should be extremely low.

Electrochemical measurements were carried out with a three-electrode cell (Fig. 6.1), which was made of polytetrafluoroethylene (PTFE) and SUS. An HOPG electrode was fixed between the PTFE component and the SUS current collector. Only the basal plane of HOPG has contact with the electrolyte solution. The contact area of the HOPG basal plane and the electrolyte was kept constant at 0.38 cm^2 with an o-ring. Platinum mesh and silver-silver chloride (Ag/AgCl) were used as counter and reference electrodes, respectively. Unless otherwise noted, the potentials in this paper are referenced to Ag/AgCl in a saturated KCl aqueous solution (0.197 V vs. NHE).

The DOS at the surface of an HOPG basal plane was evaluated from a capacitance measurement. The double-layer capacitance of an HOPG basal plane was measured by an ac

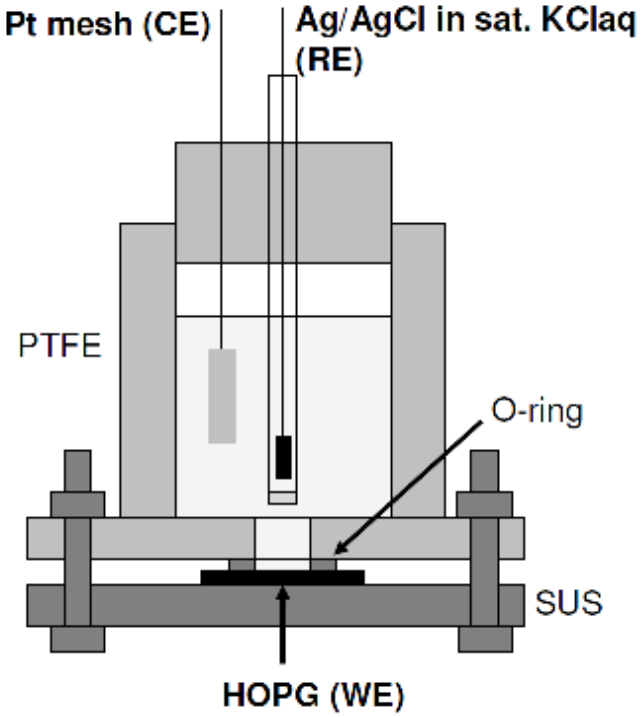

Fig. 6.1 Schematic diagram of a three-electrode cell.

method with an applied ac voltage of 10 mV. An aqueous solution containing 1 mol dm^{-3} KCl (Nacalai Tesque, Inc., Japan) was used as an electrolyte. To obtain potential dependence of the capacitance, the frequency was fixed at 100 Hz and the electrode potential was stepped by 20 mV (step duration: 10 s) in a range between –0.40 V and 0 V.

The rate constant for heterogeneous electron transfer of $Ru(NH_3)_6^{2+/3+}$ on an HOPG basal plane was evaluated from a cyclic voltammogram. An electrolyte was 1 mol dm^{-3} KCl aqueous solution containing 1 mmol dm^{-3} $Ru(NH_3)_6Cl_3$ (Aldrich). The cyclic voltammetry was conducted in a potential range between 0.2 V and –0.4 V with a scan rate of 100 mV s^{-1}. Digital simulation of cyclic voltammogram was configured under a quasi-reversible condition. The Butler-Volmer equation and the Fick's diffusion law were used for the theoretical description of cyclic voltammogram [14]. In the digital simulation, the diffusion coefficient of $Ru(NH_3)_6^{3+/2+}$ was set at 4.0×10^{-6} cm^2 s^{-1}. The electron-transfer rate constant for $Ru(NH_3)_6^{2+/3+}$ was evaluated by fitting the simulated cyclic voltammogram to the experimental one.

6.3. Results and Discussion

6.3.1. Evaluation of Surface DOS from a Capacitance Measurement.

We used Gerischer's method [8] to evaluate the DOS at an HOPG basal plane. This method starts from measuring the double-layer capacitance at an HOPG basal plane. Figure 6.2 shows the potential dependences of the double-layer capacitances of four HOPG samples in 1 mol dm^{-3} KCl aqueous solution. The ac frequency was set at 100 Hz. We confirmed in advance that the deviation in the capacitance with frequency was below 5 % (Fig. 6.3). The measured capacitance was very small (< 4.5 μF cm^{-2}) compared to those at metal electrodes (e.g. 15–20 μF cm^{-2}). Such small capacitances derived from the presence of a space-charge layer inside the HOPG electrode.

As reported by Randin et al. [11,12] and Gerischer et al. [8,9], the electric double layer at an HOPG/electrolyte interface consists of three components of capacitor: diffusion-double-layer capacitance (C_{diff}), Helmholtz-double-layer capacitance (C_H), and space-charge-layer capacitance (C_{SC}) (Fig. 6.4a). In an equivalent circuit, these three components of capacitor are connected in series (Fig. 6.4b). Therefore, the experimentally measured capacitance (C_{exp}) is given by the following equation,

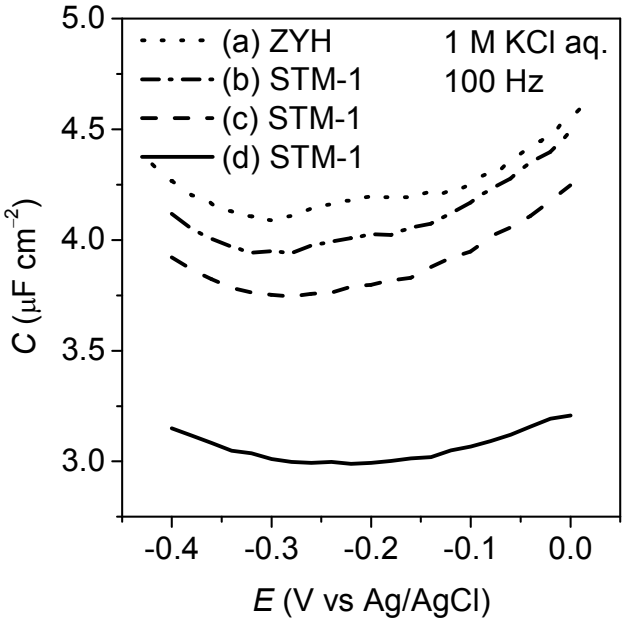

Fig. 6.2 Electric-double-layer capacitances against given potentials on four HOPG basal planes in 1 mol dm^{-3} KCl aqueous solution. The frequency was set at 100 Hz.

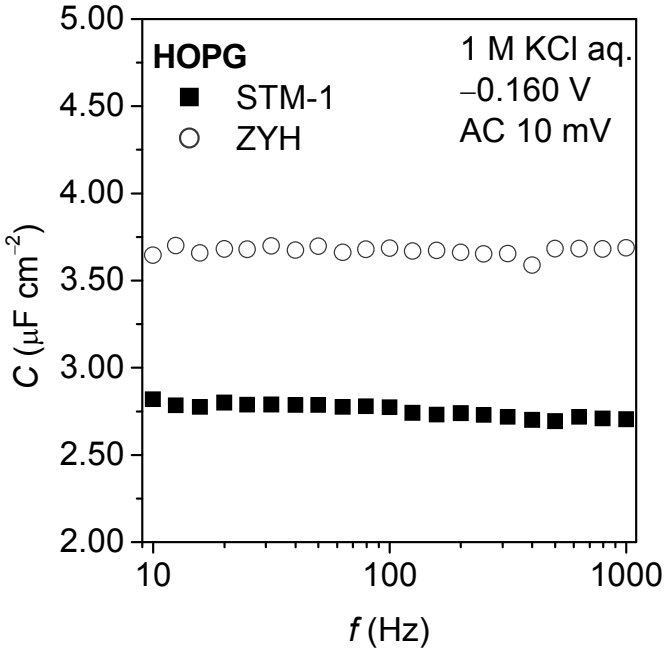

Fig. 6.3 Frequency dependences of electric-double-layer capacitances on basal planes of HOPG STM-1 and ZYH grades in 1 mol dm^{-3} KCl aqueous solution. The electrode potential was kept at −0.160 V and ac voltage was set at 10 mV.

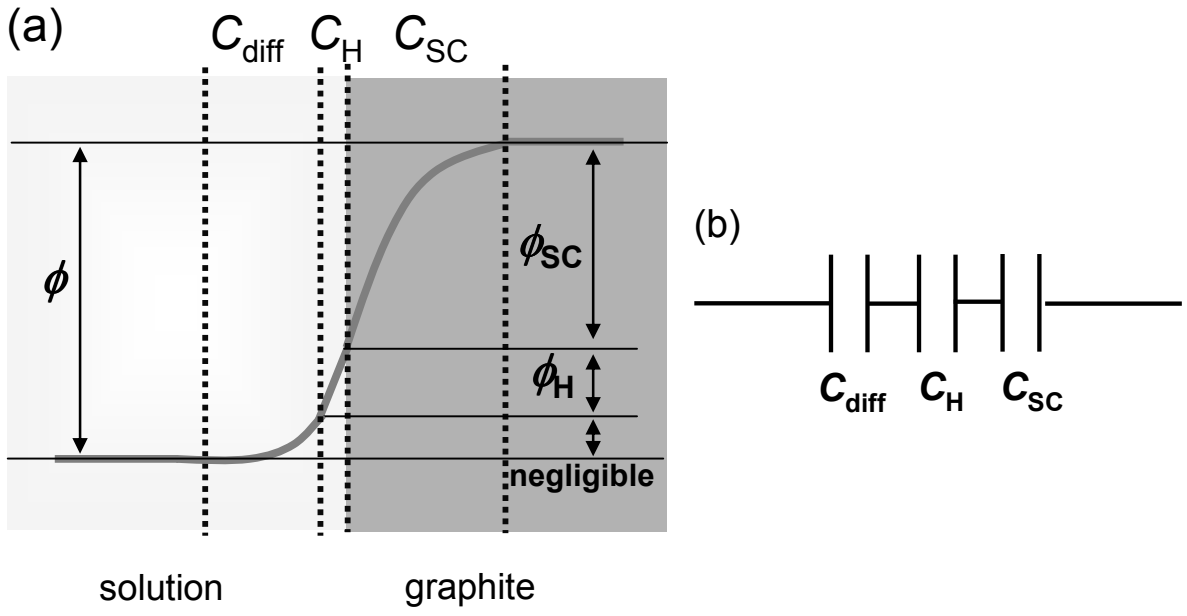

Fig. 6.4 (a) Structure of electric double layer at graphite/solution interface and (b) its equivalent circuit. There are three kinds of electric double layers in series at the interface: diffusion double layer (C_{diff}), Helmholtz double layer (C_H), and space-charge layer (C_{SC}).

$$\frac{1}{C_{exp}} = \frac{1}{C_{diff}} + \frac{1}{C_H} + \frac{1}{C_{SC}} \quad (1).$$

Among these three components of capacitor, C_{SC} is the smallest at a HOPG basal plane [12]. Hence, $1/C_{SC}$ is the largest in the right side of eq. 1, significantly contributing to $1/C_{exp}$. The space-charge layer derives from the small carrier density (i.e., low DOS) at the near-surface of a HOPG basal plane. Therefore, the surface DOS at a HOPG basal plane can be measured from C_{exp}. Gerischer *et al*. reported the following relation between surface DOS and C_{SC} as a function of the potential drop at a space-charge layer, ϕ_{SC}, in a unit of eV [8,9],

$$D(\phi_{SC}) = \frac{1}{e\varepsilon\varepsilon_0}\left[\int_0^{\phi_{SC}} C_{SC}(\phi_{SC})d\phi_{SC}\,\frac{dC_{SC}(\phi_{SC})}{d\phi_{SC}} + \{C_{SC}(\phi_{SC})\}^2\right] \quad (2)$$

where $D(\phi_{SC})$ is DOS at the energy level of ϕ_{SC}, e is the charge of electron, ε_0 is the permittivity of free space, and ε is the relative permittivity of graphite (3.28) [15], respectively. To evaluate DOS from eq. 2, we need to know C_{SC} as a function of ϕ_{SC}.

First, eq. 1 offers a way to C_{SC}. In an electrolyte with relatively high concentration, C_{diff} is generally very large and thus, $1/C_{diff}$ can be neglected in eq 1 [8,9,12]. As a result, C_{SC} at a given electrode potential can be calculated from eq. 3,

$$C_{SC} = (C_H - C_{exp})/C_H C_{exp} \quad (3).$$

We cannot measure the exact C_H value at a HOPG basal plane, but C_H can be speculated from a measured capacitance at a metal electrode. Since C_H is 15-30 μF cm^{-2} at a metal electrode with small surface charge (< 10 μC cm^{-2}) [16,17], we set 20 μF cm^{-2} for the estimated C_H value at a HOPG basal plane. Using eq. 3 and Fig. 6.2, we can obtain C_{SC} as a function of the electrode potential (Fig. 6.5). Second, ϕ_{SC} can be calculated using C_{SC} and C_H at a given electrode potential. If we neglect the contribution from diffusion double layer, the overall potential drop at the electrode / electrolyte interface, ϕ, consists of two components as shown in the following equation,

$$\phi = \phi_H + \phi_{SC} \quad (4)$$

where ϕ_H denotes the potential drop at the Helmholtz double layer and ϕ is referenced to the pzc of the HOPG electrode (–0.24 V vs Ag/AgCl). Since the same amount of charge is accumulated at C_H and C_{SC}, the following equation is given:

$$C_H\,\phi_H = C_{SC}\,\phi_{SC} \quad (5).$$

Then, the value of ϕ_{SC} can be obtained from eqs. 4 and 5. Above reasoning offers C_{SC} as a function of ϕ_{SC} (Fig. 6.6), leading to the evaluation of the surface DOS from eq. 2.

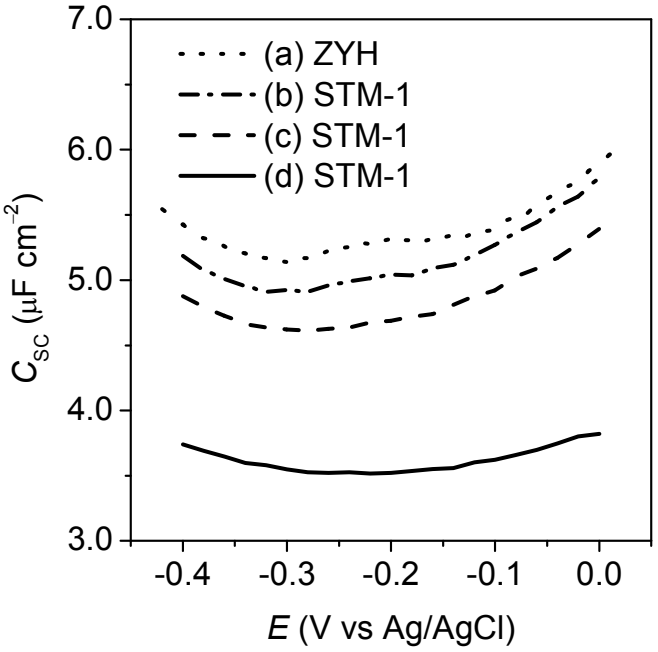

Fig. 6.5 Space-charge-layer capacitances (C_{SC}) against given potentials on four HOPG basal planes evaluated from a capacitance measurement in 1 mol dm^{-3} KCl aqueous solution.

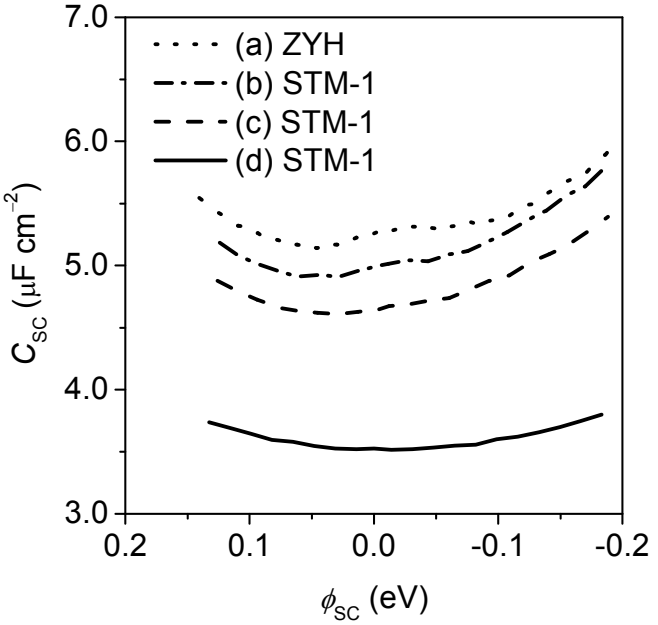

Fig. 6.6 Space-charge-layer capacitances (C_{SC}) on four HOPG basal planes as a function of the potential drop at the space-charge layer, ϕ_{SC}.

Figure 6.7 shows DOS at four HOPG basal planes as a function of ϕ_{SC}. The ϕ_{SC} value is referenced to the potential of zero charge (pzc) of an HOPG basal plane (–0.24 V). Note that the DOS evaluated here is the one at the near-surface of an HOPG basal plane where the space-charge layer exists. The minimal values of DOS range from 2×10^{20} to 7×10^{20} eV^{-1} cm^{-3}, depending on HOPG samples used. These values are in excellent agreement with those previously reported [8,18,19] and thus, the experiment in the present study is accurate and reliable.

6.3.2. Variation in Surface DOS at HOPG Basal Planes.

The variation in surface DOS is reflected in measured double-layer capacitance, because the space-charge-layer capacitance is dominant over other double-layer capacitances, Helmholtz and diffusion double layers. Randin and Yeager reported that glassy carbon and an HOPG edge plane showed a large capacitance compared to those at an HOPG basal plane [12,13]. Rice *et al*. showed that the laser activation of an HOPG basal plane resulted in a significant increase of a capacitance, which could not be explained only by the roughness of the electrode surface [20]. These results indicate that an edge orientation plays an important role in the variation in DOS. In

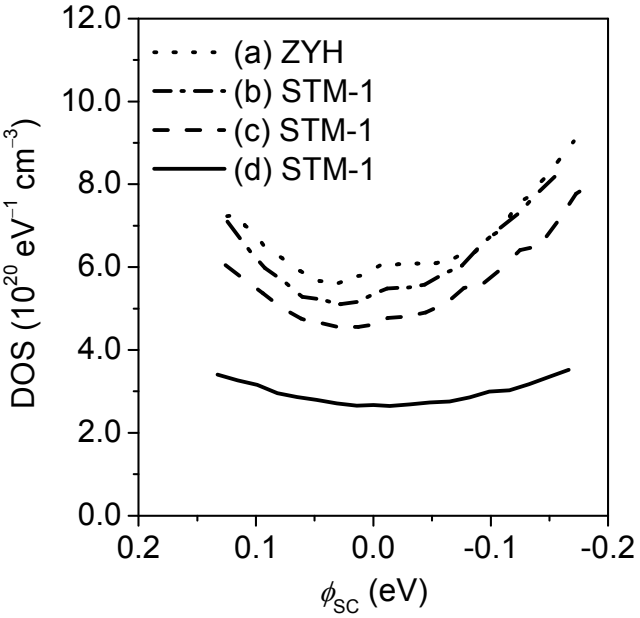

Fig. 6.7 Density of electronic states (DOS) at the surface of four HOPG basal planes measured from capacitance measurements.

Fig. 6.7, however, we cannot find a large difference between the DOS at the two HOPG grades, STM-1 and ZYH, although we expect a large number of edge orientations (e.g., defects and grain boundaries) on the basal plane of HOPG ZYH. This is because the amount of edge orientations on an HOPG basal plane is determined by the cleaving process, rather than the nature of HOPG itself. We clean the basal plane of HOPG by carefully cleaving it, but this process gives a difference in the amount of edge orientations (i.e., defects) on HOPG basal planes. Only a small amount of edge orientations significantly increases DOS at the near-surface of an HOPG basal plane to the extent that the difference in the capacitances is measurable.

It is important to consider the role of edge orientations in increasing DOS on an HOPG basal plane. Kobayashi carried out a calculation with a density functional theory to show local density of states (LDOS) at several carbon atoms on a graphite basal plane [21]. He clarified that LDOS is not homogeneous on the whole surface of graphite; LDOS is very high on an edge plane and decreases on a basal plane far away from the edge plane. Since the DOS measured here is an average on the whole surface of an HOPG basal plane, a large amount of edge orientations (e.g., defects and grain boundaries) on an HOPG basal plane leads to the increase of measured DOS. Consequently, the amount of edge orientations on an HOPG basal plane results in the variation in surface DOS.

6.3.3. Evaluation of Kinetics of Heterogeneous Electron Transfer of $Ru(NH_3)_6^{3+/2+}$ on HOPG Basal Planes.

Figure 6.8 shows cyclic voltammograms of the basal planes of four HOPG samples in 1 mol dm^{-3} KCl aqueous solution containing 1 mmol dm^{-3} $Ru(NH_3)_6Cl_3$. The HOPG samples (a)–(d) correspond to those in the results of the capacitance and DOS (Figs. 6.2, 6.5-6.7). The solid lines indicate the experimental curves at a scan rate of 100 mV s^{-1}. The redox reaction of $Ru(NH_3)_6^{3+/2+}$ was observed as cathodic and anodic peaks in each voltammogram. The peak separation, ΔE_p, of the cathodic and anodic sweeps indicates the rate of heterogeneous electron transfer at each HOPG sample. The four cyclic voltammograms differ in ΔE_p, indicating that the electron-transfer rate of $Ru(NH_3)_6^{3+/2+}$ is different on the four HOPG basal planes. Among the four HOPG samples, sample (a) showed the fastest redox reaction, and sample (d) the slowest.

We evaluated the standard rate constant, k^o, of $Ru(NH_3)_6^{3+/2+}$ from the cyclic voltammograms. The broken lines in Fig. 6.8 show the fitting curves of digital simulation to the experimental curves. The fitting of the digital simulation gives k^o of $Ru(NH_3)_6^{3+/2+}$. The k^o

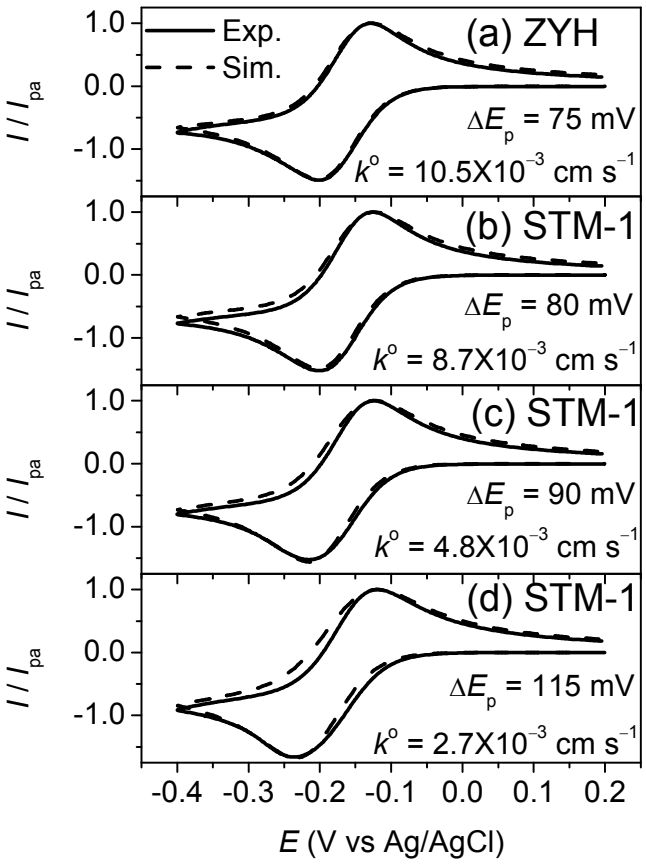

Fig. 6.8 Cyclic voltammograms (solid lines) of four HOPG basal planes in 1 mol dm^{-3} KCl aqueous solution containing 1 mmol dm^{-3} $Ru(NH_3)_6Cl_3$, with the current normalized by the anodic peak current (I_{pa}). The scan rate was set at 100 mV s^{-1}. The broken lines denote the fitting curves of digital simulation. The four HOPG basal planes correspond to those in Figs. 6.2, 6.5-6.7.

values ranged from $2X10^{-3}$ cm s^{-1} to $1X10^{-2}$ cm s^{-1}, while the transfer coefficient (α) remained constant at 0.60 in the present experimental condition. We also conducted cyclic voltammetry at various scan rates between 30 and 400 mV s^{-1} and confirmed that the deviation in k^o is below 15 % at these scan rates (Fig. 6.9). It is interesting to note the relation between surface DOS and k^o of $Ru(NH_3)_6^{3+/2+}$ on samples (a) – (d). At HOPG sample (a), both k^o and the DOS are high compared to those at other samples, while at HOPG sample (d), both of them are the smallest of those at the four.

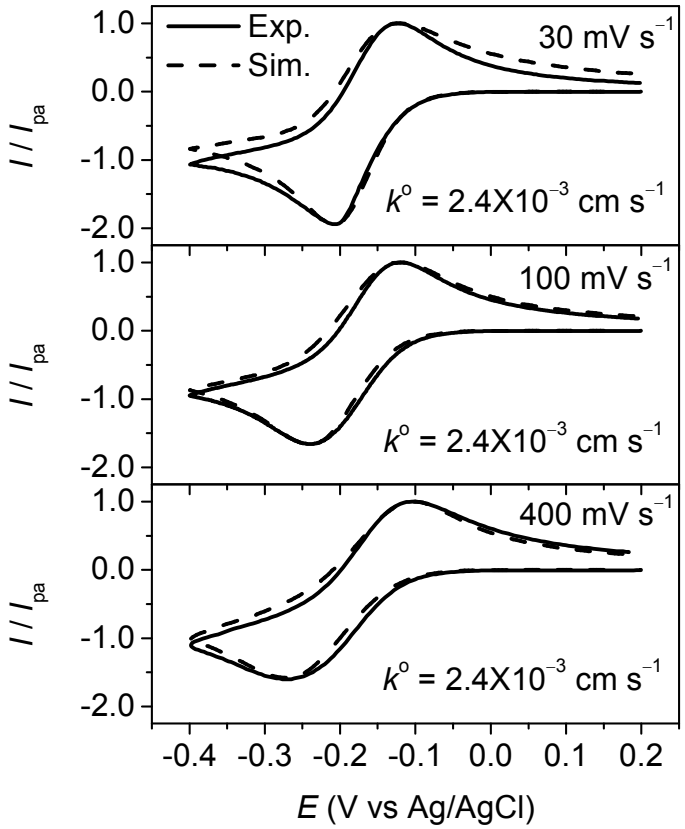

Fig. 6.9 Cyclic voltammograms (solid lines) of an HOPG basal plane (STM-1 grade) in 1 mol dm^{-3} KCl aqueous solution containing 1 mmol dm^{-3} $Ru(NH_3)_6Cl_3$. The broken lines denote the fitting curves. The scan rate was set at 30, 100, and 400 mV s^{-1}.

6.3.4. Influence of Surface DOS on Kinetics of Heterogeneous Electron Transfer.

Before moving to a discussion on the influence of DOS, we discuss several factors that may influence the kinetics of heterogeneous electron transfer: (*i*) surface area, i.e. electrode roughness, (*ii*) functional groups, (*iii*) double-layer effect, and (*iv*) DOS. Surface area (*i*) is not the cause for the variation in k^o of $Ru(NH_3)_6^{3+/2+}$. Compton's group studied the relation between the electrode roughness of glassy carbon and the shape of cyclic voltammogram [22]. They concluded that surface roughness produced by polishing or scratching does not make a significant influence on the kinetics of electron transfer of $Ru(NH_3)_6^{3+/2+}$. For an HOPG basal plane, surface roughness produced by cleaving is extremely small. Therefore, the variation in k^o at HOPG basal planes should not be attributed to surface area (i.e., surface roughness). The influence of functional groups (*ii*) is also excluded from the factors, with the mechanism of electron transfer of

$Ru(NH_3)_6^{3+/2+}$ considered. McCreery *et al.* showed that the electron transfer-reaction of $Ru(NH_3)_6^{3+/2+}$ proceeds in an outer-sphere way [1,4]. Therefore, the presence of functional groups on an edge orientation is not the reason for the variation in k^o on HOPG basal planes. Next, Royea *et al.* showed that the double-layer effect (*iii*) is negligible at a semiconductor electrode under a depletion condition, because the potential drop at Helmholtz double layer is very small [23]. Likewise, the potential drop at Helmholtz double layer is small at an HOPG basal plane. In addition, the formal potential of $Ru(NH_3)_6^{3+/2+}$ (–0.16 V) is near pzc of an HOPG basal plane (–0.24 V). Hence, it is reasonable to consider that the double-layer effect (*iii*) is negligibly small on the redox reaction of $Ru(NH_3)_6^{3+/2+}$ at an HOPG basal plane. With all of the discussion taken into consideration, DOS (*iv*) is the most plausible factor to explain the variation in k^o of $Ru(NH_3)_6^{3+/2+}$ at HOPG basal planes.

Figure 6.10 shows the relation between k^o of $Ru(NH_3)_6^{3+/2+}$ and surface DOS at more than 20 HOPG basal planes. The values of DOS used here are those at the energy level corresponding to the formal potential of $Ru(NH_3)_6^{3+/2+}$ (–0.160 V vs Ag/AgCl). It is obvious that the DOS and the electron-transfer rate constant have a proportional relationship. Such a proportional correlation has been theoretically expected at a graphite electrode. Royea *et al.* applied Fermi golden rule to

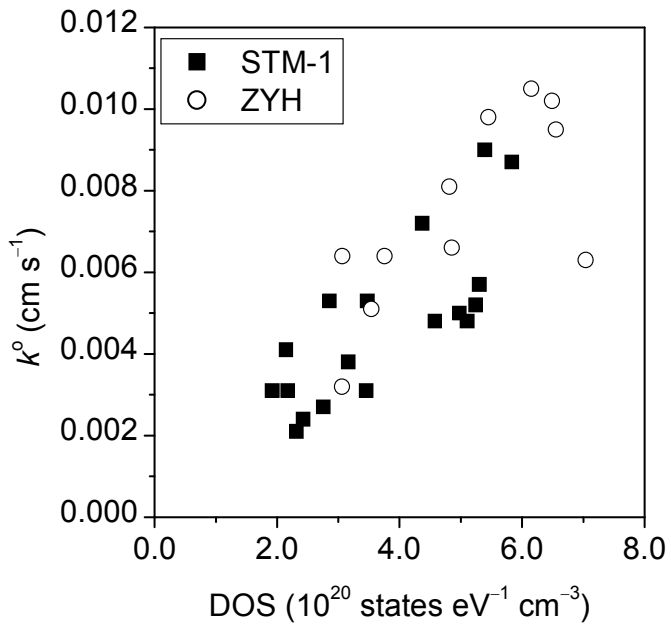

Fig. 6.10 Correlation between electron-transfer rate constant (k^o) of $Ru(NH_3)_6^{3+/2+}$ on HOPG basal planes and DOS at the energy level corresponding to the formal potential of $Ru(NH_3)_6^{3+/2+}$.

the description of the kinetics of heterogeneous electron transfer and reported a theoretical relation between the DOS and the kinetics of electron transfer at a semimetal electrode [24,25]. Their theory describes the rate constant for electron transfer as follows,

$$k^{o} \propto D(\phi_{E}) \left(\frac{T}{\lambda}\right)^{1/2} A \exp\left(-\frac{\lambda}{4k_{B}T}\right) \quad (6)$$

where $D(\phi_E)$ is DOS at the energy level corresponding to a formal potential of redox couple, A is a term regarding electronic coupling in Fermi golden rule, λ is reorganization energy, T is temperature, and k_B is Boltzmann constant. Equation 6 indicates that the rate constant is proportional to DOS at the energy level corresponding to the formal potential. This theory supports our result in Fig. 6.10, leading to the conclusion that the surface DOS determines the kinetics of heterogeneous electron transfer on an HOPG basal plane.

In the discussion above, we assume that the surface of an HOPG basal plane is homogeneous and LDOS is the same at any carbon atoms on the surface. However, as discussed in the previous section, LDOS is not homogeneous on the whole surface of an HOPG basal plane; LDOS is especially high at a carbon atom on or near an edge orientation [21]. The DOS measured in the present study is an average on the whole surface of an HOPG basal plane. Therefore, the measured DOS indirectly indicates the amount of edge orientations on an HOPG basal plane. On the other hand, it is reasonable to consider that the heterogeneous electron transfer of $Ru(NH_3)_6^{3+/2+}$ occurs exclusively near an edge orientation where LDOS is high. As a result, although LDOS is not homogeneous on the whole surface of an HOPG basal plane, the kinetics of electron transfer of $Ru(NH_3)_6^{3+/2+}$ depends on the measured DOS at an HOPG basal plane.

In the present study, we have shown that the variation in surface DOS on an HOPG basal plane plays an important role in determining the kinetics of heterogeneous electron transfer. This variation in surface DOS would be one of the unique characteristics of graphite, leading to interesting electrochemical behaviors of graphite. We believe that a consideration on the electrochemical behaviors from the aspect of surface DOS would lead us to further understandings on the electrochemistry of graphite.

6.4. Conclusions

We have clarified the variation in DOS at the surface of several HOPG basal planes. The minimal values of surface DOS measured from a capacitance measurement range from 2×10^{20} to 7×10^{20} eV^{-1} cm^{-3}, depending on HOPG samples used. The variation in surface DOS is attributed to the amount of edge orientations on the surface of an HOPG basal plane. In addition, we have shown that the rate constant of heterogeneous electron transfer of $Ru(NH_3)_6^{2+/3+}$ has a proportional correlation with surface DOS on an HOPG basal plane. This result is in excellent agreement with a previously reported theory. As a result, we have experimentally verified that surface DOS is one of the determining factors in the kinetics of heterogeneous electron transfer at a graphite electrode.

References

[1] McCreery, R. L. *Chem. Rev.* **2008**, *108*, 2646.

[2] Wightman, R. M.; Deakin, M. R.; Kovach, P. M.; Kuhr, W. G.; Stutts, K. J. *J. Electrochem. Soc.* **1984**, *131*, 1578.

[3] McDermott, M. T.; Kneten, K.; McCreery, R. L. *J. Phys. Chem.***1992**, *96*, 3124.

[4] Cline, K. K.; McDermott, M. T.; McCreery, R. L. *J. Phys. Chem.***1994**, *98*, 5314.

[5] McCreery, R. L.; Cline, K. K.; McDermott, C. A.; McDermott, M. T. *Colloids Surf. A* **1994**, *93*, 211.

[6] Chen, P.; Fryling, M. A.; McCreery, R. L. *Anal. Chem.***1995**, *67*, 3115.

[7] McDermott, C. A.; Kneten, K. R.; McCreery, R. L. *J. Electrochem. Soc.***1993**, *140*, 2593.

[8] Gerischer, H.; McIntyre, R.; Scherson, D.; Storck, W. *J. Phys. Chem.***1987**, *91*, 1930.

[9] Gerischer, H. *J. Phys. Chem.***1985**, *89*, 4249.

[10] Kokko, K.; Ojala, E.; Mansikka, K. *J. Phys.: Condens. Matter* **1990**, *2*, 4587.

[11] Randin, J. P.; Yeager, E. *J. Electrochem. Soc.* **1971**, *118*, 711.

[12] Randin, J. P.; Yeager, E. *J. Electroanal. Chem.* **1972**, *36*, 257.

[13] Randin, J. P.; Yeager, E. *J. Electroanal. Chem.* **1975**, *58*, 313.

[14] Bard, A. J.; Faulkner, L. R. "*Electrochemical Methods, Fundamentals and Applications*," Wiley, New York **1980**.

[15] Ergun, S.; Yasinsky, J. B.; Townsend, J. R. *Carbon* **1967**, *5*, 403.

[16] Grahame, D. C. *J. Am. Chem. Soc.* **1954**, *76*, 4819.

[17] Grahame, D. C. *J. Am. Chem. Soc.* **1957**, *79*, 2093.

[18] McClure, J. W. *Phys. Rev.* **1957**, *108*, 612.

[19] Tatar, R. C.; Rabii, S. *Phys. Rev. B* **1982**, *25*, 4126.

[20] Rice, R. J.; McCreery, R. L. *Anal. Chem.* **1989**, *61*, 1637.

[21] Kobayashi, K. *Phys. Rev. B* **1993**, *48*, 1757.

[22] Menshykau, D.; Streeter, I.; Compton, R. G. *J. Phys. Chem. C* **2008**, *112*, 14428.

[23] Royea, W. J.; Kruger, O.; Lewis, N. S. *J. Electroanal. Chem.* **1997**, *438*, 191.

[24] Royea, W. J.; Fajardo, A. M.; Lewis, N. S. *J. Phys. Chem. B* **1997**, *101*, 11152.

[25] Royea, W. J.; Hamann, T. W.; Brunschwig, B. S.; Lewis, N. S. *J. Phys. Chem. B* **2006**, *110*, 19433.

Chapter 7

Role of Edge Orientation in Kinetics of Electrochemical Lithium Intercalation into Graphite

7.1. Introduction

The electrochemistry of graphite has long been the focus of many researchers' attention because graphite electrodes exhibit unique properties [1]. One of the characteristic features of graphite electrodes is the relationship between surface structure and electrochemical behavior. Graphite has a layered structure, resulting in two orientations, edge and basal orientations, on the surface. The two orientations at the surface of graphite show a significant difference in electrochemical activity [2–5]. The edge orientation of graphite is active toward heterogeneous electron transfer, whereas the basal orientation is highly inactive. Such a characteristic behavior has generated a lively discussion on the role of edge orientations in electrochemical reactions.

Since graphite came into use as a negative electrode in lithium-ion batteries, much effort has been devoted to clarifying the role of edge orientation in electrochemical lithium-ion intercalation at graphite, an essential reaction in lithium-ion batteries. Of major interest so far was the relation between the presence of edge orientations and the reversibility of lithium-ion intercalation at a graphite electrode [6-9]. Chung *et al.* reported that the irreversible capacity tended to be large at graphite materials with many edge orientations [7]. This is because some side reactions (e.g., electrolyte decomposition) mainly occur at the edge orientations of graphite during the intercalation of lithium-ion. Therefore, to improve the reversibility of lithium-ion intercalation, we need to design the structure and size of a graphite electrode considering the amount of edge orientations on the surface.

Despite the vigorous study on the reversibility of lithium-ion intercalation, there are few researches on the role of edge orientations in the kinetics of lithium-ion intercalation at graphite. Funabiki *et al.* showed that the intercalation of lithium-ion was quite slow at the basal plane of highly oriented pyrolytic graphite (HOPG), leading to the conclusion that the edge orientation of graphite is the intercalation site of lithium-ion [10]. Therefore, the amount of edge orientations at the surface of graphite should significantly influence the kinetics of lithium-ion intercalation

and also the rate performance of lithium-ion batteries. However, it is not clear how the kinetics of lithium-ion intercalation is correlated with the amount of edge orientations at the surface of graphite.

In the present study, we used the basal plane of HOPG as a model electrode to study the relation between the amount of edge orientations and the kinetics of electrochemical lithium-ion intercalation. The amount of edge orientations was evaluated from the kinetics of heterogeneous electron transfer of $Ru(NH_3)_6^{3+/2+}$, which is an established method of quantifying edge orientations [11]. The kinetics of lithium-ion intercalation at the basal plane of HOPG was investigated by ac impedance spectroscopy. On the basis of results obtained, we discuss the role of edge orientations in the kinetics of lithium-ion intercalation at graphite.

7.2. Experimental Methods

A basal plane of HOPG (Momentive Performance Materials Quartz, Inc.) was used as a model electrode. The grade of HOPG was STM-1 (Mosaic Spread: 0.8 ± 0.2^{o}) and ZYH (Mosaic Spread: 3.5 ± 1.5^{o}). In advance to electrochemical measurements, the basal plane of HOPG was carefully cleaved with an adhesive tape so that the density of surface defects should be low. Polished glassy carbon (GC-10, Tokai Carbon, Co., Ltd.) was used for comparison.

The edge orientation on the basal plane of HOPG was quantified from the kinetics of heterogeneous electron transfer of $Ru(NH_3)_6^{3+/2+}$ [11]. Cyclic voltammetry was conducted with a three-electrode cell, in which platinum mesh and silver-silver chloride (Ag/AgCl) in saturated KCl aqueous solution were used as counter and reference electrodes, respectively. Only the basal plane of HOPG has contact with an electrolyte solution. The contact area of an HOPG basal plane and an electrolyte was kept constant at 0.38 cm^2 with an o-ring. An electrolyte was 1 mol dm^{-3} KCl (Nacalai Tesque, Inc.) aqueous solution containing 1 mmol dm^{-3} $Ru(NH_3)_6Cl_3$ (Aldrich). The scan rate of cyclic voltammetry was set at 100 mV s^{-1}. Digital simulation of a cyclic voltammogram was configured under a quasi-reversible and linear-diffusion condition. The Butler-Volmer equation and Fick's diffusion law were used for the theoretical description of a cyclic voltammogram. In the digital simulation, the diffusion coefficient of $Ru(NH_3)_6^{3+/2+}$ was set at 4.0×10^{-6} cm^2 s^{-1}. After the measurement, the cell was dried to remove water. The HOPG electrode remained fixed in the cell during the drying process so that the surface area of the electrode was kept constant.

The evaluation of the kinetics of lithium-ion intercalation at the basal plane of HOPG followed the quantification of edge orientations. Electrochemical measurements were carried out with a three-electrode cell [12] in an argon atmosphere. The cell employed lithium metal for counter and reference electrodes. An electrolyte solution was 1 mol dm^{-3} $LiClO_4$ dissolved in a mixture (1:1 by vol.) of ethylene carbonate (EC) and dimethyl carbonate (DMC) (Kishida Chemical Co., Ltd.). Cyclic voltammetry was conducted in the potential range of 0–3 V vs. Li/Li^+ with the scan rate of 0.1 mV s^{-1}. Ac impedance spectroscopy was conducted at the electrode potential of 0.2 V vs. Li/Li^+. The frequency range was 100 kHz – 10 mHz and the applied ac voltage was 5 mV. ZPlot software (Solartron Analytical) was used for the analysis of resultant Nyquist plots.

7.3. Results and Discussion

7.3.1. Quantification of Edge Orientations on HOPG.

Figure 7.1 shows cyclic voltammograms of the basal planes of three HOPG samples in 1 mol dm^{-3} KCl aqueous solution containing 1 mmol dm^{-3} $Ru(NH_3)_6Cl_3$. The solid lines indicate the experimental curves at the scan rate of 100 mV s^{-1}. The cathodic and anodic peaks in the voltammograms show the redox reaction of $Ru(NH_3)_6^{3+/2+}$. The peak separation of the cathodic and anodic sweeps was different in the three voltammgrams, indicating that the standard electron-transfer rate constant (k^o) of $Ru(NH_3)_6^{3+/2+}$ varied at the three HOPG samples. The dashed lines in Fig. 7.1 denote the fitting curves of digital simulation, which give the k^o value of $Ru(NH_3)_6^{3+/2+}$ at each HOPG basal plane. The obtained k^o values are summarized in Table 7.1. The k^o values varied from 1.5×10^{-3} to 5.0×10^{-3} cm s^{-1} depending on the HOPG samples used, whereas the transfer coefficient (α) remained constant at around 0.65. The variation in k^o of $Ru(NH_3)_6^{3+/2+}$ derives from the amount of edge orientations, i.e. defects and grain boundaries, on the basal plane of HOPG [3–5]. In the previous literature, the k^o value of $Ru(NH_3)_6^{3+/2+}$ on an HOPG basal plane was reported to be 0.9×10^{-3} cm s^{-1} by McCreery's group[4] and 12×10^{-3} cm s^{-1} by Compton's group [11]. The large difference in the k^o values derives from a cleaving method of the surface of HOPG: a knife blade by McCreery's group and an adhesive tape by Compton's group. On the basis of the reported k^o values, cleaving by a knife blade results in a low-defect basal plane. In the present study, we used an adhesive tape for cleaving and thus, the ko values were larger than that reported by McCreery's group. We also conducted cyclic

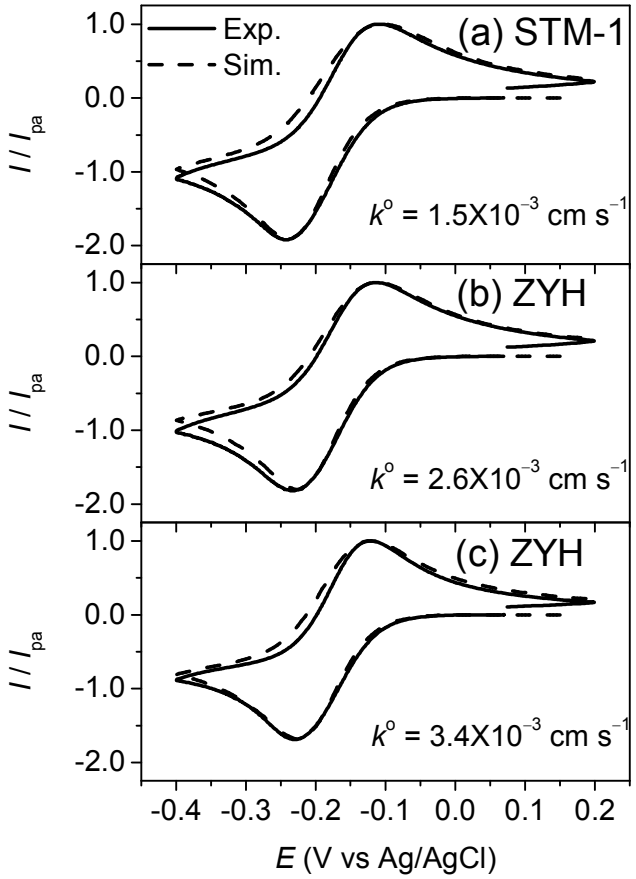

Fig. 7.1 Cyclic voltammograms (solid lines) of three HOPG basal planes in 1 mol dm^{-3} KCl aqueous solution containing 1 mmol dm^{-3} $Ru(NH_3)_6Cl_3$ at room temperature. The current was normalized by the anodic peak current (I_{pa}). The scan rate was set at 100 mV s^{-1}. The dashed lines denote the fitting curves of digital simulation.

voltammetry at various scan rates between 30 and 400 mV s^{-1} and confirmed that the deviation in k^o was below 15 % at these scan rates.

The edge orientations exposed on an HOPG basal plane can be quantified from the k^o value of $Ru(NH_3)_6^{3+/2+}$. Compton's group used the following equation to evaluate the fraction of edge orientations (f_{edge}) exposed on the basal plane of HOPG [11],

$$k^o = f_{edge}\, k^o_{edge} \quad (1),$$

where k^o_{edge} denotes the rate constant of $Ru(NH_3)_6^{3+/2+}$ on a pure edge plane of graphite. Equation 1 leads to the f_{edge} value on HOPG basal planes, as long as we know the k^o_{edge} value. Cyclic voltammetry using the edge plane of HOPG may enable us to measure the k^o_{edge} value, but it is difficult to prepare a flat surface of an HOPG edge plane. Therefore, we used a polished

Table 7.1: Standard rate constant of $Ru(NH_3)_6^{3+/2+}$ (k^o), fraction of edge orientations (f_{edge}), charge-transfer resistance for lithium-ion intercalation (R_{ct}), and edge-area specific resistance for charge transfer (ASR_{edge}) at various HOPG basal planes

Grade	k^o (10^{-3} cm s^{-1})	f_{edge}	R_{ct} (kΩ)	ASR_{edge} (10^2 Ω cm^2)
STM-1(a)	1.5	0.016	26.6	1.6
ZYH	1.6	0.017	17.9	1.2
ZYH	1.8	0.019	16.3	1.2
STM-1	1.9	0.020	23.1	1.8
STM-1	2.0	0.021	31.9	2.6
ZYH	2.0	0.021	16.8	1.3
STM-1	2.3	0.024	14.5	1.3
ZYH (b)	2.6	0.027	13.8	1.4
ZYH	2.6	0.027	11.9	1.2
STM-1	2.8	0.030	7.0	0.8
ZYH	2.9	0.031	10.7	1.2
STM-1	3.2	0.034	11.1	1.4
ZYH (c)	3.4	0.036	9.6	1.3
ZYH	4.3	0.045	3.7	0.6
ZYH	5.0	0.053	8.6	1.7

glassy carbon electrode for the measurement of the k^o_{edge} value. A glassy carbon electrode is a good alternative for a pure edge plane of graphite [11]. The solid and dashed lines in Fig. 7.2 s how

experimental and simulated cyclic voltammograms of polished glassy carbon, respectively. The fitting result of digital simulation led to the k^o_{edge} value of 0.095 cm s^{-1}. McCreery and his co-workers reported that the k^o value of $Ru(NH_3)_6^{3+/2+}$ was over 0.4 cm s^{-1} on laser-activated glassy carbon [4]. The present work employed polished glassy carbon without laser activation and thus, the value of 0.095 cm s^{-1} is reasonable. Using this value, we evaluated the f_{edge} values on the basal planes of various HOPG samples. Table 7.1 summarizes the values of k^o and f_{edge} on the basal planes of 15 HOPG samples. The values of f_{edge} ranged from 0.016 to 0.053. In the

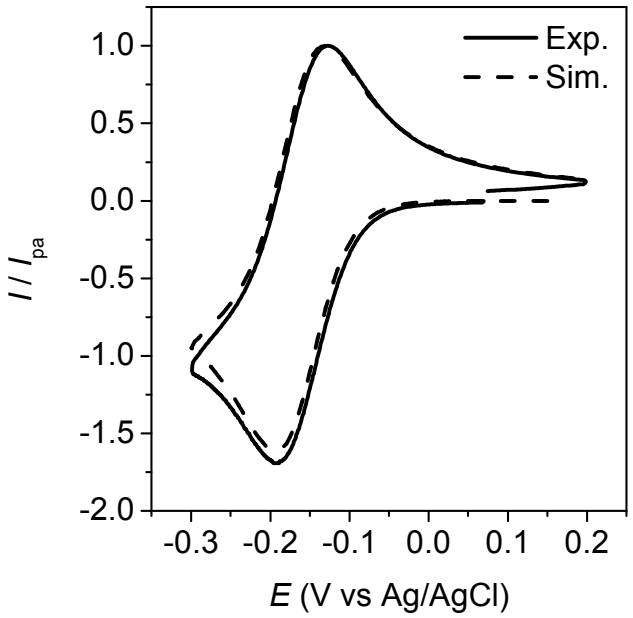

Fig. 7.2 Cyclic voltammogram (solid line) of polished glassy carbon in 1 mol dm^{-3} KCl aqueous solution containing 1 mmol dm^{-3} $Ru(NH_3)_6Cl_3$ at room temperature. The current was normalized by the anodic peak current (I_{pa}). The scan rate was set at 100 mV s^{-1}. The dashed lines denote the fitting curves of digital simulation.

previous literature, the f_{edge} value on an HOPG basal plane was reported to be 0.01–0.10 by Bard's group [13], 0.002–0.016 by McCreery's group [14], and 0.03 by Compton's group [11]. Therefore, the f_{edge} values in the present study are reasonable, indicating that our measurement is accurate and reliable. We could not find a large difference in f_{edge} at the two grades of HOPG. This is because the amount of edge orientations on an HOPG basal plane is determined by the cleaving process, rather than the nature of HOPG itself. Even careful cleaving by an adhesive tape results in surface defects on the basal plane of HOPG and thus, it is difficult to detect the difference in the nature of STM-1 and ZYH grades by this electrochemical method.

7.3.2. Evaluation of Kinetics of Lithium-Ion Intercalation at HOPG.

After obtaining f_{edge} on HOPG samples, we evaluated the kinetics of lithium-ion intercalation at the *same* HOPG samples. Figure 7.3 shows cyclic voltammograms of the basal planes of three HOPG samples in 1 mol dm^{-3} $LiClO_4$ / EC:DMC (1:1 by vol.). The three HOPG samples correspond to those in Fig. 7.1. The cathodic and anodic peaks in the potential range between 0 and 0.6 V vs. Li/Li^+ are assigned to the intercalation and deintercalation of lithium-ion

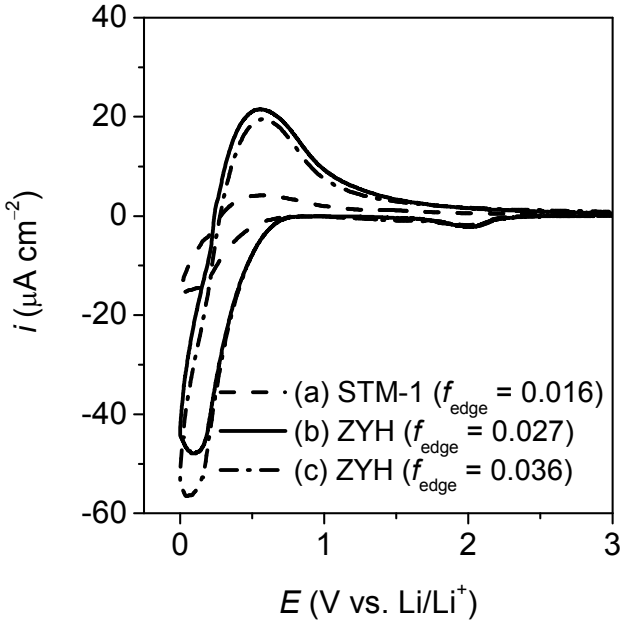

Fig. 7.3 Cyclic voltammogram of three HOPG basal planes in 1 mol dm^{-3} $LiClO_4$ EC:DMC (1:1 by vol.) at 30 ^oC. The scan rate was set at 0.1 mV s^{-1}. The three HOPG basal planes correspond to those in Fig. 7.1.

at HOPG, respectively. The peak current varied at the three HOPG basal planes, indicating that the kinetics of lithium-ion intercalation was different. An interesting point is that the kinetics of lithium-ion intercalation is correlated with that of heterogeneous electron transfer of $Ru(NH_3)_6^{3+/2+}$. Both lithium-ion intercalation and heterogeneous electron transfer were slow at sample (a), while both of them were fast at sample (c). These results imply that these two reactio ns occur at the same reaction site (i.e., edge orientation).

To evaluate the kinetics of lithium-ion intercalation, we carried out ac impedance spectroscopy at the electrode potential of 0.2 V vs. Li/Li^+ at which lithium-ion intercalation at HOPG can take place. Figures 7.4a) and 7.4b) show Nyquist plots of the three HOPG samples in 1 mol dm^{-3} $LiClO_4$ / EC:DMC (1:1 by vol.). The f_{edge} values at the three HOPG samples are also shown in Fig. 7.4a). The measurement was conducted after two cycles of lithium-ion intercalation/deintercalation to make sure that the formation of a surface film (solid electrolyte interphase, SEI) was completed. There are small and large semicircles at the characteristic frequency of 1 kHz and 1 Hz, respectively. In the lower frequency region, Warburg impedance appears as a straight line with 45^o from the *Z'* axis. The attribution process for these resistance components was described in detail in our previous literature [12]. The small semicircle at the

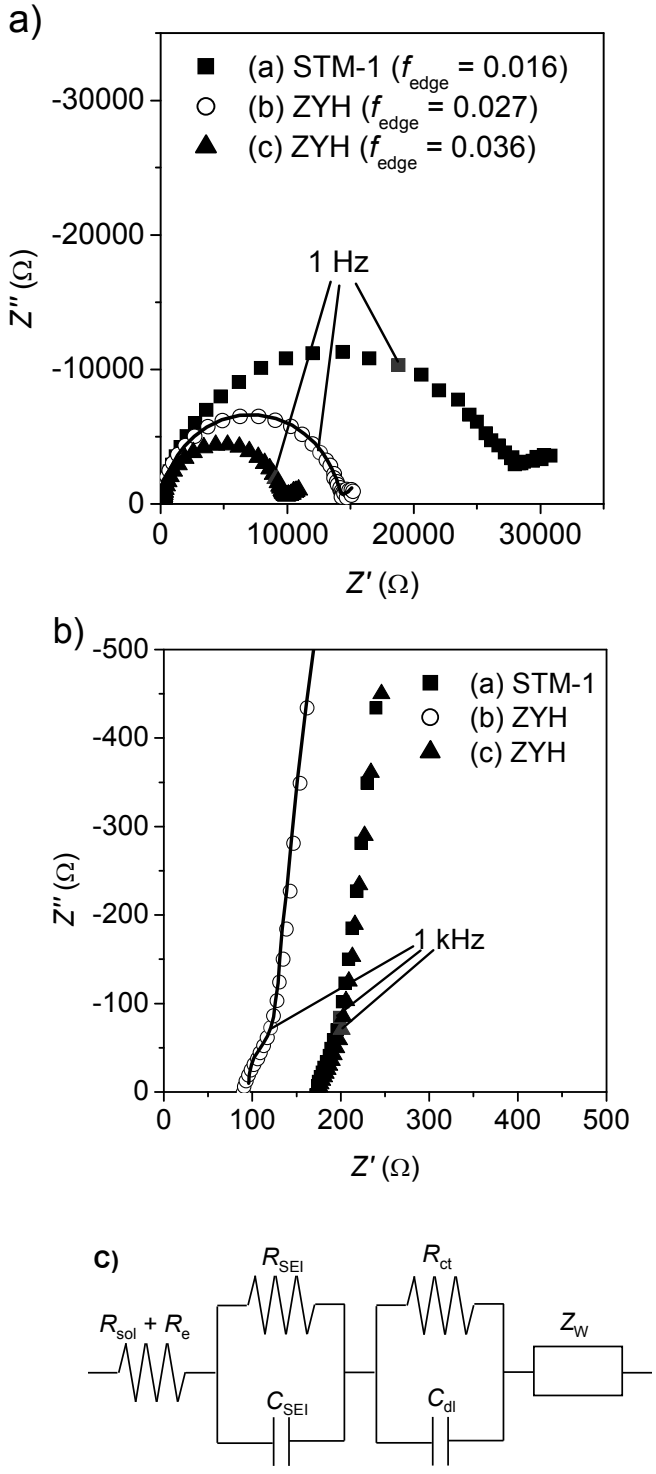

Fig. 7.4 (a) Nyquist plots of three HOPG basal planes in 1 mol dm^{-3} $LiClO_4$ EC:DMC (1:1 by vol.) at 30 ^{o}C. The three HOPG basal planes correspond to those in Figs. 7.1 and 7.3. (b) Enlarged figure of the Nyquist plots in a high-frequency region. (c) Equivalent circuit used for the analysis of the Nyquist plots.

characteristic frequency of 1 kHz is attributed to the resistance for lithium-ion transport in an SEI (R_{SEI}). The large semicircle at the characteristic frequency of 1 Hz is the charge (lithium-ion) transfer resistance at an HOPG/electrolyte interface (R_{ct}). The Warburg impedance (Z_W) derives from lithium-ion diffusion in HOPG. The *Z'* intercept indicates the resistance for lithium-ion transport in an electrolyte (R_{sol}) and the electronic resistance in HOPG and at HOPG/current collector (R_e). Figure 7.4a) shows that the R_{ct} values significantly varied at the three HOPG samples. Hence, the kinetics of lithium-ion intercalation was different depending on the f_{edge} values. On the other hand, the semicircles for R_{SEI} were almost the same at the three HOPG samples, as shown in Fig. 7.4b). Therefore, the kinetics of lithium-ion transport in the SEI was not influenced by the f_{edge} values. A difference in the *Z'* intercept at the three HOPG samples did not derive from the nature of HOPG but was inherent in the electrochemical cell used.

The attribution shown above let us to configure an equivalent circuit as shown in Fig. 7.4c), where the symbols C_{SEI} and C_{dl} denote a capacitance element in an SEI and a double-layer capacitance, respectively. An example of a fitting curve using the equivalent circuit is shown as a solid line in Figs. 7.4a) and 7.4b). The best fitting gives R_{ct} values at the basal planes of HOPG, as shown in Table 7.1. The R_{ct} values significantly varied depending on the f_{edge} values.

7.3.3. Correlation between Amount of Edge Orientations and Kinetics of Lithium-Ion Intercalation at HOPG.

Figure 7.5 shows the relation between f_{edge} and R_{ct} at the basal planes of 15 HOPG samples. A clear correlation was observed between f_{edge} and R_{ct}. HOPG samples with many edge orientations (large f_{edge}) tend to give small R_{ct} values, leading to fast intercalation of lithium-ion. The relation between f_{edge} and R_{ct} is approximate to inverse proportion. From these results, we confirmed that an edge orientation on graphite is active for lithium-ion intercalation as well as heterogeneous electron transfer.

This result provides important information about the kinetics of lithium-ion intercalation at graphite. By normalizing the R_{ct} value by the total area of edge orientations on the surface of HOPG basal planes, we can calculate the edge-area specific resistance (ASR_{edge} with a unit of Ω cm^2) as follows,

$$ASR_{edge} = R_{ct} f_{edge} S \quad (2)$$

where S denotes the surface area of an HOPG basal plane that has contact with the electrolyte. If we assume that the basal plane of HOPG is completely flat, the S value is 0.38 cm^2. Calculated

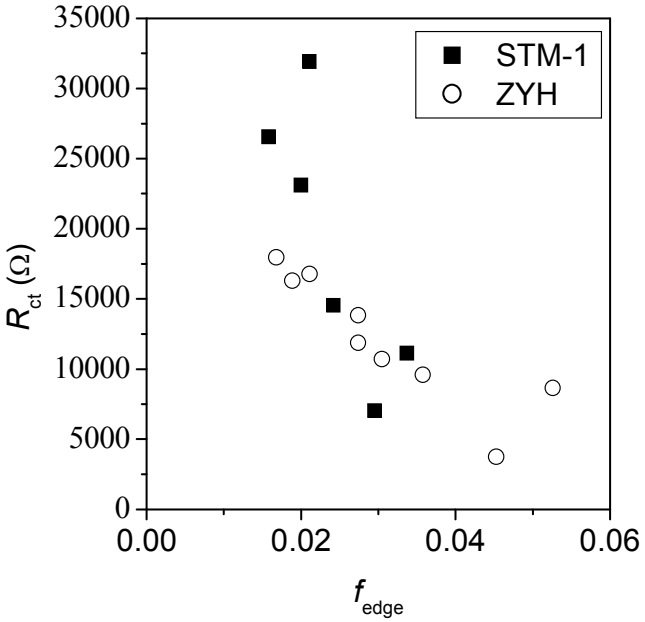

Fig. 7.5 Correlation between fraction of edge orientations (f_{edge}) and charge-transfer resistance of lithium-ion intercalation (R_{ct}) at the surface of various HOPG basal planes.

ASR_{edge} values on various HOPG basal planes are shown in Table 7.1. Although the ASR_{edge} values exhibited small dispersion, most of them were around 150 Ω cm^2. These results clarified again that the amount of edge orientations is one of the determining factors in the kinetics of lithium-ion intercalation at graphite. In addition, the obtained ASR_{edge} value is useful to control the kinetics of lithium-ion intercalation by designing the structure and size of graphite materials for lithium-ion batteries.

7.3.4. Determining Factors in Kinetics of Electrochemical Lithium-Ion Intercalation at Graphite.

The interfacial conductivity ($1/R_{ct}$) for lithium-ion intercalation obeys the Arrhenius equation as follows,

$$1/R_{ct} = A\exp(-E_a/RT) \quad (3)$$

where A is frequency factor, E_a is activation energy, R is gas constant, and T is absolute temperature. Therefore, there are two factors, A and E_a, determining the kinetics of lithium-ion intercalation at graphite. Our previous study clarified that the E_a value depends on electrolyte solvents and SEI compositions [12]. When we use an EC-based electrolyte, the E_a value is

always around 58 kJ mol^{-1}. In the present study, we used the same electrolyte for all the measurements. Therefore, the E_a value should be constant at all the HOPG samples, and the A values are different at various HOPG samples. Considering the relation between R_{ct} and f_{edge}, we concluded that the A value depends on the amount of edge orientations on the basal planes of HOPG.

In summary, we need to consider electrolyte solvents, SEI compositions, and the amount of edge orientations to achieve high rate-performance at a graphite negative electrode in lithium-ion batteries. The amount of edge orientations determines the frequency factor of lithium-ion intercalation at graphite, whereas electrolyte solvents and SEI compositions influence the activation energy of the reaction. Of course, we must take into consideration the relation between the amount of edge orientations and irreversible capacity. The irreversible capacity tends to be large at a graphite material with many edge orientations [7]. Therefore, an appropriate amount of edge orientations is a trade-off between the kinetics and the irreversible capacity of lithium-ion intercalation at graphite. The results in the present study will be useful for designing the structure and size of graphite materials with high rate-performance and low irreversible capacity as a negative electrode in lithium-ion batteries.

7.4. Conclusions

We have clarified the correlation between the amount of edge orientations and the kinetics of lithium-ion intercalation at the basal plane of HOPG. The fraction of edge orientations (f_{edge}) exposed on the basal plane of 15 HOPG samples were evaluated to be in a range of 0.016 to 0.053. The charge-transfer resistance (R_{ct}) for lithium-ion intercalation was inversely proportional to the f_{edge} value on the basal planes of HOPG. In addition, we evaluated the edge-area specific resistance (ASR_{edge}) for lithium-ion intercalation at graphite to be ca. 150 Ω cm^2 at the electrode potential of 0.2 V vs. Li/Li^+. These results indicate that the amount of edge orientations is one of the determining factors in the kinetics of lithium-ion intercalation at graphite.

References

[1] McCreery, R. L. *Chem. Rev.* **2008**, *108*, 2646.

[2] Wightman, R. M.; Deakin, M. R.; Kovach, P. M.; Kuhr, W. G.; Stutts, K. J. *J. Electrochem.*

Soc. **1984**, *131*, 1578.

[3] McDermott, M. T.; Kneten, K.; McCreery, R. L. *J. Phys. Chem.***1992**, *96*, 3124.

[4] Cline, K. K.; McDermott, M. T.; McCreery, R. L. *J. Phys. Chem.***1994**, *98*, 5314.

[5] McCreery, R. L.; Cline, K. K.; McDermott, C. A.; McDermott, M. T. *Colloids Surf. A* **1994**, *93*, 211.

[6] Winter, M.; Novak, P.; Monnier, A. *J. Electrochem. Soc.* **1998**, *145*, 428.

[7] Chung, G.-C.; Jun, S.-H; Lee, K.-Y.; Kim, M.-H. *J. Electrochem. Soc.* **1999**, *146*, 1664.

[8] Zaghib, K.; Nadeau, G.; Kinoshita, K. *J. Electrochem. Soc.* **2000**, *147*, 2110.

[9] Aurbach, D.; Teller, H.; Koltypin, M.; Levi, E. *J. Power Sources* **2003**, *119-121*, 2.

[10] Funabiki, A.; Inaba, M.; Ogumi, Z. *J. Power Sources* **1997**, *68*, 227.

[11] Davies, T. J.; Moore, R. R.; Banks, C. E.; Compton, R. G. *J. Electroanal. Chem.* **2004**, *574*, 123.

[12] Yamada, Y.; Iriyama, Y.; Abe, T.; Ogumi, Z. *Langmuir* **2009**, *25*, 12766.

[13] Chang, H.; Bard, A. J. *Langmuir* **1991**, *7*, 1143.

[14] McDermott, M. T.; McCreery, R. L. *Langmuir* **1994**, *10*, 4307.

Publication list

Part 1

Chapter 1

Correlation between Charge-Discharge Behavior of Graphite and Solvation Structure of the Lithium Ion in Propylene Carbonate-Containing Electrolytes

Yuki Yamada, Yasuhiro Koyama, Takeshi Abe, and Zempachi Ogumi

Journal of Physical Chemistry C **2009**, *113*, 8948–8953.

Chapter 2

Electrochemical Lithium Intercalation into Graphite in Dimethyl-Sulfoxide-Based Electrolytes: Effect of Solvation Structure of Lithium-Ion

Yuki Yamada, Yasuyuki Takazawa, Kohei Miyazaki, and Takeshi Abe

Journal of Physical Chemistry C, accepted.

Part 2

Chapter 3

Kinetics of Lithium-Ion Transfer at the Interface between $Li_{0.35}La_{0.55}TiO_3$ and Binary Electrolytes

Yuki Yamada, Fumihiro Sagane, Yasutoshi Iriyama, Takeshi Abe, and Zempachi Ogumi

Journal of Physical Chemistry C **2009**, *113*, 14528–14532.

Chapter 4

Kinetics of Lithium Ion Transfer at the Interface between Graphite and Liquid Electrolytes: Effects of Solvent and Surface Film

Yuki Yamada, Yasutoshi Iriyama, Takeshi Abe, and Zempachi Ogumi

Langmuir **2009**, *25*, 12766–12770.

Chapter 5

Kinetics of Electrochemical Insertion and Extraction of Lithium Ion at SiO

Yuki Yamada, Yasutoshi Iriyama, Takeshi Abe, and Zempachi Ogumi

Journal of the Electrochemical Society **2010**, *157*, A26-A30.

Part 3

Chapter 6

Variation in Density of Electronic States at the Surface of Graphite and Its Influence on the Kinetics of Heterogeneous Electron Transfer

Yuki Yamada, Kohei Miyazaki, and Takeshi Abe

Analytical Chemistry, submitted.

Chapter 7

Role of Edge Orientation in Kinetics of Electrochemical Intercalation of Lithium-Ion at Graphite

Yuki Yamada, Kohei Miyazaki, and Takeshi Abe

Langmuir, submitted.